The Dissertation Committee for Kevin Michael Eckes certifies that this is the approved version of the following dissertation:

Probing the effects of backbone ester substitution on self-assembly and biological activity of short depsipeptides

Committee:

Laura Suggs, Supervisor

Brent Iverson

Pengyu Ren

Jason Shear

Jeanne Stachowiak

Probing the effects of backbone ester substitution on self-assembly and biological activity of short depsipeptides

by

Kevin Michael Eckes, B.S., M. S. E.

Dissertation

Presented to the Faculty of the Graduate School of

The University of Texas at Austin

in Partial Fulfillment

of the Requirements

for the Degree of

Doctor of Philosophy

The University of Texas at Austin

May 2015

Dedication

To my family for their unquestioning and unending love and support.

Acknowledgements

First and foremost, I would like to thank my family. Their love and encouragement have helped to guide me through every challenge I have ever faced. To Beth, thank you for your love, dedication, and your genuine interest in understanding my work. You have helped me become a much better science communicator.

To former and current Suggs lab members, who have been a constant source of advice, assistance, and laughter: Mary, Julie, Eunna, Laura G, Laura R, Ryan, Daniela, Alicia, Kiheon, Kabir, and Shane, thank you all for making it easy and enjoyable to come to lab every day. I feel lucky to have been part of a working environment with people of such high quality. To Ryan Stowers in particular, I enjoyed our shared veracity for good, strong coffee and our frequent musings on the nature of science and the research profession, even if sometimes we were a little *too* cynical.

I also would like to acknowledge the various core facility staff for their invaluable expertise and generous help: Steve Sorey and Angela Spangenberg of the NMR Facility, Dr. Karin Keller and Ian Riddington of the Mass Spec Facility, Michelle Gadush of the Protein and Metabolite Analysis Facility, Dr. Dwight Romanowicz of the ICMB Imaging Core Facility, Dr. Steve Swinnea of the Texas Materials Institute X-ray Facility, and Dr. Eun Jeong Cho of the Texas Institute for Drug and Diagnostic Development. Additionally, I would like to thank Prof. Lauren Webb and her lab members for use and help with FTIR sample preparation and measurements.

I thank the National Science Foundation for support in the form of a Graduate Research Fellowship, without which I may have not been able to finish graduate school. The Cockrell School of Engineering also generously provided several years of

supplementary financial support, which I appreciated greatly and used wisely. Other than financial support, moral support was key to "sticking it out"; to my friends in the Biomedical Engineering department across all class years, thank you for the great conversations, encouragement, commiserations, and the social outlets you all help provide for each other through the tougher years of grad school. As I finish the final phases of my project, I would also like to thank Profs. Brent Iverson, Pengyu Ren, Jason Shear, and Jeanne Stachowiak for their willingness to advise and help me as my dissertation committee members.

Finally, I would like to thank my advisor Prof. Laura Suggs for her thoughtful guidance, encouragement, and frequent post-meeting conversations about nearly everything. Few are so lucky to have such an approachable and caring mentor who so readily puts her students' education and individual development before her personal interests.

Probing the effects of backbone ester substitution on self-assembly and biological activity of short depsipeptides

Kevin Michael Eckes, Ph.D.

The University of Texas at Austin, 2015

Supervisor: Laura J. Suggs

Hydrogel materials composed of self-assembled amphiphilic peptides show great promise for use as injectable, highly biocompatible biomaterials for tissue regeneration applications. However, peptides do not easily degrade naturally without the presence of proteolytic enzymes, which recognize specific peptide sequences and are specific to certain cell and tissue types. In this dissertation, we evaluate the self-assembly and bioactivity of backbone ester-containing depsipeptides that are degradable by alkaline or acid hydrolysis as the basis for hydrogel materials, in order to circumvent any inflammation and immunogenicity caused by peptide materials that persist in the body. The self-assembly of depsipeptides has not been widely explored, thus we first studied the self-assembly of a simple N-protected dipeptide and its depsipeptide analogue both experimentally and computationally to evaluate the relative importance of hydrogen-bonding interactions mediated by the single amide bond in driving and stabilizing self-assembly. We determined that amide-amide hydrogen bonding interactions are not strictly necessary for self-assembly. We next hypothesized that amide-mediated hydrogen bonding may not be necessary for mediating peptide-protein interactions. To test this hypothesis in a simple, well-characterized system, we synthesized a depsipeptide analogue of a peptide containing the Arg-Asp-Gly (RGD) sequence, which is found in

extracellular matrix proteins and known to promote cell adhesion through binding of cell surface integrin proteins. As before, the RGD analogue was capable of self-assembly leading to hydrogel formation. However, we found that the depsipeptide did not possess an affinity for the protein high enough to influence cell behavior in the same manner as the peptide. These results suggest that backbone amide hydrogen bonding is crucial in mediating RGD-integrin interaction affinity. Based on these results and other studies in the literature suggesting that amide-to-ester mutations have a complex and context-dependent effect on peptide-protein interactions, further development of depsipeptide-based materials should focus on exploring alternate N-protecting groups that are likely to have higher biocompatibility while driving robust self-assembly, exploring in more depth the ability to tune degradation rates and mechanical properties using alternate side chain chemistries, and exploiting depsipeptide self-assembly and degradability for non-viral gene delivery.

Table of Contents

List of Tables

List of Figures

List of Illustrations

Chapter 1: Introduction

1.1 INTRODUCTION

The overall objective of the research described herein is to develop a new class of self-assembling hydrogel biomaterials for tissue engineering applications. Tissue engineering strategies typically employ physiologically interactive materials that act as scaffolds upon which the body can rebuild native tissue. For this reason, the goal of any biomaterial to be used for regenerating critically injured or diseased tissue is to mimic the native extracellular matrix (ECM) without inhibiting deposition of new ECM during healing. Thus, an ideal biomaterial would be made from non-cytotoxic materials, promote ECM-like cell-material interactions to direct cell behavior, and degrade by nonspecific chemical pathways (i.e. not requiring enzymatic action) over the course of several months.

Peptide-based biomaterials fulfill most of these requirements. Amphiphilic and "self-complementary" oligomeric peptides have been shown to self-assemble in aqueous solution to form nanostructures that entangle and result in gelation of the solution. Furthermore, these peptides can often be engineered to have cell-adhesive or bioactive amino acid sequences without disruption of self-assembly and gelation. While peptide-based materials often exhibit *in vivo* immune tolerance over the short term, there is a lack of understanding about long-term inflammation that might result. Given the tolerance of the amide bond to non- enzyme mediated hydrolysis, peptide substituents likely persist in the tissue much longer than the time over which new cells infiltrate the injury site and begin to rebuild native ECM. Ideally, substituent molecules would degrade into very low

molecular weight components soon after disassembly of the bulk material, thereby minimizing the risk of possible complications due to chronic inflammation.

Our group has focused on the development of ester-containing *depsipeptides* as the major components of hydrogel biomaterials. Depsipeptides are peptide mimics in which amide bonds in the peptide backbone alternate with ester bonds conferred by α-hydroxy acids used in place of amino acids. Given the potential of depsipeptides to exhibit desirable degradation characteristics while potentially maintaining peptide-like bioactivity, we chose to develop a simple depsipeptide analogue of the Arginine-Glycine-Aspartic acid (RGD) sequence, the ubiquitous amino acid motif known to interact with cell integrin proteins to mediate cell interaction with the ECM. This research was intended to achieve the following goals: 1) validate the bottom-up design and synthesis of biomaterials with inherent biocompatibility, engineered bioactivity, and hydrolytic degradability, and 2) answer fundamental questions regarding how peptide backbone chemistries affect their ability to interact specifically with proteins.

1.2 ORGANIZATION OF DISSERTATION

This document is organized into chapters that correspond to discrete phases of this research project. Chapter 2 provides the background information necessary for understanding the motivation for the research and the approach taken. We discuss the motivation for the research as the poor clinical outcomes that result from tissue scarring and remodeling post-myocardial infarction and recent materials-based strategies to improve outcomes. We also provide relevant background information and recent applications of self-assembling peptide-based materials for tissue regeneration. This chapter also provides a brief review of the development and uses of peptidomimetics as a

general class of materials and includes a specific discussion of depsipeptides with special regard for their common uses and demonstrated self-assembly and protein-binding capabilities.

Chapter 3 describes a published study in which we took a combined experimental and computational approach to show that a simple gelator, Fmoc-Ala-Ala, self-assembles into fibrillar supramolecular nanostructures stabilized mainly through hydrophobic interactions between neighboring Fmoc protecting groups. The results of this work indicated that supramolecular structures formed are fairly disordered, calling into question the validity of a previously hypothesized structure model for an Fmoc-diphenylalanine hydrogelator. Furthermore, our results suggested that specific β-sheet-like hydrogen bonding between adjacent peptides within an assembly is not the predominant mode of interaction and likely contributes little to the overall stability of assemblies of such short peptides.

Chapter 4 is a published follow-up study to the work described in Chapter 3. In this work, we describe the self-assembly characteristics of Fmoc-Ala-Lac, an ester-containing analogue of the hydrogelator Fmoc-Ala-Ala. We developed Fmoc-Ala-Lac as a simple platform to test whether ester-containing Fmoc-depsipeptides might be capable of self-assembly leading to gelation. The ester linkage within Fmoc-Ala-Lac also allowed us to test the prevailing hypothesis that β-sheet interactions between adjacent peptides in a self-assembled structure are a major contributor to driving self-assembly and stabilizing the resulting structures. Our results showed that Fmoc-Ala-Lac was indeed capable of self-assembly into fibrillar nanostructures that entangled to form a gel, indicating that specific β-sheet interactions are not a requirement for self-assembly of short peptides. We compare the nanoscale morphological and spectroscopic characteristics of Fmoc-Ala-Ala and Fmoc-Ala-Lac gels and demonstrate that while the fundamental self-assembled fibril

units appear to be very similar, the morphology of high-order structures and bulk properties are very different. Computational simulations also indicate that the basic fibril units should be similar in diameter and molecular arrangement, but that Fmoc-Ala-Lac fibrils have a greater propensity to further aggregate into larger structures due to fewer hydrogen-bonding interactions with the surrounding water.

In Chapter 5, we describe recent work that attempts to understand the consequence of an amide-to-ester mutation in a system with biological relevance. Specifically, we attempted to determine whether R-Glc-D (Glc = glycolic acid), a depsipeptide analogue of the integrin-binding Arginine-Glycine-Aspartic acid (RGD) sequence, would retain integrin affinity. The results of such experiments would allow us to ascertain the necessity of backbone hydrogen bonding interactions in mediating the RGD-integrin interaction. First, we synthesized Fmoc-protected depsipeptide RGD analogues and demonstrated the self-assembly of both these analogues and of the RGD peptides. Next, in a series of trials involving RGD peptide- or depsipeptide-modified glass surfaces, we show that cells plated in serum-free conditions attach and spread greatly on surfaces presenting the native RGD peptide, whereas R-Glc-D-presenting surfaces do not promote cell attachment and spreading to the same degree. These results indicate that backbone hydrogen bonding is important in mediating RGD-integrin binding, at least at a functional level.

Finally, in Chapter 6 we present the overall conclusions of our work, and suggest future directions for the project and the material developed.

Chapter 2: Background and Significance

2.1 Motivation – Myocardial infarction and materials-based strategies for treatment

Worldwide, cardiovascular disease is the leading cause of death by non-communicable diseases in people under the age of 70 (*1*). Acute myocardial infarction (MI) occurs after massive clotting events that result from the rupture of coronary artery plaques. Cardiac tissue becomes critically ischemic, resulting in cell death and tissue damage. As in most examples of healing after tissue trauma, the body reacts to the injury swiftly to prevent infection and stop hemorrhaging at the expense of proper reconstruction of the native tissue organization, thereby leading to reduced functionality and efficiency. Post-MI prognosis is therefore usually quite grim; while MI accounts for only about 15% of all acute heart disease-related deaths in the U.S. (*2*), tissue inflammation and remodeling post-MI likely contribute significantly to ventricular wall thinning and left ventricular dilation leading to decreased ejection fraction and highly increased risk of subsequent fatal heart failure (**Figure 2.1**) (*3–5*).

The goal of tissue engineering is to develop therapies, often based on the use of cells and biomaterials, that discourage the body's natural tendency to form scar tissue and encourage tissue regeneration as in development, with proper cellular organization and function. Considering the enormous societal and economic impacts of cardiovascular disease, tissue-engineering therapies have been investigated to encourage regeneration of native-like cardiac tissue after MI to prevent pathological remodeling and hopefully restore normal function and a sufficiently high ejection fraction. Naturally derived proteinaceous materials such as fibrin glue (*6*, *7*) and decellularized myocardium (*8*) have been successfully injected into post-MI rat hearts and displayed good biocompatibility

and cell ingrowth leading to organized, vessel-like structures, as well as a slowing of the decrease in systolic function and myocardial degeneration. While promising, approaches based on naturally derived materials are limited by sourcing and availability issues, inconsistencies between donor samples, high processing costs, possible immunogenicity, and a host of other issues. Cheaper and abundant synthetic polymer gels can also be problematic, as many require chemical crosslinking conditions that are not physiologically compatible and are often not able to be degraded and excreted by the body.

2.2 SELF-ASSEMBLING PEPTIDE-BASED MATERIALS FOR TISSUE ENGINEERING

Many small molecules have been found to self assemble in solution into fibrous structures that entrap water, forming a hydrogel. These low molecular weight "hydrogelators" (LMWH) have long been of interest in the organic chemistry community (*9*), but are only recently gaining interest within the biomaterials community. The advantages of a small molecule self-assembling material for drug and cell delivery are many. They can be injected through a syringe, circumventing the need for invasive surgery. Simultaneously, they are triggered to gel *in situ* by a change in pH or temperature, change in solubility due to enzymatic action, or the addition of common ions such as calcium, in contrast to potentially harmful radical-producing photosensitizers used in light-based *in situ* cross-linking of long polymer chains. Furthermore, as small molecules they should be easily cleared from the body by the kidneys, unlike large cross-linked polymer systems that must first be hydrolyzed or oxidized into smaller fragments.

Peptide-based LMWHs gain further advantages over other systems. The peptide segments of these small self-assembling molecules can be engineered to have bioactivity

and cell-signaling capability, such as the Arginine-Glycine-Aspartic acid (RGD) motif recognized by integrins, which mediate cell binding to a surface. Peptides are also naturally degraded by proteases into amino acids, which are easily metabolized or recycled by the body. Therefore, gels from these materials would be even more easily degraded and cleared by the body than would other small molecule hydrogelators. The distinct advantages offered by peptide-based LMWHs make them potentially clinically applicable, and many investigators are performing *in vitro* and *in vivo* tests for biocompatibility, cell-binding capability, and tissue regeneration. Three well-studied classes of peptide-based LMWHs are discussed below as well as several biomedical-oriented experiments for each.

2.2.1 Self-complementary oligopeptide gelators

While attempting to show that a oligopeptides with alternating hydrophobic and hydrophilic side chain residues could preferentially bind Z-DNA, Zhang et al. discovered that these EAK- and RAD-repeat peptides (**Figure 2.2 A**) self-assembled and formed an insoluble membranous film when mixed with DMEM cell medium (*10*). The authors found that the structure was composed of many β-sheet-like structures using circular dichroism (CD), and using TEM they also found that the structure contained many entangled nanofiber features. Based on this information, they proposed that the oligopeptides assemble into supramolecular structures in the manner shown in **Figure 2.2 B**. Because of the alternating sequence of amino acids with hydrophobic and charged side chain groups, all charged groups lie on one side of the β-sheet and all hydrophobic groups like on the other side, allowing membranes to interact laterally.

Zhang et al. also observed that the membranous structures were resistant to degradation by proteases, SDS, urea, heat, and acid. Because of its stability, the authors proposed that the gel-like film could be used as a biomaterial. In a paper published shortly thereafter, Zhang et al. (*11*) demonstrated that a variety of mammalian cell types were able to attach to films made using a 16-residue peptide with a repeating Arginine-Alanine-Aspartic acid (RAD) sequence, even when pre-incubated with free RGD peptide to block RGD-binding integrins. Notably, the authors found that when injected into rabbits to produce antibodies against the oligopeptides no significant antibody titer was produced, suggesting that the synthetic peptides are non-immunogenic. This evidence favored continued use of these materials for biological applications, which have since been numerous.

RAD16 peptide gels have been shown to induce formation of capillary-like networks with single- and multi-cell lumens when human microvascular endothelial cells were encapsulated in gels *in vitro* (*12*), and *in vivo* they have been found to encourage endothelial and smooth muscle cell infiltration and capillary-like structure formation when injected into mouse hearts (*13*). Neural applications of RAD16 have also been explored, including using the scaffolds to promote neurite outgrowth in nerve cells of various species (*14*), conjugating bioactive peptides to RAD16 chains to promote neural stem cell attachment and differentiation (*15*), and entrapment of neural cells migrating from a hippocampal slice for selective enrichment of migrating cells (*16*). Similar peptide gels have been used in myriad other ways, including as a wound dressing (*17*), delivery systems for semi-controlled release of drugs (*18*, *19*) and cytokines (*20*), and as materials to encourage pre-osteoblast differentiation (*21*) and chondrogenesis (*22*). The RAD16 peptides so heavily used in all these studies are now being marketed as a product called PuraMatrix™ by the company 3DM, Inc. in Waltham, Massachusetts (*23*).

2.2.2 Peptide amphiphiles

Samuel Stupp and colleagues first developed peptide amphiphiles to form a self-assembling matrix for biomimetic crystal templating of hydroxyapatite mineral (*24*). Peptide amphiphiles (PAs) are molecules composed of a hydrophobic fatty acid tail conjugated to the N-terminus of a short (<15 residue) peptide sequence (*25*). The peptide portion of the molecule contains a β-sheet forming segment (~7 residues) to stabilize lateral interactions between adjacent molecules, a charged segment (1-2) residues to mediate responsiveness of the peptide to changes in pH or ionic strength in solution, and a terminal segment (4-7 residues) with a bioactive sequence (**Figure 2.3**). Self-assembly of PAs is triggered by a change in pH, temperature, or ionic interactions, depending on the design of the PA molecule. Radial assembly of individual PAs give rise to a larger, nanometer-dimensioned cylindrical structure with hydrophobic alkyl tails concentrated in the center of the structure. It is hypothesized that the β-sheet forming capability of the inner peptide segment stabilizes the structure along its long axis and prevents the formation of micelle-like assemblies (*25*).

Several important findings have made the use of PAs more feasible for biomedical applications. Initially, a limitation of the use of PAs for use as cell scaffolds was their tendency to self-assemble only at fairly low or high pH due to the neutralization of protonated or deprotonated side chain residues to allow close adjacent packing of PA molecules. However, Niece et al. (*26*) found that PAs that normally assemble at acidic pH can form gels at neutral pH when combined with PAs that tend to assemble at basic pH due to complementary charge interactions between side chain residues. The oppositely charged PAs contained bioactive sequences, so this work also demonstrates that PA nanofibers can incorporate and present multiple bioactive sequences. This potential for simultaneous signaling may be useful for cell and tissue engineering

applications. Also important for such applications is the ability to tune the mechanical properties of a cell substrate material. Greenfield et al. (*27*) showed that simple modulation of PA concentration and gelation technique (acidification or salt addition) allowed for modulation of the bulk mechanical properties over a range of two orders of magnitude. Among others, these findings validate the use of PAs as a tunable and broadly applicable self-assembling system for biomedical applications.

The flexibility of the PA platform has allowed for their investigation in a number of *in vitro* and *in vivo* studies. PAs have been explored as pro-angiogenesis materials; PAs engineered with a VEGF-mimicking bioactive peptide for the tail were found to induce VEGF receptor phosphorylation at a level comparable to that of soluble VEGF protein, and when injected into ischemic hind limbs of rats, these PAs were shown to enhance vascular recovery and limb motor function relative to controls (*28*). *In vivo* angiogenesis in a dorsal skin fold chamber has also observed with the use of a heparan sulfate-binding PA gel (*29*). PAs have been specifically engineered for nerve tissue regeneration as well. In one PA design the laminin-derived IKVAV sequence was included, and neural progenitor cells cultured on these PAs were found to be even more neuron-like than those cultured on laminin-coated substrates, putatively due to the extremely high density of IKVAV ligands presented on the surface of these PA nanofibers (*30*). An *in vivo* study by Angeloni et al. used a PA gel to deliver Sonic Hedgehog (SHH) protein to crushed cavernous nerves of rat penises and showed decreased apoptosis of cells surrounding crushed nerve, a decrease in myelin degradation, and an increase in erectile function by 58% relative to a BSA control (*31*). Bone tissue engineering with PAs has also been explored, including *in vitro* and *in vivo* studies that showed that PAs can induce osteogenesis in human mesenchymal stem cells (*32*) and greatly enhance the healing of critical size femoral defects when delivered with

nanoparticulate hydroxyapatite mineral (*33*). Drug delivery applications of PAs are numerous and include gel-based strategies to deliver the cancer drugs like cisplatin (*34*) and camptothecin (*35*) as well as anti-inflammatory drugs (*36*) and nucleic acids (*37*). Like Zhang, Stupp created a company to produce and market peptide amphiphiles. The company, Nanotope, Inc., has already completed preclinical trials for a PA specifically designed to enhance cartilage regeneration and is presumably preparing to carry out human clinical trials (*38*, *39*).

2.2.3 Aromatic N-terminal protected peptide gelators

One group of researchers studying molecular self assembly found in 2003 that a diphenylalanine (FF) motif found in the β-amyloid protein (implicated in Alzheimer's disease and dementia) sequence can self assemble into supramolecular nanotubes when water is used to dilute a solution of FF in a waster-miscible organic solvent (*40*). The authors hypothesized that aromatic stacking of phenylalanine side chains was responsible for driving self-assembly and nanotube formation when water was introduced to the system. Around the same time of this discovery, another research group found that *various* dipeptides composed of alanine, glycine, serine, and threonine residues conjugated to a fluorenylmethoxycarbonyl (Fmoc) protecting group would self-assemble into supramolecular structures that form hydrogels in response to an acidic pH trigger (*41*). Coming full circle, both Mahler et al. (*42*) and Jayawarna et al. (*43*) independently discovered that *Fmoc-protected* diphenylalanine (Fmoc-FF) would also form a fairly rigid gel. Also widely reported as having self-assembly and gelation capabilities are naphthalene-dipeptides (*44*, *45*), as well as some unique nucleic acid base-conjugated peptides (*46*, *47*) and dipeptides with nonsteroidal anti-inflammatory drugs as aromatic

N-protecting groups (*48–50*). Fmoc-peptides seem to be the most widely reported, however, presumably due to the ubiquitous use of the Fmoc-protected amino acids in solid-phase peptide synthesis.

The self-assembly of these small molecules is poorly understood. The main forces driving assembly are thought to be hydrophobic and π-π interactions of the Fmoc groups and hydrogen bonding through β-sheet like interactions between adjacent dipeptides (**Figure 2.4**) (*51*). The efficiency of this hydrogen bonding must be very sensitive to the chemical environment or steric hindrances created by the side chain residues, as evidenced by the fact that not all Fmoc-dipeptides can form gels (*52*, *53*). A structure has been proposed for the nanofiber assembly of Fmoc-FF (*54*), but a problem with the model is that it considers too heavily the influence of aromatic interactions due to phenylalanine's side chain group and is therefore probably not generalizable to other Fmoc-dipeptide hydrogelators. Indeed, Chapter 3 of this dissertation concerns experimental and computational work undertaken by our group to better elucidate the role of amide-amide hydrogen bonding in stabilizing an Fmoc-dipeptide supramolecular structure to understand how perturbations to the peptide backbone chemistry might disrupt self-assembly. In biomedical applications where ligand presentation may be of interest, structural knowledge of Fmoc-peptide assemblies will likely be necessary. At the current time, however, researchers have already begun investigation into the feasibility of these materials for cell proliferation and viability and to a lesser extent, drug delivery.

Because Fmoc-peptide materials have only been described fairly recently, experiments using these materials as cell promoting substrates have been mostly *in vitro* and focused on testing for cell viability, proliferation and spreading. In the first paper describing Fmoc-FF self-assembly, Jayawarna et al. showed that bovine chondrocytes displayed good viability and proliferation in Fmoc-FF gels co-assembled with a lysine-

presenting Fmoc-dipeptide (*43*). More recent studies have focused on RGD-presenting systems. In one study, a co-assembly of Fmoc-FF/Fmoc-RGD increased human dermal fibroblast (HDF) spreading and proliferation relative to an Fmoc-RGE containing co-assembly (*55*). Another group assessed the viability of Chinese hamster ovary cells in gels composed of Fmoc-FRGD molecules and found that viability was decreased to below 60% of the day one viability by the third day of culture (*56*). More recent studies have refuted these results, demonstrating good cell attachment and viability on RGD-containing Fmoc-peptides versus the GRD-containing isomers (*57*, *58*). Very recently, Zhou et al. examined the deposition of natural extracellular matrix components by dermal fibroblasts within Fmoc-FF/Fmoc-RGD co-assembled gels and found increased secretion of fibronectin and collagen type I relative to Fmoc-RGE containing gels (*59*).

Only a few reports of *in vivo* application of N-protected peptides have been published. Yang et al. demonstrated in a rat model the subcutaneous and intraperitoneal phosphatase-triggered gelation of a naphthalene-peptide containing a phosphorylated tyrosine residue, but beyond showing that naturally secreted phosphatases are able to cause gelation *in situ*, the authors did not examine a specific application of the material (*60*). The same group investigated an *in vivo* drug delivery application of a similar naphthalene-dipeptide, showing that release of a radiolabeled drug (as monitored by single photon emission computed tomography) from subcutaneously injected gels was slower than bolus injection of the drug (*61*). A different lab evaluated the ability of a laminin-labeled Fmoc-trileucine peptide gel to be retained *in vivo* in a laminin-deficient dystrophic zebrafish model, and while they did not demonstrate any functional improvement in muscle function, they showed through fluorescent histology and TEM that nanofibers of the injected gel were retained in the tissue over four days post-implantation (*62*).

Rein Ulijn, one of the most prominent researchers in the field of Fmoc-peptide self assembly, co-founded a company in Scotland called Biogelx for the production and commercialization of Fmoc-peptide based gel systems used to support cells in 3D cell culture (*63*). The exact formulation of the product is proprietary, and the company's website lists possible applications for human mesenchymal stem cells, therapy resistant cancer cells, HDFs, and osteosarcoma cell lines. Only a cursory mention to *in vivo* or therapeutic applications is given, suggesting perhaps that Fmoc-peptides' inherent limitations may restrict their usefulness to *in vitro* cell culture.

2.2.4 Important limitations of peptide-based self-assembling materials

Despite the advantages of peptide-based materials, there are several important disadvantages. RAD16 oligopeptides do not have any well-understood biological action; indeed, the only clinical applications for PuraMatrix™ currently under study for FDA approval are as a dental bone void filler and as a hemostatic material (*64*). Neither application necessitates that the material be cell-instructive, and since these peptides self-assemble based on sequence-mediated self-complementarity, engineering bioactivity into them may disrupt their self-assembly capability. Stupp's peptide amphiphiles and aromatic N-protected di- and tri- peptides may offer more robust self-assembly capability, but to our knowledge the *in vitro* and long-term *in vivo* degradation of any such materials have not been characterized and/or published. Unless these materials degrade within the course of several weeks to months in the body, long-term inflammation could result and limit their clinical application. Because of these limitations, we believe peptide-mimicking materials engineered to have controllable

degradability and peptide-like bioactivity may represent a more favorable alternative to peptides for clinical applications.

2.3 PEPTIDOMIMETICS

Peptidomimetic-based hydrogel biomaterials have not been widely explored but may have properties advantageous for biomedical applications, including biocompatibility and tailored bioactivity. Peptidomimetics are synthetic molecules that attempt to mimic the functional group presentation and/or conformation of native peptides (*65*). Peptidomimetics are often designed to be scaffold molecules that retain a similar presentation of side chain groups as peptides, but are less susceptible to denaturation and unfolding. In many cases, the chemical backbone of the molecule is modified to resist degradation and retain secondary folding characteristics, as many peptidomimetics are developed as therapeutic drugs for oral delivery and/or requiring a long residence time in the body (*66*). Depending on the application, peptidomimetics may also be engineered to have greatly enhanced binding affinity for a protein target or increased uptake efficiency and bioavailability relative to a native peptide.

In general, peptidomimetics can be classified in one of three main categories: mimics with peptide main-chains only, mimics with amino acid side-chain groups only, and mimics with both peptide main-chains and amino acid side chains (**Figure 2.5 A**). The first category is considered to be largely uninteresting due to the importance of side chain chemistry in mediating binding interactions of peptides and proteins (*67*). The second category is composed of peptidomimetics designed with little regard to the native peptide backbone chemistry, except for preserving atomic distances between side chains relevant for their binding function. These molecules can be either conformationally rigid

"minimalist" mimics that are designed in an attempt to bind tightly and specifically to a known structure within a well-characterized protein, or more flexible "universalist" mimics designed to interact with protein features in which only sequence and side-chain information, and not specific binding conformation, may be known. The final category includes mimics in which the native peptide backbone is only slightly modified but retains chemical and conformational characteristics of the native peptide backbone. These mimics may best approximate the native conformation and side-chain presentation of a native peptide, but they are often more difficult to synthesize than side-chain-only mimics and therefore less amenable to creating combinatorial libraries used for drug screening (*66*, *67*). Still, backbone-modified peptidomimetics remain useful as potential drugs, as well as for fundamental studies of protein folding, protein structure-function relationships, and peptide-protein interactions (*68*).

Numerous chemistries have been evaluated as amide bond replacements in backbone-modified peptidomimetics. Each is designed to approximate the steric or electronic characteristics of the native amide bond but decrease susceptibility to enzymatic degradation, increase membrane transport and cellular uptake, and enhance protein binding (*66*). A few of the various chemical groups that have been evaluated as amide bond substitutes are summarized in **Figure 2.5 B** (*66*). Peptidomimetics with these modifications have shown promise as HIV protease inhibitors (*69*, *70*), thrombin inhibitors (*71*), opioid agonists (*72*), and as neurotensin analogues (*73*) among other applications. In particular, α-aza-amino acid-containing mimics (termed "azapeptides") have proven to be important industrially and clinically as effective protease inhibitors (*66*); Atazanavir, one of the most effective FDA-approved HIV antiretrovirals to date is an azapeptide and is currently on the World Health Organization's list of Essential Medicines (*74*, *75*).

While peptidomimetics have found utility in the drug and therapeutic space, there exist few examples of peptidomimetics as the basis for self-assembling, potentially bioactive biomaterials. Peptoids, constitutional isomers of peptides, have been demonstrated to be capable of self-assembly leading to gelation (*76*), but these materials are more resistant to protease degradation than peptide-based materials and are therefore not suitable for most tissue engineering applications. Degradable, ester-containing peptidomimetics known as "depsipeptides," however, may be promising candidates for *in vivo* biomaterials.

2.4 DEPSIPEPTIDES

One class of peptidomimetics comprises the depsipeptides, peptide analogues containing ester substitutions in the backbone. Because side chain chemistry often dictates peptide-protein interactions and the ester bond is rotationally and electronically similar to the amide bond (*77*, *78*), depsipeptides may bind proteins at affinities similar to peptides and in some cases may be functionally indistinct from their peptide analogues. However, given the hydrolytic sensitivity of esters relative to amide bonds (*79*), depsipeptides are unlike many other synthetic peptidomimetics in that they are likely substantially *more* susceptible to degradation than peptides in the absence of proteolytic enzymes. This section introduces depsipeptides and discusses their natural origin, synthesis, and applications of depsipeptides in studying the role of hydrogen bonding in protein folding and peptide-protein interactions.

2.4.1 Depsipeptides in nature

In contrast to most peptidomimetics, depsipeptides can be found in nature. Marine sponges, bacteria, fungi, and actinomycetes produce many of the natural depsipeptides that have been described, and most are cyclic molecules with antimicrobial and/or anti-tumor properties (*80–82*). A recent Nature article that received considerable media attention described the discovery of a new depsipeptide antibiotic produced by a previously uncultured bacterial species that was cultivated *in situ* in soil with the use of a multichannel culture device called an iChip (*83*). The depsipeptide, named teixobactin, displayed excellent antimicrobial activity against methicillin-resistant *Staphylococcus aureus* bacteria (MRSA), one of the organisms responsible for hospital-acquired infections, and no bacterial strain tested developed resistance to the depsipeptide over a month of serial passaging. The antibiotic activity of many depsipeptides is achieved through disruption of cell wall peptidoglycan biosynthesis during bacterial replication (*82*, *83*).

Anti-tumor depsipeptides exert biological action through protein binding. One small cyclic depsipeptide "FK228" produced by *Chromobacterium violaceum* was discovered in the early 1990s and was found to be a potent histone deacetylase inhibitor and inhibitor of mitogen-activated protein kinases, and therefore induces apoptosis in various cancer cell types (*84*). This molecule, now with the commercial name Romidepsin, was fast tracked for approval by the FDA in 2004, underwent a phase II clinical trial, and approved as a chemotherapeutic drug for use in treating cutaneous T-cell lymphoma (CTCL) in 2009 (*85*, *86*). Another notable depsipeptide, cryptophycin-1, is synthesized by certain cyanobacteria and inhibits tubulin assembly into microtubules (*87*). Cryptophycin-1 was shown to be effective against multiple drug-resistant solid

tumors in mice, and several cryptophycins and their analogues have undergone clinical trials for cancer treatments (*88–91*).

2.4.2 Synthesis of depsipeptides

In the chemical synthesis of depsipeptides, ester inclusions are created by incorporating α-hydroxy acids that have side chain chemical groups analogous to those in proteinogenic amino acids. Several α-hydroxy acid analogues of amino acids are naturally occurring and/or commercially available, including analogues of glycine, alanine, phenylalanine, valine, leucine, and isoleucine. Additionally, most tert-Butyloxycarbonyl- (Boc-) protected amino acids with appropriately protected reactive side chain groups can be converted into their α-hydroxy analogues by a chemical process known as diaotization (*92*). The inclusion of α-hydroxy acids is typically achieved through modified solid-phase peptide synthesis techniques involving direct coupling of a hydroxyl-unprotected α-hydroxy acid to a growing peptide chain by conventional amide coupling chemistries, followed by esterification of the subsequent amino acid using dimethylaminopyridine (DMAP)-catalyzed carbodiimide coupling (*93*, *94*).

Other approaches, including one developed by our group, have sought to synthesize N-protected depsipeptide units containing one amino acid coupled via ester bond to one α-hydroxy acid, leaving a free terminal carboxylic acid group that can be coupled directly on solid phase with normal amide coupling chemistry (*95–97*). The advantages of this approach are avoidance of low crude purity due to inefficient α-hydroxy acid coupling or esterification and potential for automated solid-phase synthesis of long depsipeptides using commercially available automated synthesizer instruments.

All the depsipeptides described later in this dissertation were all synthesized using solution-coupled depsipeptide units as substituents.

Long depsipeptides can also be efficiently synthesized through recombinant techniques in which a stop-codon-specific tRNA is pre-charged with the desired α-hydroxy acid of interest (*98*, *99*). Given the complications of pre-charging tRNAs with α-hydroxy acids, this method has found utility mostly in synthesizing long peptides and proteins with one or only a few ester-substitutions in order to study the structural role of backbone hydrogen bonding in the context of a large protein (*100*, *101*).

2.4.3 Depsipeptide self-assembly

Despite the decreased ability of their ester residues to participate in hydrogen bonding, several depsipeptides have been shown to self-assemble into nanostructures that in some cases form hydrogels (*96*, *102–104*). That depsipeptides are capable of supramolecular self-assembly was discovered serendipitously; Elgersma et al. designed amylin (20-29) derivatives with ester substitutions at three different positions as "β-breaker" molecules that would inhibit amyloid fiber formation by disrupting inter-chain hydrogen bonding, but found that the depsipeptide alone formed helical nanostructures that caused solution gelation (*96*). In an interesting follow up study, the same researchers synthesized the amylin derivative depsipeptides with either all L- or all D-form amino and α-hydroxy acids and found that D-form depsipeptides formed right-handed helical nanostructures, whereas L-form depsipeptides formed left-handed helices (**Figure 2.6 A**) (*102*). Intriguingly, when the two were mixed in equimolar quantities, no helices were observed in TEM; only flat ribbon structures formed, suggesting that the right- and left-

handed forms of the depsipeptides interact closely and do not self-sort during the self-assembly process.

A more recent study examined the self-assembly of single-ester depsipeptides as potentially useful degradable biomaterials. Tian et al. showed that 11-residue depsipeptides formed hydrogels when dispersed in water, and the degradation rate of these hydrogels was somewhat controllable based on the steric bulk of the side-chain group on the ester-conferring α-hydroxy acid (**Figure 2.6 B**) (*103*). These depsipeptides were also unexpectedly stiffer than the analogous peptide, but softened over time as ester bond hydrolysis led to bulk degradation and disassembly. Murine mesenchymal stem cells cultured in the stiffer depsipeptide gels spread to a greater extent than in the peptide gels, and cell proliferation was greater in depsipeptide gels over 5 days as the gels degraded.

While this study effectively highlights the potential of self-assembling depsipeptide-based hydrogel materials for use as biomaterials, the design approach is derivative; the material is a single-ester-containing analogue of a known hydrogelator. In an attempt to design depsipeptide-based materials with a bottom up approach based on exploiting the properties of hydrophobicity and charge-charge interactions, our group developed a small library of Fmoc-protected, charged depsipeptides to further understand the more fundamental requirements for depsipeptide self-assembly (*104*). We found that depsipeptide self-assembly into nanofiber structures (**Figure 2.6 C**) and the rate of subsequent gelation were highly dependent on side chain sequence, charge complementarity, and solution salt concentration. We also found that increasing the overall hydrophobicity of the molecule by adding a C-terminal phenylalanine residue dramatically increased the rate of self-assembly and thus shortened the time to gelation. The degradation rate of the depsipeptides was also highly dependent on the state of the

assembly (sol vs. gel, controlled by concentration) and the concentration of salts, with salt-containing solutions causing faster degradation. With this knowledge, we gained a better understanding of the design requirements for controlling self-assembly and rate of degradation, factors that are important for application-driven design of depsipeptide-based materials.

2.4.4 Depsipeptides for understanding protein folding

As with other peptidomimetics, depsipeptides have been widely utilized as tools for understanding protein-folding processes. Producing depsipeptides by introducing specific amide-to-ester mutations into peptides and proteins of interest has long been a strategy for understanding the role of specific amide bonds in determining the secondary structure features of these peptides and proteins.

The role of specific backbone hydrogen bonding interactions in stabilizing α-helices has been studied through site-specific replacement of amide bonds with esters in peptides. The stability of an α-helix within the T4 lysozyme protein was studied by recombinant synthesis of lysozyme mutants with α-hydroxy acids incorporated at three sites within the helix region (**Figure 2.7**) (*98*). The hydroxy acids were introduced by means of leucic- or isoleucic-acid-acylated tRNAs encoded by an "amber" suppressor sequence. The mutant proteins were cleaved at the ester site under alkaline conditions, whereas wild type (WT) proteins remained intact. Mutant lysozymes also had lower melting temperatures and positive $\Delta\Delta G°$ of folding relative to the WT proteins, indicating a decreased stability of the helix containing the ester mutation in the folded state. Interestingly, all mutant proteins retained catalytic activity suggesting that native-like conformation was achieved even in less stable ester-containing mutants.

In a more dramatic example of a peptide's ability to retain secondary folding with ester modifications, Beligere and Dawson (*94*) synthesized chymotrypsin inhibitor 2 analogues with 4 ester modifications in an α-helix region of the polypeptide. These replacements had the effect of knocking out half of the intra-chain hydrogen bonding interactions in the helix, and indeed the authors demonstrated through monitoring fluorescence of tryptophan residues during guanidine denaturation that the 4-ester mutant was less stable than the wild type peptide. Despite the decreased stability, the 4-ester mutant retained the ability to inhibit subtilisin at a K_I of 2.1 nM, on the same order of magnitude as the wild type peptide's K_I of 0.25 nM, suggesting that the depsipeptide mutant was folded in a near-native state.

Hydrogen bonding's role in β-sheet stability has also been studied through amide-to-ester mutations. In one example, researchers synthesized several amide-to-ester variants of a 34-residue peptide (specifically, the PIN WW domain) to understand the contributions of specific hydrogen bonding patterns along the peptide backbone to β-sheet formation (*105*). Through systematic amide-to-ester mutations, they were able to show that the most energetically important residues for maintaining stability of secondary structures were those that interacted via backbone-backbone hydrogen bonds formed within the hydrophobic core of the peptide, rather than near the strand termini. Therefore, the importance of backbone hydrogen bonding in this case was considered not to be absolute but rather highly context-dependent.

2.4.5 Depsipeptide-protein binding

In one of the very few examples of systematic studies to ascertain the importance of hydrogen bonding on peptide-protein interactions, PDZ protein domains (protein

domains known to facilitate protein-protein interactions for cellular signaling) (*106*) or their complementary peptide ligands (*107*) were synthesized with amide-to-ester mutations near the known interaction site (**Figure 2.8, top**). Using this approach, the authors were able to determine the relative effect of individual amide bonds on the affinity of the peptide for the PDZ protein domain and found that ester inclusions generally decreased the affinity of the interaction relative to the wild type PDZ/ligand pair (**Figure 2.8, bottom**). However, the reduction in affinity was highly context-dependent; amide-to-ester mutations further away from the depsipeptide C-terminus had far less of a detrimental impact on PDZ binding than mutations nearer to the C-terminus. Thus, it may not be appropriate to generalize the importance of backbone hydrogen bonding to all peptide-protein interactions. Additionally, no functional outcome was assessed in these studies, i.e. no experiments involving live cells to determine the functional consequences of the amide-to-ester mutations were performed.

2.5 RESEARCH GOALS

The overall aim of work described herein is to develop a *platform* for new self-assembling materials with properties optimal for cardiac tissue engineering. Depsipeptides' potential for self-assembly, degradability, and bioactivity make them theoretically well suited as the basis for synthetic hydrogel biomaterials; however, these characteristics have not been extensively studied, nor have they been assessed within a biomaterials design context. Furthermore, the ability of engineered depsipeptides to interact specifically with proteins has not been previously evaluated in cell surface proteins relevant to cell adhesion or cell-biomaterial interactions. Therefore, the main goals of this project are: 1) to demonstrate in a simple system that short, N-protected

depsipeptide analogues of known self-assembling peptides are similarly able to self-assemble in aqueous solution and form hydrogels, and 2) to investigate both the self-assembly and integrin-binding properties of the depsipeptide analogue of an RGD peptide.

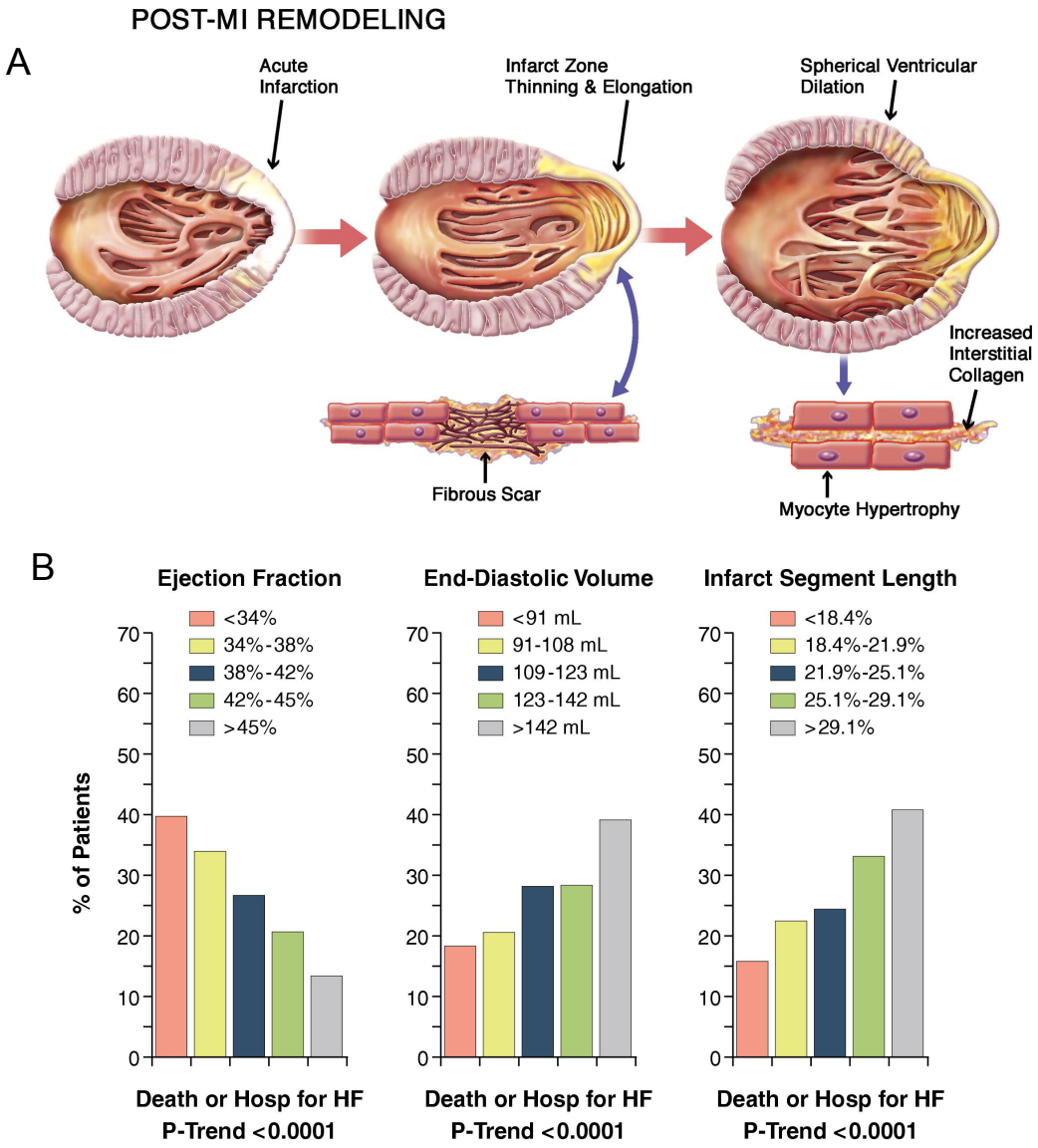

Figure 2.1 Tissue remodeling post-myocardial infarction leads to fibrous scar formation (A) and rates of death or hospitalization are significantly increased in patients with lowered ejection fraction, greater end-diastolic volume, and greater infarct segment length post-MI (B). (Adapted with permission from refs. 4 and 5)

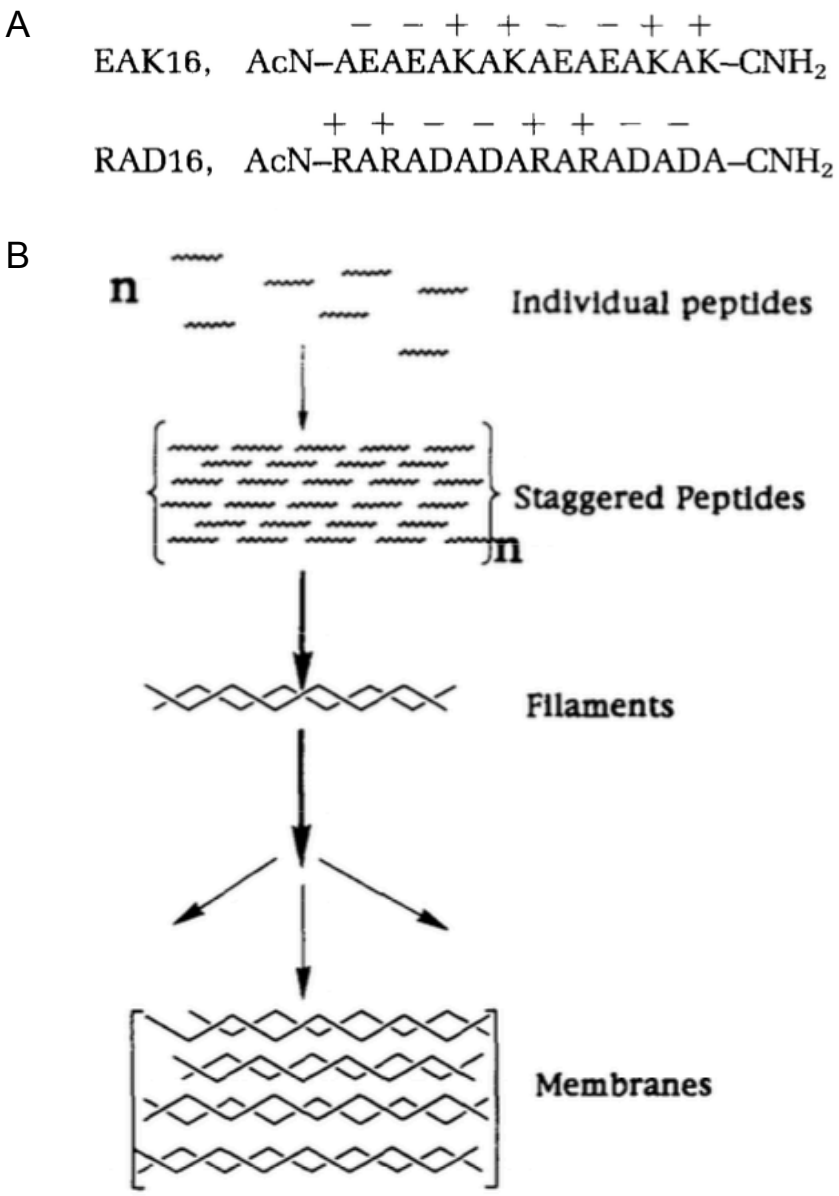

Figure 2.2 Self-complementary charged oligopeptides (A) self-assemble in a process that forms nanofibrillar filaments that organize into membranous sheets (B). (Adapted with permission from from ref. 11)

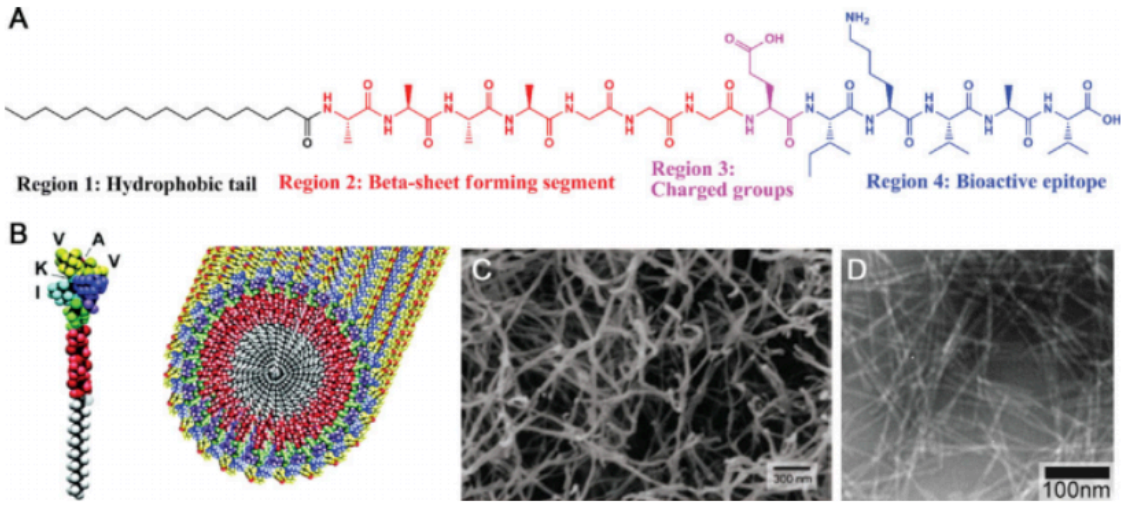

Figure 2.3 Peptide amphiphile structure (A) and proposed self-assembled fibril structure (B). Scanning electron (C) and transmission electron (D) micrographs show the nanofibrillar nature of the hydrogels that result from self-assembly. (Adapted with permission from ref. 25)

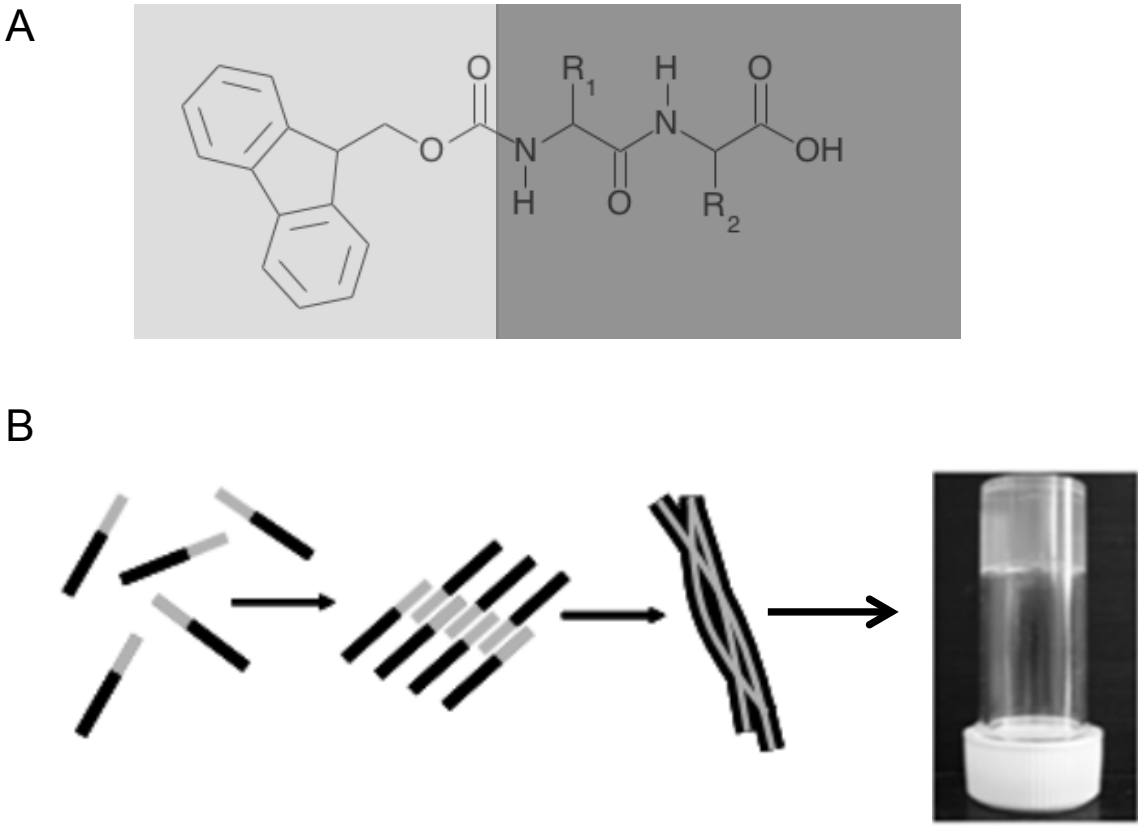

Figure 2.4 General structure of an Fmoc-dipeptide (A), with hydrophobic region shaded in light gray and peptide (hydrophilic) region in dark gray. Mode of self-assembly (B) involving interactions among aromatic N-protecting groups leading to fibril formation, ultimately causing gelation in aqueous solution. (Adapted with permission from refs. 43 and 52)

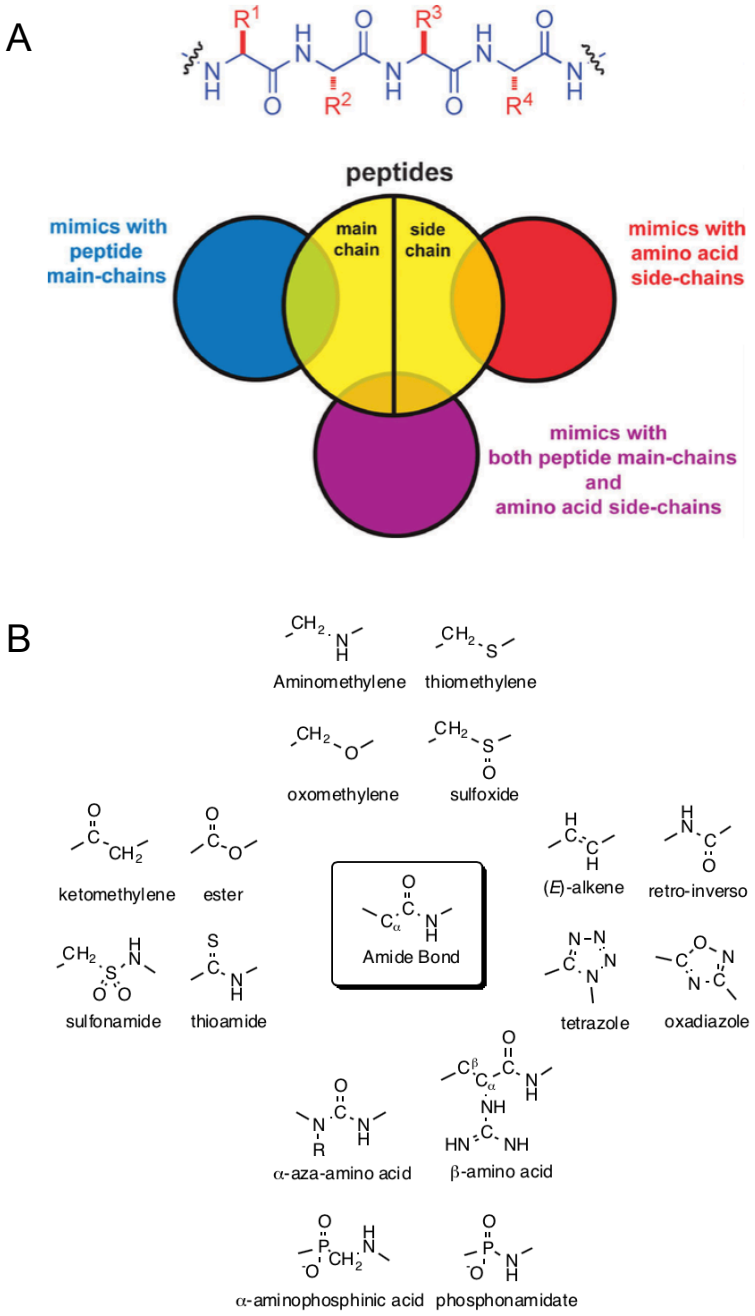

Figure 2.5 General classes of peptidomimetics (A) and common peptide backbone replacements (B). (Adapted with permission from refs. 66 and 67)

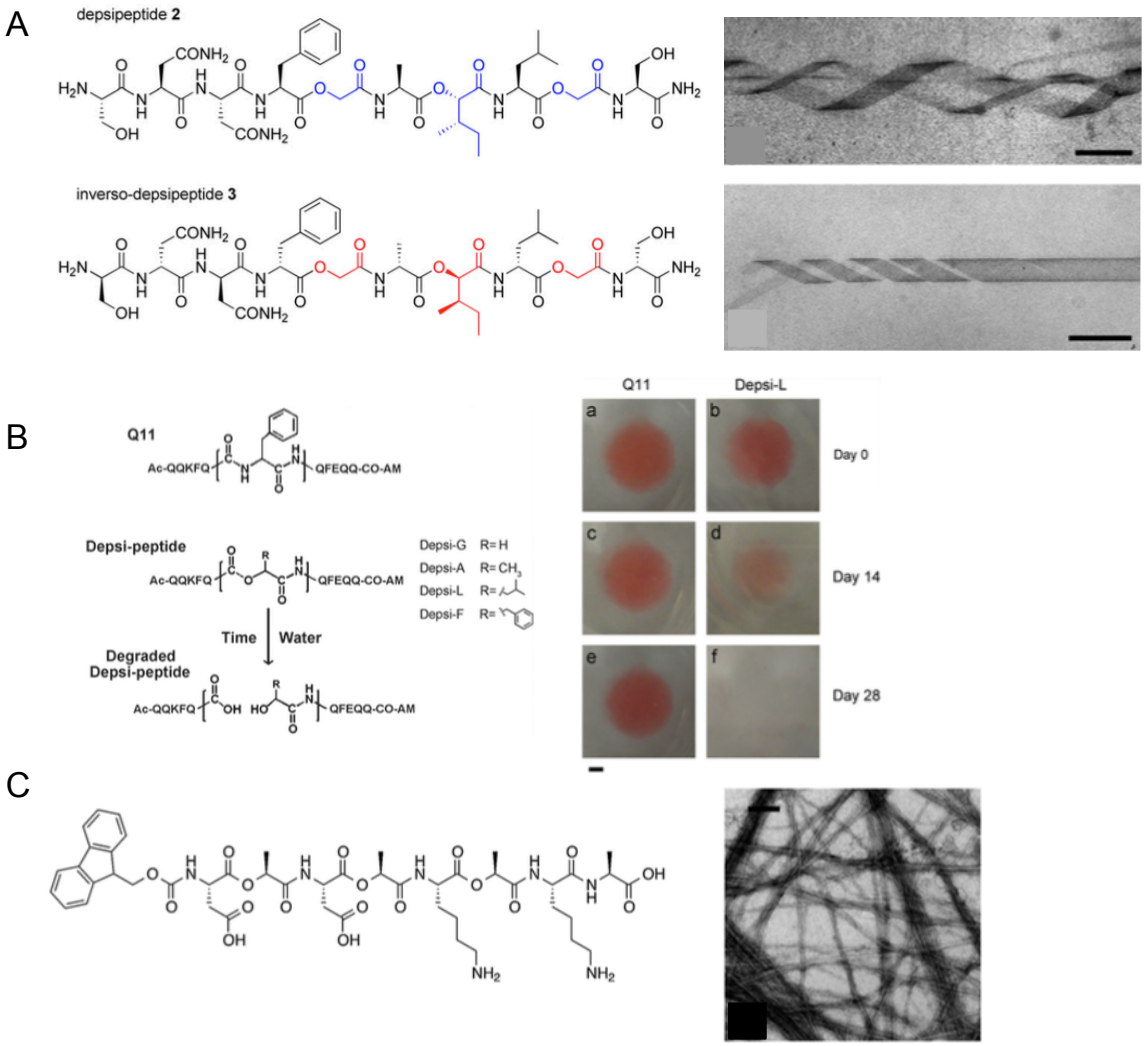

Figure 2.6 Depsipeptides have been previously demonstrated to self-assemble into left and right hand helical structures (A), and have been shown to be non-enzymatically degradable relative to peptide analogues (B). Fmoc-protected self-complementary depsipeptides are also capable of self-assembly into fibrils that form hydrogels (C). (Adapted with permission from refs. 102-104)

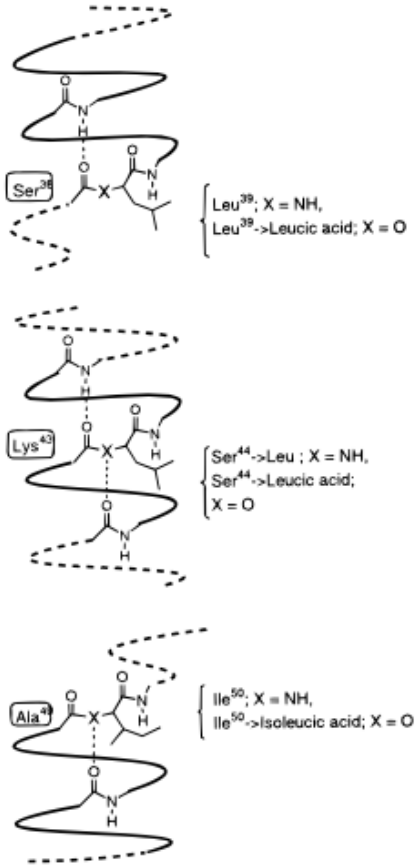

Table 1: Relative Thermodynamic Stabilities of the T4 Lysozyme Mutants Containing Amide and Ester Backbone Linkages[a]

protein	T_M (°C)	ΔT_M (°C)	$\Delta\Delta G°$ (kcal/mol)
wt (Leu^{39})	45.19 ± 0.04	–	–
Leu^{39} → leucic acid	41.95 ± 0.06	-3.24 ± 0.10	0.89 ± 0.03
Ser^{44} → Leu	47.19 ± 0.19	–	–
Ser^{44} → leucic acid	40.87 ± 0.10	-6.31 ± 0.30	1.73 ± 0.08
wt (Ile^{50})	45.19 ± 0.04	–	–
Ile^{50} → isoleucic acid	42.55 ± 0.10	-2.64 ± 0.10	0.72 ± 0.03

[a]The ΔT_M and $\Delta\Delta G°$ reported refer to the difference in stability between the ester- and the amide-containing proteins. A positive $\Delta\Delta G°$ indicates that the wt protein is more stable than the corresponding ester-containing protein.

Figure 2.7 Systematic amide-to-ester mutations in proteins enable quantification of the contribution of specific backbone hydrogen bonding modes to α-helix stability. In this example, T4 lysozyme mutants (left) are made with side-chain analogous α-hydroxy acids. The table at right shows the relative change in melting temperature and difference in folding free energy change between mutated and wild type proteins. A marked decrease in melting temperature and increase in free energy change of folding were observed with site-specific amide-to-ester mutations, but overall protein function was retained. (Adapted with permission from ref. 98)

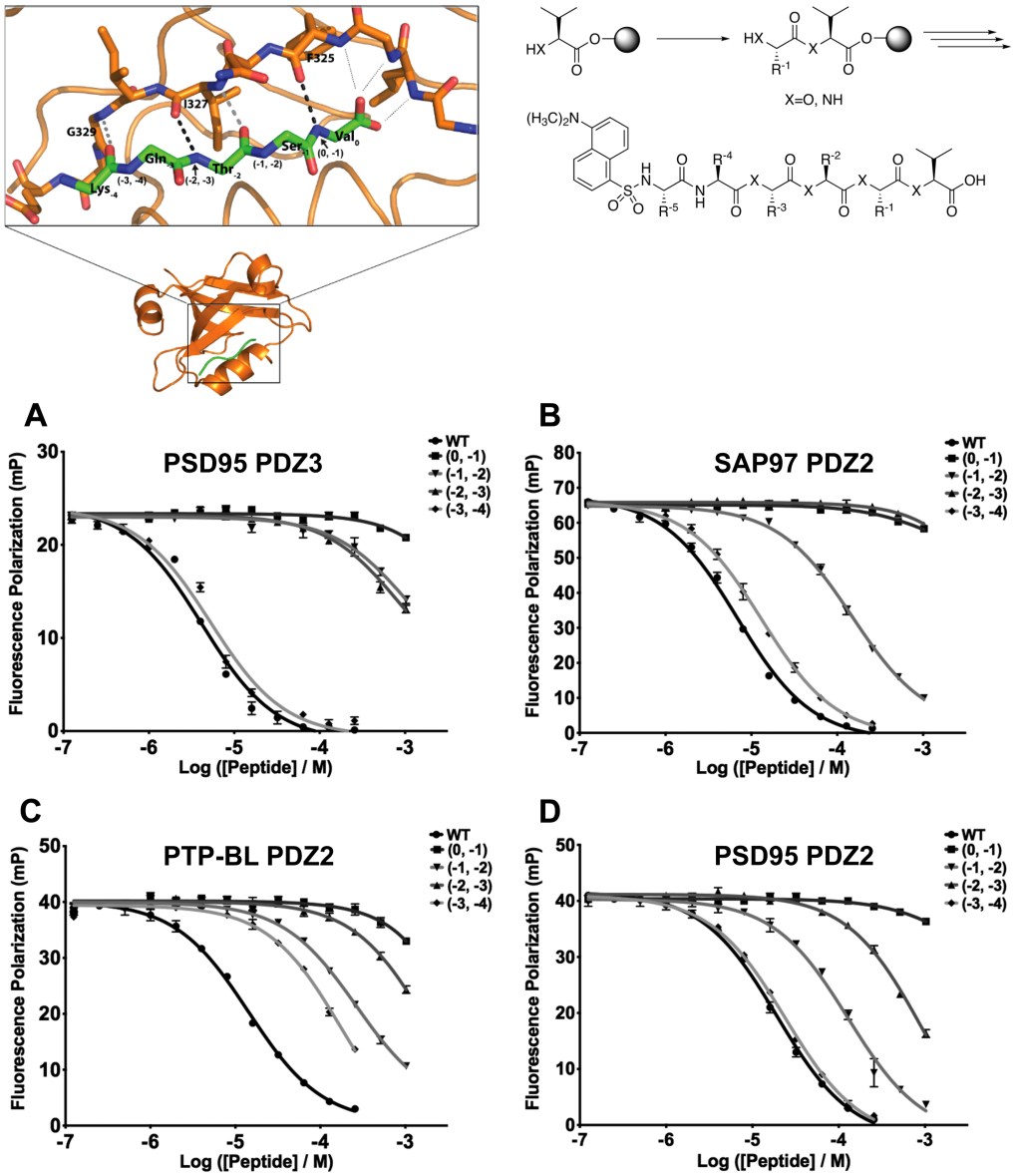

Figure 2.8 Structure of PSD-95 PDZ3 domain in complex with wild type peptide (top left), and general synthesis for dansyl-labeled depsipeptides (top right). Bottom: fluorescence polarization assays of displacement of Cy5-labeled peptide by various depsipeptides indicate that competitive binding by depsipeptides is in all cases lower than the wild type peptide, but that the efficiency of displacement is highly dependent on the position of the ester bond (denoted by (0,-1), (-1,-2), etc.) within the depsipeptide. Esters placed near the C-terminus of the depsipeptide decreased binding affinity most. (Adapted with permission from ref. 107)

2.6 REFERENCES

1. A. Alwan, World Health Organization, *Global status report on noncommunicable diseases 2010*. (World Health Organization, Geneva, Switzerland, 2011).
2. FASTSTATS - Heart Disease (2012), (available at http://www.cdc.gov/nchs/fastats/heart.htm).
3. K. L. Christman, R. J. Lee, Biomaterials for the Treatment of Myocardial Infarction. *Journal of the American College of Cardiology*. **48**, 907–913 (2006).
4. M. A. Konstam, D. G. Kramer, A. R. Patel, M. S. Maron, J. E. Udelson, Left Ventricular Remodeling in Heart Failure: Current Concepts in Clinical Significance and Assessment. *J Am Coll Cardiol Img*. **4**, 98–108 (2011).
5. S. D. Solomon *et al*., Changes in Ventricular Size and Function in Patients Treated With Valsartan, Captopril, or Both After Myocardial Infarction. *Circulation*. **111**, 3411–3419 (2005).
6. K. L. Christman *et al*., Injectable Fibrin Scaffold Improves Cell Transplant Survival, Reduces Infarct Expansion, and Induces Neovasculature Formation in Ischemic Myocardium. *J Am Coll Cardiol*. **44**, 654–660 (2004).
7. K. L. Christman, H. H. Fok, R. E. Sievers, Q. Fang, R. J. Lee, Fibrin Glue Alone and Skeletal Myoblasts in a Fibrin Scaffold Preserve Cardiac Function after Myocardial Infarction. *Tissue Engineering*. **10**, 403–409 (2004).
8. J. M. Singelyn *et al*., Naturally derived myocardial matrix as an injectable scaffold for cardiac tissue engineering. *Biomaterials*. **30**, 5409–5416 (2009).
9. L. A. Estroff, A. D. Hamilton, Water Gelation by Small Organic Molecules. *Chem. Rev*. **104**, 1201–1218 (2004).
10. S. Zhang, T. Holmes, C. Lockshin, A. Rich, Spontaneous assembly of a self-complementary oligopeptide to form a stable macroscopic membrane. *Proceedings of the National Academy of Sciences*. **90**, 3334 –3338 (1993).
11. S. Zhang *et al*., Self-complementary oligopeptide matrices support mammalian cell attachment. *Biomaterials*. **16**, 1385–1393 (1995).
12. D. A. Narmoneva *et al*., Self-assembling short oligopeptides and the promotion of angiogenesis. *Biomaterials*. **26**, 4837–4846 (2005).
13. M. E. Davis *et al*., Injectable Self-Assembling Peptide Nanofibers Create Intramyocardial Microenvironments for Endothelial Cells. *Circulation*. **111**, 442 – 450 (2005).
14. T. C. Holmes *et al*., Extensive neurite outgrowth and active synapse formation on self-assembling peptide scaffolds. *Proceedings of the National Academy of Sciences*. **97**, 6728 –6733 (2000).

15. F. Gelain, D. Bottai, A. Vescovi, S. Zhang, Designer Self-Assembling Peptide Nanofiber Scaffolds for Adult Mouse Neural Stem Cell 3-Dimensional Cultures. *PLoS ONE*. **1**, e119 (2006).

16. C. E. Semino, J. Kasahara, Y. Hayashi, S. Zhang, Entrapment of Migrating Hippocampal Neural Cells in Three-Dimensional Peptide Nanofiber Scaffold. *Tissue Engineering*. **10**, 643–655 (2004).

17. A. Schneider, J. A. Garlick, C. Egles, Self-Assembling Peptide Nanofiber Scaffolds Accelerate Wound Healing. *PLoS ONE*. **3**, e1410 (2008).

18. Y. Nagai, L. D. Unsworth, S. Koutsopoulos, S. Zhang, Slow release of molecules in self-assembling peptide nanofiber scaffold. *Journal of Controlled Release*. **115**, 18–25 (2006).

19. S. Koutsopoulos, L. D. Unsworth, Y. Nagai, S. Zhang, Controlled release of functional proteins through designer self-assembling peptide nanofiber hydrogel scaffold. *Proceedings of the National Academy of Sciences*. **106**, 4623 –4628 (2009).

20. F. Gelain, L. D. Unsworth, S. Zhang, Slow and sustained release of active cytokines from self-assembling peptide scaffolds. *Journal of Controlled Release*. **145**, 231–239 (2010).

21. A. Horii, X. Wang, F. Gelain, S. Zhang, Biological Designer Self-Assembling Peptide Nanofiber Scaffolds Significantly Enhance Osteoblast Proliferation, Differentiation and 3-D Migration. *PLoS ONE*. **2**, e190 (2007).

22. P. W. Kopesky, E. J. Vanderploeg, J. S. Sandy, B. Kurz, A. J. Grodzinsky, Self-Assembling Peptide Hydrogels Modulate In Vitro Chondrogenesis of Bovine Bone Marrow Stromal Cells. *Tissue Engineering Part A*. **16**, 465–477 (2010).

23. PuraMatrix. *3D Matrix Medical Technology-PuraMatrix-Technology* (2014), (available at http://www.puramatrix.com/index.html).

24. J. D. Hartgerink, E. Beniash, S. I. Stupp, Self-Assembly and Mineralization of Peptide-Amphiphile Nanofibers. *Science*. **294**, 1684 –1688 (2001).

25. H. Cui, M. J. Webber, S. I. Stupp, Self-assembly of peptide amphiphiles: From molecules to nanostructures to biomaterials. *Peptide Science*. **94**, 1–18 (2010).

26. K. L. Niece, J. D. Hartgerink, J. J. J. M. Donners, S. I. Stupp, Self-Assembly Combining Two Bioactive Peptide-Amphiphile Molecules into Nanofibers by Electrostatic Attraction. *J. Am. Chem. Soc*. **125**, 7146–7147 (2003).

27. M. A. Greenfield, J. R. Hoffman, M. Olvera de la Cruz, S. I. Stupp, Tunable Mechanics of Peptide Nanofiber Gels. *Langmuir*. **26**, 3641–3647 (2009).

28. M. J. Webber *et al*., Supramolecular nanostructures that mimic VEGF as a strategy for ischemic tissue repair. *Proceedings of the National Academy of Sciences*. **108**, 13438 –13443 (2011).

29. S. Ghanaati *et al*., Dynamic in vivo biocompatibility of angiogenic peptide amphiphile nanofibers. *Biomaterials*. **30**, 6202–6212 (2009).

30. G. A. Silva *et al*., Selective Differentiation of Neural Progenitor Cells by High-Epitope Density Nanofibers. *Science*. **303**, 1352 –1355 (2004).

31. N. L. Angeloni *et al*., Regeneration of the cavernous nerve by Sonic hedgehog using aligned peptide amphiphile nanofibers. *Biomaterials*. **32**, 1091–1101 (2011).

32. J. M. Anderson *et al*., Osteogenic differentiation of human mesenchymal stem cells synergistically enhanced by biomimetic peptide amphiphiles combined with conditioned medium. *Acta Biomaterialia*. **7**, 675–682 (2011).

33. J. M. Anderson *et al*., Biphasic Peptide Amphiphile Nanomatrix Embedded with Hydroxyapatite Nanoparticles for Stimulated Osteoinductive Response. *ACS Nano* (2011), doi:10.1021/nn203247m.

34. J.-K. Kim, J. Anderson, H.-W. Jun, M. A. Repka, S. Jo, Self-Assembling Peptide Amphiphile-Based Nanofiber Gel for Bioresponsive Cisplatin Delivery. *Mol. Pharmaceutics*. **6**, 978–985 (2009).

35. S. Soukasene *et al*., Antitumor Activity of Peptide Amphiphile Nanofiber-Encapsulated Camptothecin. *ACS Nano*. **5**, 9113–9121 (2011).

36. J. B. Matson, S. I. Stupp, Drug release from hydrazone-containing peptide amphiphiles. *Chem. Commun*. **47**, 7962–7964 (2011).

37. S. Bulut *et al*., Slow Release and Delivery of Antisense Oligonucleotide Drug by Self-Assembled Peptide Amphiphile Nanofibers. *Biomacromolecules*. **12**, 3007–3014 (2011).

38. Nanotope, Inc. *Nanotope, Inc*. (2014), (available at http://www.nanotope.com).

39. E. Svoboda, How Samuel Stupp Is Rebuilding Your Body, One Molecule at a Time. *Fast Company*, (available at http://www.fastcompany.com/1715179/how-samuel-stupp-rebuilding-your-body-one-molecule-time).

40. M. Reches, E. Gazit, Casting Metal Nanowires Within Discrete Self-Assembled Peptide Nanotubes. *Science*. **300**, 625 –627 (2003).

41. Y. Zhang, H. Gu, Z. Yang, B. Xu, Supramolecular Hydrogels Respond to Ligand–Receptor Interaction. *J. Am. Chem. Soc*. **125**, 13680–13681 (2003).

42. A. Mahler, M. Reches, M. Rechter, S. Cohen, E. Gazit, Rigid, Self-Assembled Hydrogel Composed of a Modified Aromatic Dipeptide. *Advanced Materials*. **18**, 1365–1370 (2006).

43. V. Jayawarna *et al*., Nanostructured Hydrogels for Three-Dimensional Cell Culture Through Self-Assembly of Fluorenylmethoxycarbonyl–Dipeptides. *Advanced Materials*. **18**, 611–614 (2006).

44. Z. Yang, G. Liang, M. Ma, Y. Gao, B. Xu, Conjugates of naphthalene and dipeptides produce molecular hydrogelators with high efficiency of hydrogelation and superhelical nanofibers. *Journal of Materials Chemistry*. **17**, 850–854 (2007).

45. L. Chen, S. Revel, K. Morris, L. C. Serpell, D. J. Adams, Effect of Molecular Structure on the Properties of Naphthalene–Dipeptide Hydrogelators. *Langmuir*. **26**, 13466–13471 (2010).

46. X. Li *et al*., Supramolecular Nanofibers and Hydrogels of Nucleopeptides. *Angewandte Chemie International Edition*. **50**, 9365–9369 (2011).

47. X. Li, Y. Kuang, B. Xu, "Molecular trinity" for soft nanomaterials: integrating nucleobases, amino acids, and glycosides to construct multifunctional hydrogelators. *Soft Matter*. **8**, 2801–2806 (2012).

48. J. Li *et al*., The conjugation of nonsteroidal anti-inflammatory drugs (NSAID) to small peptides for generating multifunctional supramolecular nanofibers/hydrogels. *Beilstein Journal of Organic Chemistry*. **9**, 908–917 (2013).

49. S. Bhuniya, Y. J. Seo, B. H. Kim, (S)-(+)-Ibuprofen-based hydrogelators: an approach toward anti-inflammatory drug delivery. *Tetrahedron Letters*. **47**, 7153–7156 (2006).

50. J. Li *et al*., d-Amino Acids Boost the Selectivity and Confer Supramolecular Hydrogels of a Nonsteroidal Anti-Inflammatory Drug (NSAID). *J. Am. Chem. Soc*. **135**, 542–545 (2013).

51. D. J. Adams, P. D. Topham, Peptide conjugate hydrogelators. *Soft Matter*. **6**, 3707–3721 (2010).

52. D. J. Adams, Dipeptide and Tripeptide Conjugates as Low-Molecular-Weight Hydrogelators. *Macromolecular Bioscience*. **11**, 160–173 (2011).

53. D. J. Adams, L. M. Mullen, M. Berta, L. Chen, W. J. Frith, Relationship between molecular structure, gelation behaviour and gel properties of Fmoc-dipeptides. *Soft Matter*. **6**, 1971–1980 (2010).

54. A. M. Smith *et al*., Fmoc-Diphenylalanine Self Assembles to a Hydrogel via a Novel Architecture Based on π–π Interlocked β-Sheets. *Advanced Materials*. **20**, 37–41 (2008).

55. M. Zhou *et al*., Self-assembled peptide-based hydrogels as scaffolds for anchorage-dependent cells. *Biomaterials*. **30**, 2523–2530 (2009).

56. R. Orbach *et al*., Self-Assembled Fmoc-Peptides as a Platform for the Formation of Nanostructures and Hydrogels. *Biomacromolecules*. **10**, 2646–2651 (2009).

57. G. Cheng, V. Castelletto, R. R. Jones, C. J. Connon, I. W. Hamley, Hydrogelation of self-assembling RGD-based peptides. *Soft Matter*. **7**, 1326–1333 (2010).

58. V. N. Modepalli *et al*., In vitro response to functionalized self-assembled peptide scaffolds for three-dimensional cell culture. *Biopolymers*. **102**, 197–205 (2014).

59. M. Zhou, R. V. Ulijn, J. E. Gough, Extracellular matrix formation in self-assembled minimalistic bioactive hydrogels based on aromatic peptide amphiphiles. *J Tissue Eng*. **5**, 2041731414531593 (2014).

60. Z. Yang, G. Liang, L. Wang, B. Xu, Using a Kinase/Phosphatase Switch to Regulate a Supramolecular Hydrogel and Forming the Supramolecular Hydrogel in Vivo. *Journal of the American Chemical Society*. **128**, 3038–3043 (2006).

61. G. Liang *et al*., Supramolecular Hydrogel of a d-Amino Acid Dipeptide for Controlled Drug Release in Vivo†. *Langmuir*. **25**, 8419–8422 (2009).

62. R. J. Williams *et al*., The in vivo performance of an enzyme-assisted self-assembled peptide/protein hydrogel. *Biomaterials*. **32**, 5304–5310 (2011).

63. Biogelx - Pushing Forward BIO-INSPIRED Applications. *Biogelx, Ltd*. (2015), (available at http://www.biogelx.com).

64. Clinical Trials. *3D Matrix Medical Technology - Company* (2014), (available at http://www.puramatrix.com/clinical_trials.html).

65. A. Giannis, T. Kolter, Peptidomimetics for Receptor Ligands—Discovery, Development, and Medical Perspectives. *Angewandte Chemie International Edition in English*. **32**, 1244–1267 (1993).

66. J.-M. Ahn, N. A. Boyle, M. T. MacDonald, K. D. Janda, Peptidomimetics and peptide backbone modifications. *Mini Reviews in Medicinal Chemistry*. **2**, 463–473 (2002).

67. E. Ko, J. Liu, K. Burgess, Minimalist and universal peptidomimetics. *Chemical Society Reviews*. **40**, 4411 (2011).

68. W. S. Horne, S. H. Gellman, Foldamers with Heterogeneous Backbones. *Acc. Chem. Res*. **41**, 1399–1408 (2008).

69. B. Munoz, C.-Z. Giam, C.-H. Wong, α-Ketoamide Phe—Pro isostere as a new core structure for the inhibition of HIV protease. *Bioorganic & Medicinal Chemistry*. **2**, 1085–1090 (1994).

70. Y. Kiso, Design and synthesis of substrate-based peptidomimetic human immunodeficiency virus protease inhibitors containing the hydroxymethylcarbonyl isostere. *Biopolymers*. **40**, 235–244 (1996).

71. R. T. Shuman *et al*., Highly selective tripeptide thrombin inhibitors. *Journal of medicinal chemistry*. **36**, 314–319 (1993).

72. N. S. Chandrakumar *et al*., Preparation and opioid activity of analogues of the analgesic dipeptide 2,6-dimethyl-L-tyrosyl-N-(3-phenylpropyl)-D-alaninamide. *J. Med. Chem.* **35**, 223–233 (1992).

73. R. Gonzalez-Muniz *et al*., Ketomethylene and (cyanomethylene) amino pseudopeptide analogues of the C-terminal hexapeptide of neurotensin. *Journal of medicinal chemistry*. **38**, 1015–1021 (1995).

74. C. L. Tiec, A. Barrail, C. Goujard, D. A.-M. Taburet, Clinical Pharmacokinetics and Summary of Efficacy and Tolerability of Atazanavir. *Clin Pharmacokinet*. **44**, 1035–1050 (2012).

75. WHO | WHO Model Lists of Essential Medicines. *World Health Organization*, (available at http://www.who.int/medicines/publications/essentialmedicines/en/).

76. K. H. A. Lau, Peptoids for biomaterials science. *Biomater. Sci.* **2**, 627–633 (2014).

77. K. B. Wiberg, K. E. Laidig, Barriers to rotation adjacent to double bonds. 3. The carbon-oxygen barrier in formic acid, methyl formate, acetic acid, and methyl acetate. The origin of ester and amide resonance. *J. Am. Chem. Soc.* **109**, 5935–5943 (1987).

78. R. T. Ingwall, M. Goodman, Polydepsipeptides. III. Theoretical Conformational Analysis of Randomly Coiling and Ordered Depsipeptide Chains. *Macromolecules*. **7**, 598–605 (1974).

79. W. Mabey, T. Mill, Critical review of hydrolysis of organic compounds in water under environmental conditions. *Journal of Physical and Chemical Reference Data*. **7**, 383–415 (1978).

80. S. Sivanathan, J. Scherkenbeck, Cyclodepsipeptides: A Rich Source of Biologically Active Compounds for Drug Research. *Molecules*. **19**, 12368–12420 (2014).

81. R. E. Moore, Cyclic peptides and depsipeptides from cyanobacteria: A review. *Journal of Industrial Microbiology*. **16**, 134–143 (1996).

82. W. Li, A. Schlecker, D. Ma, Total synthesis of antimicrobial and antitumor cyclic depsipeptides. *Chem. Commun.* **46**, 5403–5420 (2010).

83. L. L. Ling *et al*., A new antibiotic kills pathogens without detectable resistance. *Nature*. **517**, 455–459 (2015).

84. P. A. Konstantinopoulos, G. P. Vandoros, A. G. Papavassiliou, FK228 (depsipeptide): a HDAC inhibitor with pleiotropic antitumor activities. *Cancer Chemotherapy and Pharmacology*. **58**, 711–715 (2006).

85. R. L. Piekarz *et al*., Phase II Multi-Institutional Trial of the Histone Deacetylase Inhibitor Romidepsin As Monotherapy for Patients With Cutaneous T-Cell Lymphoma. *JCO*. **27**, 5410–5417 (2009).

86. FDA Approval for Romidepsin. *National Cancer Institute*, (available at http://www.cancer.gov/cancertopics/druginfo/fda-romidepsin).

87. C. D. Smith, X. Zhang, S. L. Mooberry, G. M. L. Patterson, R. E. Moore, Cryptophycin: A New Antimicrotubule Agent Active against Drug-resistant Cells. *Cancer Res*. **54**, 3779–3784 (1994).

88. D. J. Newman, G. M. Cragg, Marine natural products and related compounds in clinical and advanced preclinical trials. *Journal of natural products*. **67**, 1216–1238 (2004).

89. J. P. Stevenson *et al*., Phase I trial of the cryptophycin analogue LY355703 administered as an intravenous infusion on a day 1 and 8 schedule every 21 days. *Clinical cancer research*. **8**, 2524–2529 (2002).

90. J. Liang *et al*., Cryptophycins-309, 249 and other cryptophycin analogues: preclinical efficacy studies with mouse and human tumors. *Investigational new drugs*. **23**, 213–224 (2005).

91. M. J. Edelman *et al*., Phase 2 study of cryptophycin 52 (LY355703) in patients previously treated with platinum based chemotherapy for advanced non-small cell lung cancer. *Lung Cancer*. **39**, 197–199 (2003).

92. S. Deechongkit, S.-L. You, J. W. Kelly, Synthesis of All Nineteen Appropriately Protected Chiral α-Hydroxy Acid Equivalents of the α-Amino Acids for Boc Solid-Phase Depsi-Peptide Synthesis. *Org. Lett*. **6**, 497–500 (2004).

93. D. J. Gordon, S. C. Meredith, Probing the Role of Backbone Hydrogen Bonding in β-Amyloid Fibrils with Inhibitor Peptides Containing Ester Bonds at Alternate Positions. *Biochemistry*. **42**, 475–485 (2003).

94. G. S. Beligere, P. E. Dawson, Design, Synthesis, and Characterization of 4-Ester CI2, a Model for Backbone Hydrogen Bonding in Protein α-Helices. *Journal of the American Chemical Society*. **122**, 12079–12082 (2000).

95. M. M. Nguyen, N. Ong, L. Suggs, A general solid phase method for the synthesis of depsipeptides. *Organic & Biomolecular Chemistry*. **11**, 1167 (2013).

96. R. C. Elgersma, T. Meijneke, G. Posthuma, D. T. S. Rijkers, R. M. J. Liskamp, Self-Assembly of Amylin(20–29) Amide-Bond Derivatives into Helical Ribbons and Peptide Nanotubes rather than Fibrils. *Chemistry - A European Journal*. **12**, 3714–3725 (2006).

97. O. Kuisle, E. Quiñoá, R. Riguera, A General Methodology for Automated Solid-Phase Synthesis of Depsides and Depsipeptides. Preparation of a Valinomycin Analogue. *J. Org. Chem*. **64**, 8063–8075 (1999).

98. J. T. Koh, V. W. Cornish, P. G. Schultz, An Experimental Approach to Evaluating the Role of Backbone Interactions in Proteins Using Unnatural Amino Acid Mutagenesis†. *Biochemistry*. **36**, 11314–11322 (1997).

99. E. Chapman, J. S. Thorson, P. G. Schultz, Mutational analysis of backbone hydrogen bonds in staphylococcal nuclease. *Journal of the American Chemical Society*. **119**, 7151–7152 (1997).

100. J. Guo, J. Wang, J. C. Anderson, P. G. Schultz, Addition of an α-Hydroxy Acid to the Genetic Code of Bacteria. *Angewandte Chemie International Edition*. **47**, 722–725 (2008).

101. P. M. England, Y. Zhang, D. A. Dougherty, H. A. Lester, Backbone Mutations in Transmembrane Domains of a Ligand-Gated Ion Channel: Implications for the Mechanism of Gating. *Cell*. **96**, 89–98 (1999).

102. R. C. Elgersma, G. E. Mulder, G. Posthuma, D. T. S. Rijkers, R. M. J. Liskamp, Mirror image supramolecular helical tapes formed by the enantiomeric-depsipeptide derivatives of the amyloidogenic peptide amylin(20–29). *Tetrahedron Letters*. **49**, 987–991 (2008).

103. Y. F. Tian, G. A. Hudalla, H. Han, J. H. Collier, Controllably degradable β-sheet nanofibers and gels from self-assembling depsipeptides. *Biomaterials Science*. **1**, 1037 (2013).

104. M. M. Nguyen, K. M. Eckes, L. J. Suggs, Charge and sequence effects on the self-assembly and subsequent hydrogelation of Fmoc-depsipeptides. *Soft Matter*. **10**, 2693 (2014).

105. S. Deechongkit *et al*., Context-dependent contributions of backbone hydrogen bonding to β-sheet folding energetics. *Nature*. **430**, 101–105 (2004).

106. S. W. Pedersen *et al*., Probing backbone hydrogen bonding in PDZ/ligand interactions by protein amide-to-ester mutations. *Nat Commun*. **5** (2014), doi:10.1038/ncomms4215.

107. J. N. N. Eildal *et al*., Probing the Role of Backbone Hydrogen Bonds in Protein–Peptide Interactions by Amide-to-Ester Mutations. *Journal of the American Chemical Society*. **135**, 12998–13007 (2013).

Chapter 3: Experimental and computational studies reveal an alternative supramolecular structure for Fmoc-dipeptide self-assembly

3.0 FOREWORD

This chapter is based on an article we published in 2012.[1] It describes a collaborative effort by our group and the group of Dr. Pengyu Ren to evaluate and compare the experimental and computational features of Fmoc-dipeptide self-assembly. Xiaojia Mu designed and performed all computational simulations, wrote the associated methods and results sections, and contributed to the introduction, and thus is listed as a co-first author. My contribution was to design experimental work and write up much of the introduction, methods, and experimental results and discussion. Dr. Mary Nguyen and Profs. Laura Suggs and Pengyu Ren conceptualized the research and aided in research design.

3.1 INTRODUCTION

Molecular self-assembly continues to be explored as a powerful approach for fabricating functional nanostructured materials (*1–4*). Artificial self-assembly methods offer a "bottom-up" route to fabricating novel complex structures with nanometer precision. Numerous examples of the self-assembly of low molecular weight organic molecules leading to hydrogel formation can be found in literature (*5–7*), and of these, hydrogels composed of self-assembling, peptide-based small molecules have recently gained interest for their potential uses in biomedical applications such as tissue engineering and drug delivery (*8*). In contrast to traditional hydrogels composed of

[1] X. Mu, K. M. Eckes, M. M. Nguyen, L. J. Suggs, P. Ren, Experimental and Computational Studies Reveal an Alternative Supramolecular Structure for Fmoc-Dipeptide Self-Assembly. *Biomacromolecules*. **13**, 3562–3571 (2012).

chemically cross-linked high molecular weight polymers, gel materials based on self-assembling peptide conjugates consist of low molecular weight components that associate based on non-covalent interactions, such as hydrophobic forces, π-stacking and hydrogen bonding. These materials may therefore be more sensitive to *in vivo* chemical and physical stimuli than polymeric hydrogels, and more easily degraded by the body and cleared by the kidneys (*5*). Also unlike many polymer hydrogel systems, these molecules self-assemble via a pH or temperature trigger and can therefore be delivered through transdermal injection and gelled *in situ*, minimizing the invasiveness of the procedure required to place the material. Being peptide-derived, these materials are easily customized with bioactive sequences that may serve to enhance cell adhesion or induce specific signaling pathways.

Notable among self-assembling peptide-based gel materials are those created by Stupp and co-workers (*9*). These engineered peptide amphihiles (PAs) consist of a hydrocarbon tail conjugated to a short (8-12 residue) peptide sequence, with the inner residues having a high propensity to form β-sheet type hydrogen bonding interactions with neighboring molecules (*10*). The putative supramolecular arrangement of these molecules is a cylindrical fibril, stabilized by hydrophobic interactions among the hydrocarbon tails within the core of a fibril and by hydrogen bonding between the β-sheet forming segments. A recent molecular dynamics study of the proposed assembly confirmed this general structure, demonstrating the water- and ion-excluding properties of the hydrophobic core as well as the extensive hydrogen bonding between adjacent peptide segments (*11*).

Recently it has been shown that much shorter (2-5 residues) peptides conjugated to aromatic N-terminal protecting groups (such as fluorenylmethoxycarbonyl, naphthalene, pyrene, and even DNA nucleotide bases) can also self-assemble to form gels

(*7*, *8*, *11–17*). Of these, the fluorenylmethoxycarbonyl (Fmoc) derivatives were the first such molecules that were shown to gel in part because Fmoc-protected peptides and dipeptides are widely available for use in solid phase peptide synthesis. Their gelation ability was likely discovered serendipitously during attempts to drive aqueous dissolution; gelation of certain Fmoc-peptides has been demonstrated by raising then lowering the solution temperature, adding an excess of water to a miscible organic solvent containing the peptide conjugate, or by raising then lowering the solution pH (*8*).

Like PAs, these conjugate peptides are thought to form nanometer diameter fibril structures stabilized by noncovalent interactions between aromatic protecting groups and β-sheet-like hydrogen bonding between amide bonds on adjacent molecules. However, the proposed supramolecular arrangement of the conjugated peptides is markedly different from that of the PA system. Researchers observed, using Fourier-transform infrared spectroscopy (FTIR), circular dichroism (CD) spectroscopy, and x-ray diffraction (XRD) techniques, that these gels contain hydrogen-bonding patterns, molecular configurations, and intermolecular dimensions indicative of antiparallel β-sheet structures (*12*, *18*). Smith *et al*. (*18*) proposed a model in which pairs of Fmoc-diphenylalanine molecules are arranged in a helix around the long axis of a tubular fibril in an anti-parallel manner, with the aromatic rings of the Fmoc group on one molecule located near the peptide carboxyl terminus of the adjacent molecule. The authors offer a computational/theoretical confirmation of the energetic feasibility of this structure, involving a potential energy minimization using the AMBER force field; however, potential energy minimization typically leads to local minima and excludes the contribution of thermal energy and entropic effects.

Considering the potential conformational changes during the time evolution in self-assembly, molecular dynamics (MD) simulations are more favorable than simple

energy minimization to study the self-assembly of biomolecules (*19*, *20*). Besides providing atomistic information on kinetics, thermodynamics, and time evolution of molecular conformations, MD can also remove unfavorable interactions that remain after energy minimization. Therefore, MD can overcome the minimization's inadequacy in predicting the entropically favored conformations and therefore has been widely used in other self-assembly studies in recent years (*11*, *21–23*). In one example, MD simulations were used to study the self-assembly of Fmoc-tetrapeptides based on the RGD cell adhesion sequence (*24*). However, the simulations were relatively short (10-20 ns), consisted of assemblies of only 21 molecules, and there was no clear evidence that the structures had converged. Furthermore, the study concerned Fmoc-tetrapeptides, which have two more peptide bonds available for hydrogen bonding than do Fmoc-dipeptides and is therefore an arguably more "peptide-like" system.

In our preliminary molecular dynamics study, the Fmoc-dipeptide fibril model proposed by Smith *et al*. (*18*) did not maintain its hollow tube structure; instead, it shrunk into a more compact aggregate with water molecules excluded from the center (see **Appendix Figure A.1**). We thus focus on models in which the aromatic protecting groups are concentrated toward the center of the fibril with the attached peptide chains radiating outward, as is the case for PAs.

In this work, we sought to answer two questions about the self-assembly of Fmoc-dipeptides: 1) What are the major driving forces for self-assembly? and 2) How are individual molecules arranged within the gel-forming fibril structures? To this end we performed experimental validation of past results along with the first demonstration of the use of extensive molecular dynamics simulations to gain insight into the supramolecular structure of the Fmoc-dipeptide assembly. By answering these questions we will improve our understanding of the nano-scale properties of these materials and

can therefore assess the feasibility of using self-assembling short peptide conjugates for *in vivo* biomedical applications. Our system and approach may also be extended to investigate the dependence of side chain identity and sequence on self-assembly (*25*, *26*) in order to move toward rational design of peptide-based small molecule hydrogelators.

3.2 MATERIALS AND METHODS

3.2.1 Experimental details

3.2.1.1 Preparation of Fmoc-AA gels.

Fmoc-L-Ala-L-Ala-OH was purchased from Bachem, Inc. (Torrance, CA) and used without further purification. To form gels via a pH trigger, Fmoc-AA was added to deionized water, vortexed, and sonicated for several minutes. 1 eq 0.5 M NaOH was added and mixture was vortexed until completely clear. The mixture was then added quickly to a vial containing 1 eq 0.1 M HCl, to trigger gelation.

3.2.1.2 Wide angle X-ray scattering.

Fmoc-AA gel samples were prepared at 10 mg/ml (final pH = 2.6-2.8) by a pH trigger method (1 eq 0.5 M NaOH added to dissolve Fmoc-AA, then 1 eq 0.1 M HCl added to induce gelation, as described above) and were spread out onto a quartz slide and allowed to dry for two days. Samples were run on a Scintag X1 theta-theta powder diffractometer with a Cu x-ray source. Peak analysis was performed using Jade v9.1.1 (Materials Data Inc.) software, and *d*-spacings were calculated assuming an x-ray wavelength of 1.54059Å (Cu K-α1).

3.2.1.3 Transmission Electron Microscopy.

Gels for TEM analysis were prepared at a final concentration of 5 mg/ml (final pH = 3.3-3.4). Approximately 10 μl of gel was placed on the shiny side of

Formvar/Carbon coated 300 mesh nickel grids (Electron Microcopy Sciences, Hatfield, PA) and was allowed to adsorb for 2 minutes. Excess solvent was removed using a Kimwipe, and the grid was further allowed to air dry for 1 minute, after which the grid was washed with 10 μl deionized water for 1 minute and dried with a Kimwipe. Finally, the grids were placed on 10 μl drops of 2% uranyl acetate for 1.5 minutes, then dried with a Kimwipe and allowed to air dry before placing in the instrument. Samples were imaged using a FEI Tecnai instrument operating at 80 kV, and the associated AMT Advantage HR 1kX1k digital camera was used both for sample navigation and image capture.

3.2.1.4 Fourier Transform Infrared spectroscopy.

Gels were prepared at 5 mg/ml (final pH = 3.3-3.4) as described above, except D_2O was used in place of deionized water in all solutions. Concentrated stock solutions of NaOH and HCl solutions were diluted to the concentrations described above using D_2O. Gel samples were sandwiched tightly between two calcium fluoride (CaF_2) windows (25 mm wide by 2 mm thick) and placed in line with the beam in a transmission configuration within the instrument. A Thermo-Mattson Infinity Gold FTIR instrument was used to collect spectra, which were averaged over 200 scans.

3.2.1.5 Circular Dichroism spectroscopy.

Fmoc-AA gels for circular dichroism were prepared at a concentration of 5 mg/ml. ~2.5 eq of Glucono-delta-lactone (GdL), a slowly-hydrolyzing lactone that ring-opens to form gluconic acid, was used to acidify and hence gel a solution of Fmoc-AA and 1 eq 0.5 M NaOH in deionized water, as described previously (*27*). Prior to GdL addition, a background spectrum was taken using deionized water with 1 eq 0.5 M NaOH added. After GdL addition and dissolution the Fmoc-AA solution was pipetted into a cylindrical demountable quartz cuvette with a 0.1 mm pathlength. Spectra were measured

using a Jasco J-810 CD Spectrometer every 10 minutes after GdL addition. The instrument was operated with a data pitch of 0.5 nm, scan speed of 200 nm/min, and response time of 1 second. Three spectra were taken for each time point then averaged. After the final time point we checked for linear dichroism (LD) artifacts by performing the scan again with the cuvette rotated 90, 180, and 270 degrees from its starting position, but we observed no significant change in the CD signal and thus concluded that LD effects were minimal. The final pH of GdL-formed gels after 24 hours was in all cases between 3.5 and 3.7.

3.2.2 Molecular models and dynamics simulations

3.2.2.1 Initial structures preparations.

Fmoc-AA molecules were built in TINKER (*28*). As shown in **Figure 3.1**, all the fibrils are cylindrical nanofibrils, "Cubic 4" has 4 molecules placed as a "cross" on each layer; "Cubic 5" has 5 molecules with the alanines radiating outward; "Cubic 6" and "400 ns" has parallel placed Fmoc-AAs also with alanines radiating outward. Except Cubic 4's fibril, the plate layers are rotated 35.9 degrees relative to the adjacent layer. The distance between each layer is 4.5 Å for SA and 400 ns models, and 5 Å for all Cubic models. A lower density of molecules on each layer (like 2 or 3 Fmoc-AA molecules on each layer) will result in an unstable fibril.

3.2.2.2 Details of atomistic simulations.

Individual Fmoc-AA molecules were built and parameterized using TINKER and GROMACS (version 4.5.4) (*29*). For the Fmoc residue, an OPLS-AA-type molecular mechanics model was developed in both TINKER and GROMACS. The atomic charges for new atom types in the Fmoc residue were derived by quantum mechanical (QM)

calculations; the bond, angle and vdW parameters were transferred from OPLS-AA, OPLS-AA/L (*30–32*) and MM3 (*33*) force fields; the torsion parameters were derived by fitting the molecular mechanics (MM) calculations to the QM potential surface.

Some of our molecular dynamics simulations were performed on the Texas Advanced Computing Center (TACC) Ranger (3,936 16-way SMP compute, 15,744 AMD Opteron™ processors for a total of 62,976 compute cores, 579 TFLops Peak) and TACC Lonestar (Dell PowerEdge 1955 Blade, 55.5 TFlops Peak, 1300 nodes, 2 Dual-Core Xeon 5100 at 2.66 GHz, InfiniBand interconnection).

All simulations and calculations were performed using GROMACS 4.5.4 and 4.5.3 (*29*) with OPLS-AA force field (*30*, *34*), and applied periodic boxes with explicit water molecules. All starting structures for MD simulation, except simulated annealing and replica exchange molecular dynamics (REMD), were subjected to steepest descent energy minimizations with 5000 maximum steps to remove high-energy contacts. Before the productive MD, in order to keep the system stable at 300 K and 1 bar, a 100 ps NVT and a 100 ps NPT equilibration were applied respectively. During the productive MD, all bonds were constrained using LINCS algorithm (*35*, *36*); for every 10 fs, neighbors were searched in grid cells with 1 nm as cutoff values for short-range neighbor list, electrostatic and van der Waals; long-range electrostatics were treated with the particle mesh Ewald method (*37*) with a grid spacing of 0.16 nm; constant temperature and pressure were maintained by coupling the system to an external bath at 300 K and 1 bar, using velocity rescaling (*38*) and Parrinello–Rahman(*39*), respectively. A 2 ps pressure coupling time was applied and the isothermal compressibility of water is 4.5×10^{-5} bar^{-1}. A leap-frog integrator with the integration time step of 2 fs was used (*40*). GROMACS OPLS-AA force field with our fitted parameters for Fmoc group was used for the Fmoc-AA, and a TIP3P model was applied for water (*41*). In SA of Fmoc-AA molecules self-

assembly, the initial fibril structure was the first 15 layers of the 400 ns model. The system temperature was firstly heated up from 288 to 300 K in 0.5 ns, then linearly and gradually cooled down to 0 K in the following 39.5 ns. We randomly extracted 120 frames during the temperature drop from 700 to 290 K in SA that covered the conformational space broadly, and those frames were then used in REMD as initial structures; a set of temperatures ranging from 280 to 600 K was estimated and preset in order to maintain the success rates of exchange within 20-30%.

3.3 RESULTS AND DISCUSSION

3.3.1 Experimental validation of self-assembly and gelation

Our model gelator, Fmoc-Ala-Ala (or Fmoc-AA, **Figure 3.1 A**), is a simple molecule known to self-assemble in aqueous solution to form a self-supporting gel (*12*, *26*). We confirm that Fmoc-AA does indeed form a self-supporting gel at 0.5% w/v by vial inversion (**Figure 3.1 B**) with circular dichroism (CD) experiments (**Figure 3.1 C**) and transmission electron microscopy (TEM) (**Figure 3.1 D**) showing chiral and nanostructural evidence of self-assembly, respectively.

Circular dichroism measurements confirm the assembly of Fmoc-AA. **Figure 3.1 C** illustrates the increase in dichroism over time when glucono-δ-lactone (GdL), a ring molecule that slowly hydrolyzes to gluconic acid, is used to slowly lower the pH and hence slowly gel a solution of Fmoc-AA (see Methods section for experimental details). The increase in dichroism can be attributed to an increase in the apparent chirality of the sample; this increase in "nanoscale chirality" is a known hallmark of the self-assembly process (*42*). Therefore, the data in **Figure 3.1 C** corresponds to the progression of self-assembly over the course of an hour, and the concomitant tendency of individual Fmoc-

AA molecules to adopt preferred orientations, giving rise to an overall "handedness" of the assembly. We confirmed that the hydrolysis of GdL itself does not contribute to the increase in dichroism over time (see **Appendix Figure A.2**). Within the data there are several important features: a broad positive peak centered at ~210 nm, a negative peak at 228 nm, and peaks at higher wavelengths (> 260 nm). The broad peak at ~210 nm is roughly 10 nm higher than a characteristic β-sheet peak typically between 195 nm and 202 nm (*43*). The negative peak at 228 nm is similar to what has been suggested as a "β-sheet peak" in previous studies (*12*, *18*, *44*), although it is also shifted about 10 nm higher than typical characteristic β-sheet-type peaks. It is important to note that there are published CD data for other Fmoc-dipeptide hydrogelators that do not contain this negative peak (*27*). The high wavelength peaks likely arise due to the induced chirality of aromatic residues (specifically, the Fmoc group) placed within the environment of a supramolecular assembly (*43*). Though slight wavelength variations exist, the CD data presented here are generally in good agreement with published data for Fmoc-dipeptides. Interestingly, the peaks in our CD align well with those reported for Fmoc-Leu-Gly by Adams *et al*. (*27*) but are opposite in sign, indicating similar supramolecular structural features that give rise to nanoscale chirality, but with reversed handedness (e.g. left- vs. right-hand helix). Given the wavelength discrepancies with protein data and the fact that not all Fmoc-dipeptide gelators exhibit β-sheet-like peaks in CD, we hesitate to use CD to make specific conclusions regarding the structural arrangement of molecules within a fibril assembly. Rather, these data serve as confirmation that Fmoc-AA self-assembles in a manner similar to other Fmoc-dipeptide systems.

TEM analysis was also performed to confirm that the nanoscale morphological features of Fmoc-AA gels were similar to those reported for other Fmoc-dipeptide gels. **Figure 3.1 D** clearly shows the ribbon-like morphology seen in previous studies of

various Fmoc-dipeptide gelators. The ribbon width ranges from 10 to 50 nm; these dimensions are also noted in previous studies (*12*, *18*, *27*, *45*, *46*).

3.3.2 Molecular simulations of self-assembly and stability analysis

Next we carried out molecular dynamics simulations to investigate the self-assembly of Fmoc-AA fibrils. We performed several simulations on different initial fibril structures consisting of loosely stacked "layers" with four, five, or six fully protonated Fmoc-AA molecules, as is shown in **Figure 3.2**. These potential fibril structures were inspired by previous work on PAs and the duplex structure of DNA. Each fibril model was named according to the number of Fmoc-AA molecules in a single plate and the geometry of the water boundary, i.e. "Cubic 4" refers to the model in which the initial structure is a 20-layer containing 4 Fmoc-AA molecules each, and this structure is placed in a cubic box of water molecules for the simulation. The rationale for running several different initial configurations was to determine what effect initial conditions might have on the final assembled structures. Each system was subjected to 160 ns or longer room-temperature MD simulations.

Additionally, we attempted *ab initio* predictions using simulated annealing (SA) (*47*) to investigate the assembly process without well-defined initial structures. SA is a global optimization algorithm designed to search for an optimal configuration. In SA, the system is "heated up" to yield random configurations and slowly "cooled back" down to a low temperature using molecular dynamics simulations. As shown in **Figure 3.2 E**, during the SA procedure the initial fibril is heated up and the structure falls apart; Fmoc-AA molecules are randomly distributed in the water box without any aggregation. As the system is cooled, Fmoc-AA molecules begin to assemble together into a fibril. However,

with finite simulation time length, SA cannot guarantee to output the optimal structure (at a global energy minimum). Therefore we performed further simulations using replica exchange molecular dynamics (REMD), a technique that utilizes the faster kinetics at the high temperature to accelerate the sampling at room temperature (*48*). REMD has been utilized to successfully fold small proteins (*49–52*) and study self-assembly (*53–55*). In our REMD, simulations are performed in parallel on 120 replicas of the molecular system, each at different temperatures from 280 to 600 K for 100 ns. The structures in the neighboring replicas are allowed to exchange with a success rate greater than 0.18. In this work, the initial structures for REMD are a collection of structures at different temperatures extracted from the SA process. Due to the computational cost, we used a smaller system with 60 Fmoc-AA molecules in a 396 nm^3 rectangular water-containing box.

Snapshots of the last frame of each simulation (**Figures 3.2 A to D**) show that each model has been compacted and reorganized during the simulation but all maintain a fibril shape. The REMD ensemble at 299 K also lead to a similar fibril shape to the SA assembled fibrils in **Figure 3.2 E**. It is also apparent from these snapshots that the hydrophobic fluorenyl rings are mostly buried but not completely inaccessible to water, and this feature may help to explain why lateral aggregation of fibrils into larger fiber structures is observed in TEM.

We also assessed the stability of each model's assembly by calculating the solvent accessible surface area (SASA) per molecule over the course of the simulation. Results of this analysis are displayed in **Figure 3.2 F**. SASA represents quantitatively the contact between solute and the solvent and therefore depicts the changes and rearrangements of hydrophobic surfaces during the molecular assembly and aggregation (*56*). During the assembly process, the space between Fmoc-AA plate layers lessens and the structure

becomes more compact. Water molecules initially located in the hydrophobic "hollow" between the Fmoc rings in the starting structures are expelled out of the fibrils during the simulations, and therefore the SASA per molecule decreases, suggesting the process of molecular aggregation. Additionally, analysis of hydrogen bonding between water and Fmoc-AA provides information about the assembly stability.

Figures 3.2 F and G show, respectively, the convergence of the SASA of each fibril model and the number of hydrogen bonds between water and Fmoc-AA during the simulations. During the first few nanoseconds of the simulation, SASA and hydrogen bond numbers drop dramatically, suggesting the rapid aggregation and assembly of Fmoc-AA molecules. After 50ns, all systems become stable; the constant values of both SASA (~1.7 nm^2/molecule) and hydrogen bonds (~4/molecule) per molecule between simulations with different starting structures suggest similar self-assembled fibrils are formed regardless of the nature of the initial starting structures.

In the 299 K REMD ensemble, the initial structure was taken from the simulated annealing at a high temperature, and thus the Fmoc-AA units are not in a fibril form, but randomly distributed in the water box (as in **Figure 3.2 E** the middle, the snapshot at 12 ns). However, during the exchanges of replicas between different temperature conditions, the stacked fibril-like configurations are quickly exchanged to and stayed in the 299 K ensemble. As a result, the REMD 299K ensemble gives remarkably similar results as the "traditional" MD results as shown in **Figures 2 F and G**. These MD simulations confirm that the self-assembly is a rather robust phenomenon and the fibril structure is energetically very favorable.

In our simulations, we also observed that the fibril composed of completely deprotonated Fmoc-AA molecules would fall apart very quickly. This observation is confirmed by experiment: at high pH (wherein Fmoc-AA is likely totally deprotonated),

the solution is free flowing and not gel-like, indicating that long, entangled fibrils are not present.

3.3.3 Experimental WAXS results confirm the molecular dimensions derived from simulations

We further validated our computational simulations by comparing molecular dimensions calculated from Radial Distribution Functions (RDF) with actual *d*-spacings obtained from Wide Angle X-ray Scattering (WAXS) experiments on dried films of Fmoc-AA gels triggered by a pH change. RDF describes the variation of the density of an atom (or group of atoms) with the distance from a reference particle (*57*), providing dimensional information that can be experimentally determined using X-ray scattering techniques. WAXS can give information about local order in non-crystalline polymers (*58*), and therefore is employed in this study to compare with RDF computational results. We recognize that drying gel films on quartz single crystal slides yields results likely unrepresentative of the gel phase (*59*); however, for the sake of comparison with previous studies we opted to use a similar sample preparation method.

Our WAXS analysis of dried Fmoc-AA gel films gives molecular dimensions similar to those reported previously. The diffraction pattern is shown in **Figure 3.3 A**. Similar to Smith *et al*. (*18*), we found a reflection corresponding to a *d*-spacing of 26.3 Å (green arrow in **Figure 3.3 A**), with subsequent higher order reflections up to n=6, indicated by green lines. Distinct from the higher order reflections is a peak corresponding to a dimension of 4.35 Å (orange arrow). This dimension is also similar to one observed by Smith *et al*. (*18*) and is seen in other self-assembling dipeptide-conjugate gel systems (*25*, *46*) in which the dimension has frequently been attributed to a β-sheet like spacing between adjacent molecules within the fibril assembly.

The obtained characteristic dimensions from WAXS are consistent with our radial distribution analyses of simulated fibrils. Note that due to the various simulation box sizes and concentrations of Fmoc-AA, it is more meaningful to compare the non-normalized RDF, i.e. without dividing the probability density by the average density in the whole box. Otherwise, doubling the box size without increasing the number of peptides, reduces the RDF intensity by factor of two since the final fibril structure remains the same. The positions of peaks are not affected by the normalization. During self-assembly simulation, the fluorenyl rings (colored yellow in **Figure 3.2**) are stacked in an ordered way, as seen within differently-colored Fmoc-AA pairs highlighted in **Figure 3.3 E**. The non-normalized RDF between fluorenyl rings is shown in **Figure 3.3 B**. All atoms in the fluorenyl rings were used for the RDF calculation. The high peaks correspond to distances of around 0.41 to 0.5 nm, indicating an ordered stacking patterning between the fluorenyl rings within the Fmoc group. A similar distance at d= 4.35 Å also appears in the WAXS in **Figure 3.3 A**, suggesting that this distance may be characteristic of the π-π π-πstacking between fluorenyl rings, rather than a specific β-sheet-like spacing between peptide bonds on adjacent molecules. This interpretation was offered by Braun and Cardoso (*60*), who argued that reflections of this dimension likely arise due to spacing of the aromatic groups (in this case, Fmoc) along the fibril axis. Furthermore, by inspecting the fluorenyl rings in the simulated structures, we observed a few well-recognized π-π stacking geometries (**Figure 3.3 E** right) (*61–63*), which likely explain the range of distances seen in the non-normalized RDF of fluorenyl rings.

By calculating the non-normalized RDF between the terminal alanine's hydroxyl hydrogen and the center of the fibril (the "center" here is defined by a set of dummy atoms along the z-axis of the fibril, as shown **Figure 3.3 C**, inset), the radius of the fibril

can be estimated as a range between 1 to 1.5 nm as shown in **Figure 3.3 C**. This radius range, which corresponds to a diameter range of 20-30 Å, is also consistent with the experimental results obtained from our WAXS in **Figure 3.3 A**, which shows a pronounced peak at 26.3 Å. Smith *et al*. (*18*) observed a very similar value (26.0 Å) in their WAXS experiments using dried gel films of Fmoc-diphenylalanine.

Figure 3.3 D shows the non-normalized RDF of the distance between adjacent peptide backbones (including α-carbons, amide nitrogens and amide carbons) along the axis of the assembled fiber. The predominant value is 0.46-0.48 nm, which corresponds well with typical antiparallel β-sheet chain-to-chain distances (*64*, *65*). However, we do not see a distinct reflection corresponding to this dimension in our WAXS results (**Figure 3.3 A**). Given the broadness of the peak corresponding to d=4.35 Å in WAXS and the simulated non-normalized RDF of fluorenyl suggesting multiple preferred interaction distances from 4.1 – 5.0 Å, it is possible that a reflection corresponding to d=4.8 Å is present but convoluted with reflections arising from π-π stacking dimensions. While it is not present in our experimental data, the presence of this dimension in our non-normalized RDF calculations may serve to explain why others have observed a similar d-spacing and ascribed it to the presence of β-sheets. We further explored the secondary structures using FTIR experiments and conformational analysis of the simulations, as discussed below.

3.3.4 Analysis of hydrogen bonding patterns within assembled structure

Table 3.1 shows the hydrogen bond distribution between the Fmoc, middle alanine ("Ala-mid"), and terminal alanine ("Ala-term") residues of adjacent Fmoc-AA molecules during the last 50 ns of the simulations. We found that the carbonyl oxygen of

the Fmoc carbamate (-OC(O)NH-) group is particularly active in forming hydrogen bonds with alanine residues, especially the terminal alanines on adjacent molecules. The high degree of interaction between the Fmoc carbamate and the terminal alanine residue may help explain why single residue Fmoc-protected amino acids with *non-aromatic* side chain groups have not, to our knowledge, been shown to form stable gels. The only examples of gel-forming single residue Fmoc-protected amino acids in literature are phenylalanine, tyrosine, and derivatives of the two (*66–68*) —all of which have side chain groups capable of π-π stacking interactions that likely contribute to fibril stability.

We also calculated the fraction of hydrogen bonds formed between Fmoc-AAs and the solvent (water) molecules, as shown in **Table 3.2**. The Fmoc group's carbonyl oxygen is almost as active as the terminal alanine carboxyl group in making hydrogen bonds with the surrounding water molecules. These data suggest, different from Stupp's proposed structure for the PA assembly (*11*), that in the fibril composed of short peptide conjugates like Fmoc-AA, the hydrophobic Fmoc groups are not completely buried within the core of the fiber. Instead, our simulations indicate that, although the Fmoc groups are mostly concentrated toward the core of the fiber, both the Fmoc carbamate and the aromatic fluorenyl groups are somewhat accessible to water molecules, making the fibril surface amphiphilic. This observation becomes quite apparent looking at **Figure 3.2** (bottom illustrations); the highly hydrophobic fluorenyl rings (yellow) are exposed to the water molecules, as well as the hydrophilic alanine residues (blue), and thus the fibril surfaces are composed of both hydrophobic and hydrophilic components, as suggested in part by Smith *et al*. (*18*) This property may also explain why fibrils can further assemble into fibers; interactions between hydrophobic regions on adjacent fibrils may force their aggregation into ribbon-like fibers.

3.3.5 Backbone conformational and secondary-structure analysis by FTIR and Ramachandran plots

In transmission FTIR spectroscopy, Fmoc-AA gels formed from D_2O show pronounced shifts in the amide I absorption region (~1600-1700 cm^{-1}). Protein secondary structures involve specific hydrogen bonding interactions between amide bonds that shift the amide C=O stretch frequency resonance in an often-characteristic manner (*69*). FTIR can therefore be used to elucidate which secondary structures are most prevalent in a protein of unknown structure. Naturally, this technique has been applied to peptide-based self-assembled gel materials to probe for interactions that might point to certain secondary structures. **Figure 3.4 A** shows the amide I absorption spectrum for an Fmoc-AA gel, with clear peaks centered at 1686 cm^{-1}, 1644 cm^{-1}, and a shoulder peak at 1634 cm^{-1}. The 1686 cm^{-1} peak and 1634 cm^{-1} shoulder are within characteristic absorption frequency ranges seen in proteins with β-sheet content (blue overlay in **Figure 3.4 A**) (*69*). These peak locations and relative intensities are also quite consistent with previous FTIR data given for Fmoc-dipeptides (*8*, *12*, *18*, *45*). The large absorption at 1644 cm^{-1}, similarly observed in related naphthalene-dipeptide gelator systems (*46*), lies outside the typical range of frequencies for β-sheet structures; instead, it falls within a frequency range indicative of hydrogen bonding within unordered protein structures (purple overlay) (*69*) but the maximum absorption value itself is characteristic of polyproline-like hydrogen bonding interactions within collagen that are shown to decrease upon heating (*70*). The spectroscopic data alone would seem to indicate that hydrogen bonding interactions indicative of polyproline-like or random coil structure are present in numbers similar to or possibly even greater than those typical of β-sheet structures. However, the above analysis of hydrogen bonding patterns in our computational simulations showed a

lack of significant β-sheet-like interactions (hydrogen bonding between amide groups on adjacent Fmoc-AA molecules).

Therefore, while the *spectroscopic* data suggest it is reasonable to construct a supramolecular model based on the assumption of β-sheet-like hydrogen bonding between amide bonds on adjacent Fmoc-AA molecules, *computational* data suggest that other significant interactions may be present and may point to an alternate model for the assembly. Given this contradiction and given that conjugate peptides are structurally quite distinct from long peptides and proteins, we comment that it may not always be appropriate to extrapolate from peptide/protein-level spectroscopic data to make structural conclusions about these conjugate peptide gel systems.

Analysis of the predominant peptide torsion angles indicative of specific secondary structures present in the simulated assemblies shows a strong preference for polyproline II (PPII) and antiparallel β-sheet-like conformations. The ϕ,ψ angles of each alanine residue for the population of Fmoc-AA molecules in a given simulation are illustrated with a Ramachandran plot for backbone conformational analysis, a classical approach to investigate the secondary structure of amino acids. In **Figures 3.4 B and C**, Ramachandran plots of the middle and terminal alanines of our systems are calculated for the Cubic 5 model during the last 50 ns (results are representative of all fibril geometries simulated). **Figure 3.4 B** demonstrates that most of the middle alanine ("Ala-mid") residues are likely to adopt a PPII conformation: 64.1% of residues have ϕ,ψ angles in the range ϕ,ψ = (-100° to 0°, 100° to 180°) and a peak at ϕ,ψ = (-78°, 152°), whereas 10.6% of residues have backbone torsions in the range ϕ,ψ = (-180° to -100°, 100° to 180°) indicative of β-sheet conformation. For terminal alanine ("Ala-term") residues, within the same ϕ,ψ ranges 54.7% have mostly PPII-like conformation, and 16.3% have β-sheet conformation. **Figure 3.4 C** shows that the PPII conformation is preferred among

the terminal alanine ("Ala-term") residues. It is known that within the PPII structure, amide linkages preferably form hydrogen bonds with water rather than with other amide groups (*71*). Since our FTIR analysis showed distinct PPII character, we counted the hydrogen bonds of residues on Fmoc-AA (Fmoc, Ala-mid and Ala-term) with other Fmoc-AA versus with water (**Table 3.3**). We indeed observed that hydrogen-bond capable residues of Fmoc-AA all prefer to form hydrogen bonds with water rather than with other Fmoc-AA molecules even in the assembled form, further corroborating our computational observation of the alanine residues' preference for adopting a PPII-like conformation.

Besides the PPII conformation, the terminal alanine also displays a notable population at ϕ,ψ = (-148°, 164°), which is close to typical antiparallel β-sheet's ϕ,ψ angles around (-140°, 135°). In **Figure 3.3 D**, the distance between Fmoc-AA strands is presented using non-normalized RDF, and the peak at around 0.46-0.48 nm also suggest a β-sheet like conformation according to previous X-ray diffraction patterns studies of protein secondary structures (*64*, *65*). We did not observe a pronounced peak around 0.48 nm in our WAXS results in **Figure 3.3 A**, but in our FTIR experiments we have observed absorbance shifts indicative both of β-sheet-like interactions between Fmoc-AA molecules and of PPII-like interactions with the solvent. While we observe β-sheet-like character in FTIR and in backbone conformational analysis of the simulated assemblies, our hydrogen bonding analysis shows that hydrogen bonding between peptides on adjacent strands (the mode of interaction for β-sheet structures) is not the predominant interaction. Rather, the Fmoc carbonyl oxygen and terminal alanine form hydrogen bonds most readily, both with each other and the surrounding water molecules. Clearly, hydrogen bonding plays a role in stabilizing the fibril structure; however, based on our

data it becomes apparent that the importance of the β-sheet forming ability of these Fmoc-dipeptides in stabilizing the fiber assembly may have been previously overstated.

3.4 CONCLUSIONS

In this paper, we presented a computational molecular dynamics simulations alongside experimental analyses to gain new insight into the structure of the Fmoc-dipeptide supramolecular assembly. We have shown in our simulations that Fmoc-AA molecules assemble into well-defined fibril structures independent of starting conditions. Furthermore, we show that alternate molecular dynamics methods (REMD and SA) give nearly identical results, further confirming the convergence of the computational data. Our experimental data show that Fmoc-AA indeed assembles into gel-forming fiber structures. Computational analysis of characteristic dimensions for fibril diameter and π-π stacking interactions are consistent with results from WAXS experiments, and comparison of FTIR spectra with typical protein FTIR data suggests the presence of β-sheet- and polyproline II-like features. However, assigning typical secondary structure motifs to these short conjugated peptides is challenging. The alanine residues adopt mostly PPII conformations with limited β-sheet-like torsion angles, according to the simulations. From the analysis of hydrogen bonding patterns we find that the majority of hydrogen bonding interactions are between the Fmoc carbonyl oxygen and either the terminal alanine hydroxyl group or the surrounding water, potentially explaining why single Fmoc-protected amino acids with non-aromatic side chain groups have not been shown to form stable gels. It appears also that hydrogen bonding between peptide bonds on adjacent Fmoc-AA molecules is far less common, and therefore we argue that the putative β-sheet character observed in Fmoc-AA gels arises due to the preferential

conformation of Fmoc-AA molecules within the assembled fibril and the chemical environment of the fibril, rather than from "typical" interactions specific to β-sheet strands. It is important to remember that no single spectroscopic analytical tool can provide information about *both* of the two main characteristics of protein secondary structure: hydrogen bonding and conformation (i.e. backbone torsion angles). Here, FTIR gives information about bond stretching affected by hydrogen bonding and CD gives information about sample chirality resulting from preferred molecular conformations. In the case of proteins and polypeptides with repeated secondary structural patterns, the hydrogen bonding effects on bond stretching and the sample chirality resulting from preferred backbone dihedrals are well characterized and can be correlated with secondary structure features thought or known to be present in the protein based on its primary sequence. However, Fmoc-dipeptides are far shorter, less complex, and contain non-native conjugate groups; therefore, they likely interact with each other in a manner distinct from peptide bonds within classical protein secondary structures. For this reason, it is our belief that a) researchers should exercise caution when extrapolating spectroscopic and other analytical data from pure protein solutions to small, conjugated peptide systems such as these, and b) computational tools can help us understand these systems where experimental analytical tools are unable to provide explicit details. By combining computational studies and experiments, we obtained missing critical insights into the supramolecular structure and mechanism of Fmoc-dipeptide self-assembly.

Finally, we show that hydrophobic groups, while mainly concentrated toward the center of the fibril, are partially exposed to the solvent and may therefore aid in aggregating fibrils into larger fibers seen in TEM, although the exact mechanism is unclear. It was reported by Tang *et al*. (*45*) that there is a dependence on gel pH on fibril aggregation. However, current analytical techniques are unable to provide detailed

supramolecular information that would give insight into this process. This "gap" may be addressed using computational models beyond atomic resolutions.

Fmoc-AA was chosen for comparison with the only other proposed structural model to date (also an Fmoc-dipeptide) and because its side chain uniformity and simplicity decrease the complexity of computational calculations performed during MD simulations. However, the knowledge and approaches established in this study will enable us to explore and rationally design novel self-assembling peptide-based materials that have bioactive sequences and biological functionality for biomedical applications.

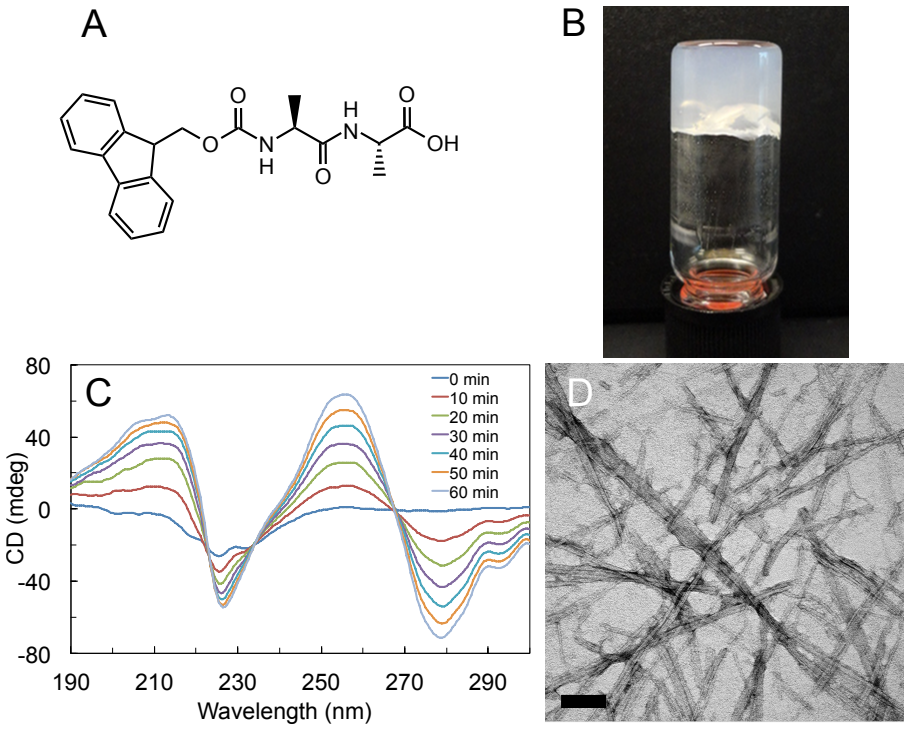

Figure 3.1 Experimental analysis of Fmoc-AA gels. (A) Fmoc-AA chemical structure; (B) Vial inversion test confirms that self-assembly leads to formation of self-supporting gel. (C) CD of Fmoc-AA gels formed via slow acidification with GdL shows increase in dichroism over time due to handedness induced by self-assembly. Spectra shown were taken from 0 to 60 minutes at 10 minute intervals; (D) TEM shows nanoscale "ribbon" like features from 10-50 nm in width, similar to those seen in previous studies. Scale bar = 100 nm.

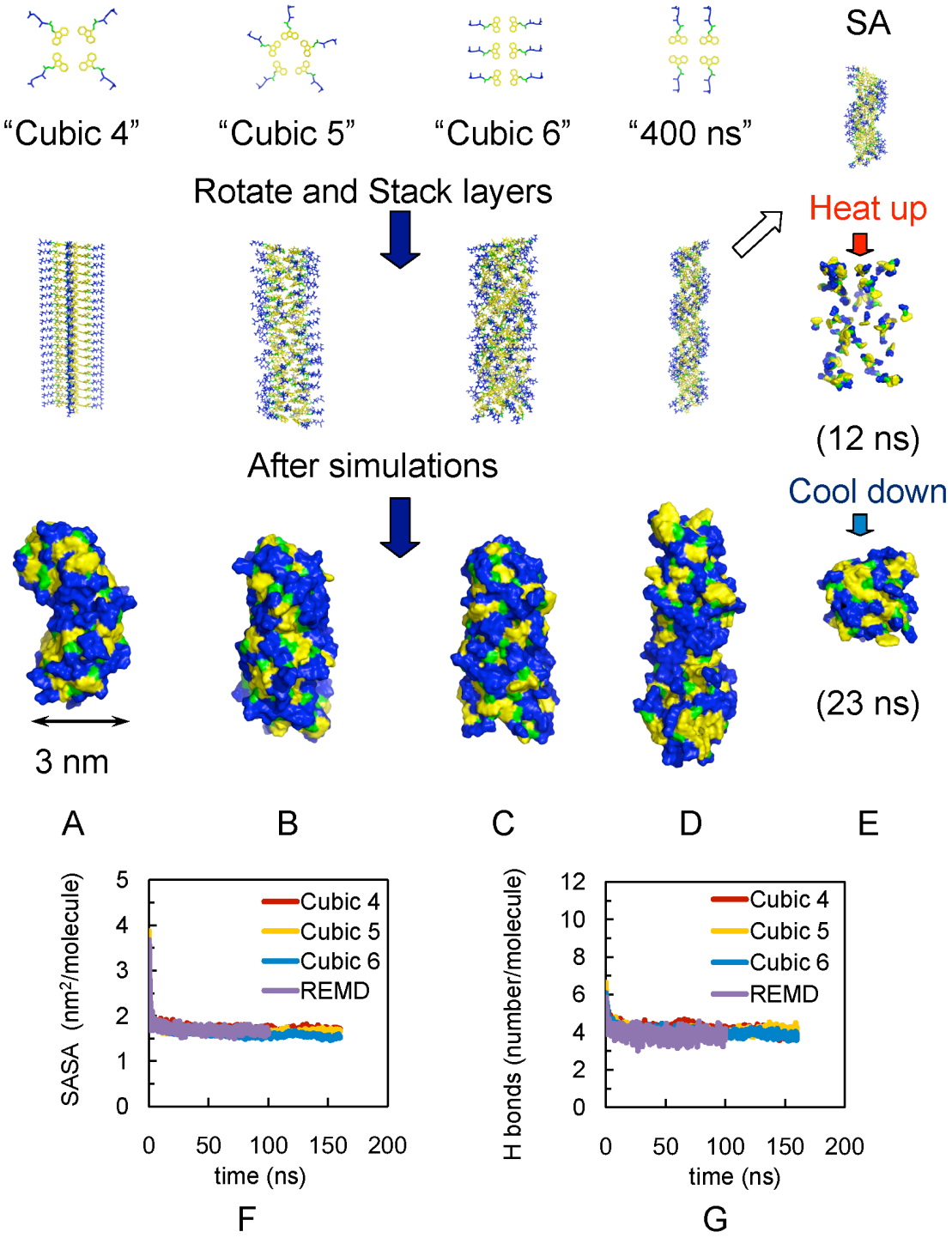
"Cubic 4"
"Cubic 5"
"Cubic 6"
"400 ns"
SA
Rotate and Stack layers
Heat up
(12 ns)
After simulations
Cool down
(23 ns)
3 nm
A
B
C
D
E
SASA (nm²/molecule)
Cubic 4
Cubic 5
Cubic 6
REMD
time (ns)
F
H bonds (number/molecule)
Cubic 4
Cubic 5
Cubic 6
REMD
time (ns)
G

Figure 3.2

Figure 3.2 caption: Models of fibrils in simulations show independence of final assembly of initial structures. (A) Fibril with 4 Fmoc-AA per layer soaked in cubic box ("Cubic 4"). (B) Fibril with 5 Fmoc-AA per layer soaked in cubic box ("Cubic 5"). (C) Fibril with 6 Fmoc-AA per layer soaked in cubic box ("Cubic 6"). (D) Fibril with 4 Fmoc-AA per layer soaked in long rectangular box with 400 ns simulation ("400 ns"). For A-C, all simulations were 160 ns. (E) Simulated annealing of 15 layers from model in (D); also used as initial structures for REMD simulations. Note: yellow indicates fluorenyl group of Fmoc, green is the carbamate linker, and blue is the peptide chain. For A-D, Top: the arrangement of Fmoc-AA molecules (hydrogens are not shown) on each layer. Middle: initial structures for simulations. Bottom: snapshots of the solvent accessible surfaces from the last frames of simulations show self-assembled fibril structures. The convergence of SASA and hydrogen bonding calculations over time indicates structural stability: (F) SASA per molecule for Cubic 4, Cubic 5, Cubic 6 and REMD ensemble at 299 K ("REMD"); all converge to ~1.7 nm^2/molecule, and (G) Number of hydrogen bonds per molecule for Cubic 4 to 6 and REMD simulations (~ 4).

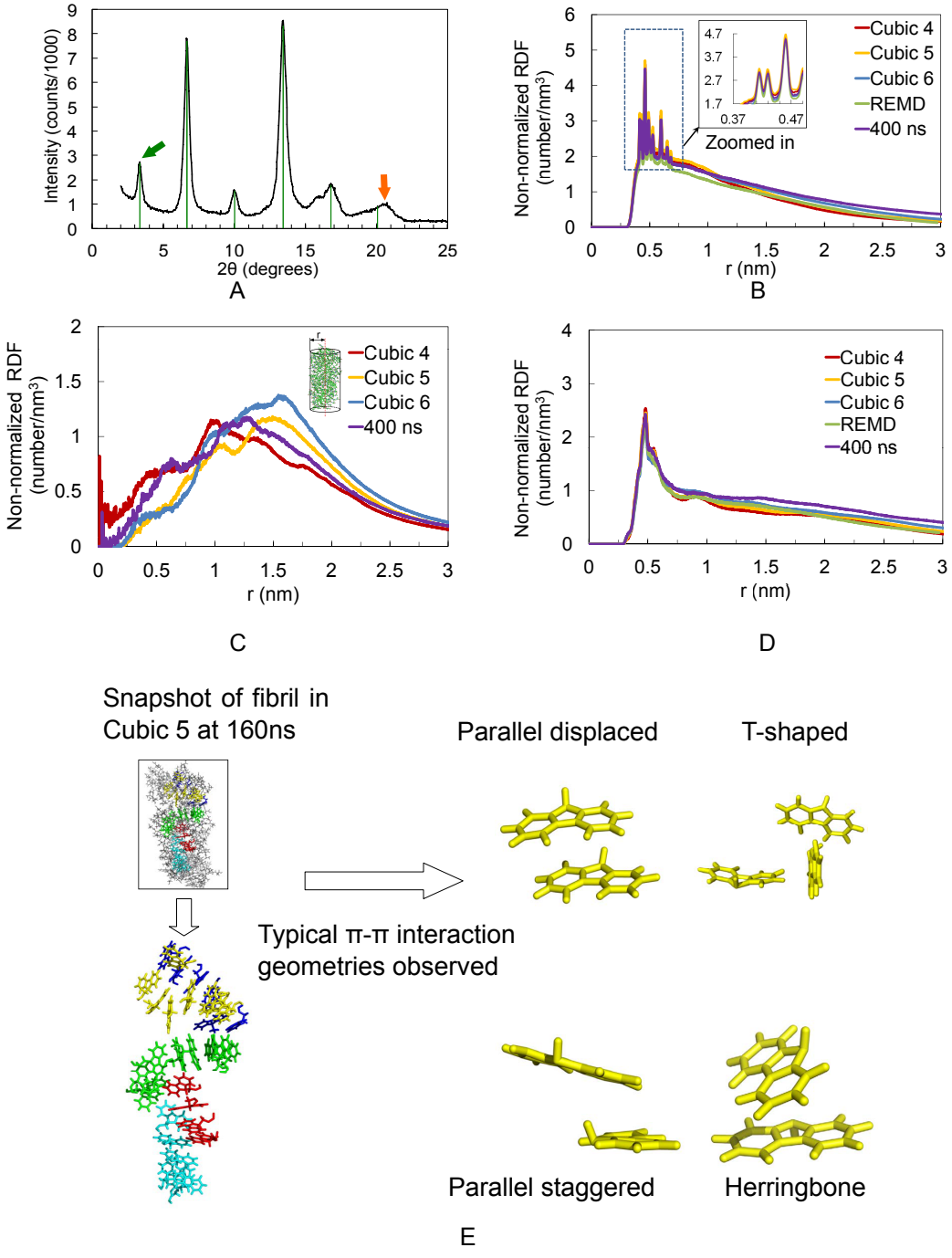
Intensity (counts/1000)
2θ (degrees)
A
Non-normalized RDF (number/nm³)
r (nm)
Cubic 4
Cubic 5
Cubic 6
REMD
400 ns
Zoomed in
B
C
D
Snapshot of fibril in Cubic 5 at 160ns
Typical π-π interaction geometries observed
Parallel displaced
T-shaped
Parallel staggered
Herringbone
E

Figure 3.3

Figure 3.3 caption: WAXS experiments confirm non-normalized RDF calculations. (A) WAXS diffraction pattern for Fmoc-AA gel film shows strong reflection (green arrow) and higher order reflections (green lines) corresponding to a d-spacing of 26.3 Å (n=1). Orange arrow indicates a reflection with d=4.35 Å. (B) Last 50 ns non-normalized RDF plot of distance between fluorenyl rings of Cubic 4, 5, and 6, REMD and the 400 ns simulations. (C) Last 50 ns non-normalized RDF plot of distance between terminal alanine's hydroxyl hydrogen and fibril axis. (D) Last 50 ns non-normalized RDF plot of Fmoc-AAs' strand-to-strand distance, showing predominance of a 0.46-0.48 nm (4.6-4.8 Å) distance between adjacent dipeptides. (E) Representative snapshot taken from Cubic 5 MD simulation displays the π-π stacking in fibril after 160 ns simulation.

Table 3.1 Hydrogen bonds distribution between individual residues on adjacent Fmoc-AA molecules *

Cubic 4	Fmoc	Ala-mid	Ala-term
Fmoc	0 %	28 %	30 %
Ala-mid		15 %	22 %
Ala-term			5 %
Cubic 5	Fmoc	Ala-mid	Ala-term
Fmoc	0 %	31 %	26 %
Ala-mid		19 %	20 %
Ala-term			4 %
Cubic 6	Fmoc	Ala-mid	Ala-term
Fmoc	0 %	17 %	37 %
Ala-mid		15 %	22 %
Ala-term			9 %

* Each matrix adds to 100%. The number of hydrogen bonds is determined with a donor-acceptor distance ≤ 3.5 Å and interaction angle ≤ 30°. The middle and terminal alanines are named “Ala-mid” and “Ala-term”, respectively.

Table 3.2 Distribution of total hydrogen bonds formed between hydrogen bond-capable groups on Fmoc-AA molecules and water molecules *

	Fmoc-O	Ala-mid-O	Ala-mid-NH	Ala-term-O	Ala-term-NH	Ala-term-OH
Cubic 4	25 %	17 %	6 %	17 %	10 %	25 %
Cubic 5	25 %	17 %	5 %	17 %	11 %	25 %
Cubic 6	27 %	19 %	7 %	14 %	11 %	22 %

* Each row adds to 100%.

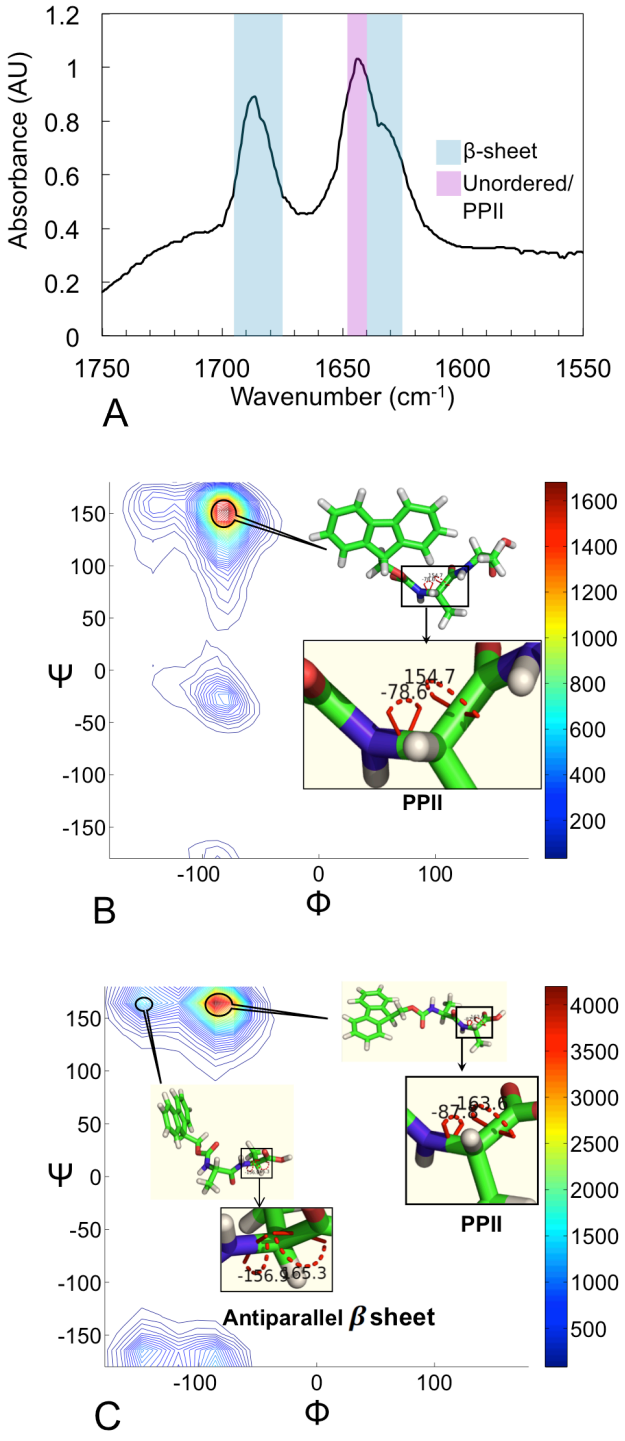
1.2
1
0.8
0.6
0.4
0.2
0
Absorbance (AU)
β-sheet
Unordered/
PPII
1750
1700
1650
1600
1550
Wavenumber (cm-1)
A
150
100
50
Ψ 0
-50
-100
-150
-100
0
100
Φ
154.7
-78.6
PPII
B
1600
1400
1200
1000
800
600
400
200
4000
3500
3000
2500
2000
1500
1000
500
-156.9
65.3
Antiparallel β sheet
C

Figure 3.4

Figure 3.4 caption: Experimental FTIR results and backbone conformational analysis (Ramachandran plot) of simulated assemblies show preferred conformations for Fmoc-AA molecules within fibril assembly. (A) FTIR amide I absorbance data give a peak at 1686 cm^{-1} and a shoulder at 1634 cm^{-1}, similar to that seen in predominantly β-sheet proteins. Another strong absorbance at 1644 cm^{-1} correlates to random coil- or polyproline-like shift in amide C=O stretch frequency. (B) Backbone conformational analysis of middle alanine in Cubic 5 model during the last 50 ns of simulation; PPII-like peak is at ϕ,ψ = (-78°, 152°). (C) Backbone conformational analysis of terminal alanine in Cubic 5 model during the last 50 ns of simulation; PPII-like peak is at ϕ,ψ = (-86°, 164°), β-sheet-like peak is at ϕ,ψ = (-148°, 164°). Results are representative of all simulations performed. In B and C, the color bar represents the population of residues in a range of angles defined by the contour lines.

Table 3.3 Average number of hydrogen bonds between each residue and water, versus each residue and adjacent Fmoc-AA *

	Fmoc··· Fmoc-AA	Fmoc···water	Ala-mid···Fmoc-AA	Ala-mid···water	Ala-term···Fmoc-AA	Ala-term···water
Cubic 4	0.59	1.00	0.66	1.06	0.58	2.23
Cubic 5	0.58	1.00	0.71	1.03	0.51	2.28
Cubic 6	0.51	1.05	0.51	1.09	0.66	1.95

*Unit: hydrogen bonds per residue. "···" denotes hydrogen bonding between the two objects/residues.

3.5 REFERENCES

1. G. M. Whitesides, J. P. Mathias, C. T. Seto, Molecular self-assembly and nanochemistry: a chemical strategy for the synthesis of nanostructures. *Science*. **254**, 1312–1319 (1991).
2. D. J. Adams, P. D. Topham, Peptide conjugate hydrogelators. *Soft Matter*. **6**, 3707–3721 (2010).
3. A. Aggeli *et al*., Hierarchical self-assembly of chiral rod-like molecules as a model for peptide β-sheet tapes, ribbons, fibrils, and fibers. *Proceedings of the National Academy of Sciences*. **98**, 11857–11862 (2001).
4. S. M. Douglas *et al*., Self-assembly of DNA into nanoscale three-dimensional shapes. *Nature*. **459**, 414–418 (2009).
5. L. A. Estroff, A. D. Hamilton, Water Gelation by Small Organic Molecules. *Chem. Rev*. **104**, 1201–1218 (2004).
6. S. Zhang, D. M. Marini, W. Hwang, S. Santoso, Design of nanostructured biological materials through self-assembly of peptides and proteins. *Current Opinion in Chemical Biology*. **6**, 865–871 (2002).
7. V. Jayawarna *et al*., Introducing chemical functionality in Fmoc-peptide gels for cell culture. *Acta Biomater*. **5**, 934–943 (2009).
8. D. J. Adams, Dipeptide and Tripeptide Conjugates as Low-Molecular-Weight Hydrogelators. *Macromol. Biosci*. **11**, 160–173 (2011).
9. J. D. Hartgerink, E. Beniash, S. I. Stupp, Self-Assembly and Mineralization of Peptide-Amphiphile Nanofibers. *Science*. **294**, 1684 –1688 (2001).
10. H. Cui, M. J. Webber, S. I. Stupp, Self-assembly of peptide amphiphiles: From molecules to nanostructures to biomaterials. *Peptide Science*. **94**, 1–18 (2010).
11. O.-S. Lee, S. I. Stupp, G. C. Schatz, Atomistic Molecular Dynamics Simulations of Peptide Amphiphile Self-Assembly into Cylindrical Nanofibers. *J. Am. Chem. Soc*. **133**, 3677–3683 (2011).
12. V. Jayawarna *et al*., Nanostructured Hydrogels for Three-Dimensional Cell Culture Through Self-Assembly of Fluorenylmethoxycarbonyl–Dipeptides. *Advanced Materials*. **18**, 611–614 (2006).
13. X. Li, Y. Kuang, B. Xu, "Molecular trinity" for soft nanomaterials: integrating nucleobases, amino acids, and glycosides to construct multifunctional hydrogelators. *Soft Matter*. **8**, 2801–2806 (2012).
14. R. Orbach *et al*., Self-Assembled Fmoc-Peptides as a Platform for the Formation of Nanostructures and Hydrogels. *Biomacromolecules*. **10**, 2646–2651 (2009).

15. B. Adhikari, A. Banerjee, Short peptide based hydrogels: incorporation of graphene into the hydrogel. *Soft Matter*. **7**, 9259–9266 (2011).

16. B. Adhikari, A. Banerjee, Short-Peptide-Based Hydrogel: A Template for the In Situ Synthesis of Fluorescent Silver Nanoclusters by Using Sunlight. *Chemistry – A European Journal*. **16**, 13698–13705 (2010).

17. Y. Zhang, Y. Kuang, Y. Gao, B. Xu, Versatile Small-Molecule Motifs for Self-Assembly in Water and the Formation of Biofunctional Supramolecular Hydrogels. *Langmuir*. **27**, 529–537 (2011).

18. A. M. Smith *et al*., Fmoc-Diphenylalanine Self Assembles to a Hydrogel via a Novel Architecture Based on π–π Interlocked β-Sheets. *Advanced Materials*. **20**, 37–41 (2008).

19. J. McCammon, B. Gelin, M. Karplus, Dynamics of folded proteins. *Nature*. **267**, 585–590 (1977).

20. M. Karplus, J. A. McCammon, Molecular dynamics simulations of biomolecules. *Nat Struct Mol Biol*. **9**, 646–652 (2002).

21. R. R. Johnson, A. T. C. Johnson, M. L. Klein, Probing the Structure of DNA–Carbon Nanotube Hybrids with Molecular Dynamics. *Nano Lett*. **8**, 69–75 (2008).

22. S. Sun, J. T. Y. Wong, T.-Y. Zhang, Effects of external electric fields on the self-assembly of phospholipids/water mixtures—coarse-grained molecular dynamics simulations. *Soft Matter*. **7**, 9307–9310 (2011).

23. B. Saha, S. Shindo, S. Irle, K. Morokuma, Quantum Chemical Molecular Dynamics Simulations of Dynamic Fullerene Self-Assembly in Benzene Combustion. *ACS Nano*. **3**, 2241–2257 (2009).

24. V. Castelletto *et al*., Self-assembly of Fmoc-tetrapeptides based on the RGDS cell adhesion motif. *Soft Matter*. **7**, 11405 (2011).

25. D. J. Adams *et al*., The delicate balance between gelation and crystallisation: structural and computational investigations. *Soft Matter*. **6**, 4144–4156 (2010).

26. D. J. Adams, L. M. Mullen, M. Berta, L. Chen, W. J. Frith, Relationship between molecular structure, gelation behaviour and gel properties of Fmoc-dipeptides. *Soft Matter*. **6**, 1971–1980 (2010).

27. D. J. Adams *et al*., A new method for maintaining homogeneity during liquid–hydrogel transitions using low molecular weight hydrogelators. *Soft Matter*. **5**, 1856 (2009).

28. J. W. Ponder, F. M. Richards, An efficient newton-like method for molecular mechanics energy minimization of large molecules. *J. Comput. Chem*. **8**, 1016–1024 (1987).

29. B. Hess, C. Kutzner, D. van der Spoel, E. Lindahl, GROMACS 4: Algorithms for Highly Efficient, Load-Balanced, and Scalable Molecular Simulation. *J. Chem. Theory Comput.* **4**, 435–447 (2008).

30. W. L. Jorgensen, D. S. Maxwell, J. Tirado-Rives, Development and Testing of the OPLS All-Atom Force Field on Conformational Energetics and Properties of Organic Liquids. *J. Am. Chem. Soc.* **118**, 11225–11236 (1996).

31. W. L. Jorgensen, J. Tirado-Rives, Potential energy functions for atomic-level simulations of water and organic and biomolecular systems. *PNAS.* **102**, 6665–6670 (2005).

32. J. Zhang, M. King, L. Suggs, P. Ren, Molecular Modeling of Conformational Properties of Oligodepsipeptides. *Biomacromolecules.* **8**, 3015–3024 (2007).

33. N. L. Allinger, Y. H. Yuh, J. H. Lii, Molecular mechanics. The MM3 force field for hydrocarbons. 1. *Journal of the American Chemical Society.* **111**, 8551–8566 (1989).

34. G. A. Kaminski, R. A. Friesner, J. Tirado-Rives, W. L. Jorgensen, Evaluation and Reparametrization of the OPLS-AA Force Field for Proteins via Comparison with Accurate Quantum Chemical Calculations on Peptides†. *J. Phys. Chem. B.* **105**, 6474–6487 (2001).

35. B. Hess, H. Bekker, H. J. C. Berendsen, J. G. E. M. Fraaije, LINCS: A linear constraint solver for molecular simulations. *J. Comput. Chem.* **18**, 1463–1472 (1997).

36. B. Hess, P-LINCS: A Parallel Linear Constraint Solver for Molecular Simulation. *J. Chem. Theory Comput.* **4**, 116–122 (2007).

37. T. Darden, D. York, L. Pedersen, Particle mesh Ewald: An N [center-dot] log(N) method for Ewald sums in large systems. *The Journal of Chemical Physics.* **98**, 10089–10092 (1993).

38. G. Bussi, D. Donadio, M. Parrinello, Canonical sampling through velocity rescaling. *J. Chem. Phys.* **126**, 014101–7 (2007).

39. M. Parrinello, A. Rahman, Polymorphic transitions in single crystals: A new molecular dynamics method. *J. Appl. Phys.* **52**, 7182–7190 (1981).

40. W. F. Van Gunsteren, H. J. C. Berendsen, A Leap-frog Algorithm for Stochastic Dynamics. *Molecular Simulation.* **1**, 173–185 (1988).

41. W. L. Jorgensen, J. Chandrasekhar, J. D. Madura, R. W. Impey, M. L. Klein, Comparison of simple potential functions for simulating liquid water. *J. Chem. Phys.* **79**, 926–935 (1983).

42. D. K. Smith, Lost in translation? Chirality effects in the self-assembly of nanostructured gel-phase materials. *Chem. Soc. Rev.* **38**, 684–694 (2009).

43. B. Nordén, A. Rodger, T. Dafforn, *Linear Dichroism and Circular Dichroism: A Textbook on Polarized-Light Spectroscopy* (Royal Society of Chemistry, 2010).

44. Y. Zhang, H. Gu, Z. Yang, B. Xu, Supramolecular Hydrogels Respond to Ligand–Receptor Interaction. *J. Am. Chem. Soc.* **125**, 13680–13681 (2003).

45. C. Tang, A. M. Smith, R. F. Collins, R. V. Ulijn, A. Saiani, Fmoc-Diphenylalanine Self-Assembly Mechanism Induces Apparent pKa Shifts. *Langmuir*. **25**, 9447–9453 (2009).

46. L. Chen *et al.*, Self-Assembly Mechanism for a Naphthalene–Dipeptide Leading to Hydrogelation. *Langmuir*. **26**, 5232–5242 (2009).

47. S. Kirkpatrick, C. D. Gelatt, M. P. Vecchi, Optimization by Simulated Annealing. *Science*. **220**, 671 –680 (1983).

48. Y. Sugita, Y. Okamoto, Replica-exchange molecular dynamics method for protein folding. *Chemical Physics Letters*. **314**, 141–151 (1999).

49. A. E. García, J. N. Onuchic, Folding a protein in a computer: An atomic description of the folding/unfolding of protein A. *PNAS*. **100**, 13898–13903 (2003).

50. H. Nymeyer, S. Gnanakaran, A. E. García, in *Methods in Enzymology*, L. B. and M. L. Johnson, Ed. (Academic Press, 2004; http://www.sciencedirect.com/science/article/pii/S0076687904830064), vol. 383 of *Numerical Computer Methods, Part D*, pp. 119–149.

51. R. Zhou, in *AIP Conference Proceedings* (AIP Publishing, 2003; http://scitation.aip.org/content/aip/proceeding/aipcp/10.1063/1.1632168), vol. 690, pp. 406–408.

52. R. Zhou, in *Protein Folding Protocols* (Springer, 2006; http://link.springer.com/protocol/10.1385/1-59745-189-4:205), pp. 205–223.

53. R. R. Johnson, A. Kohlmeyer, A. T. C. Johnson, M. L. Klein, Free Energy Landscape of a DNA–Carbon Nanotube Hybrid Using Replica Exchange Molecular Dynamics. *Nano Lett.* **9**, 537–541 (2009).

54. M. G. Wolf, J. A. Jongejan, J. D. Laman, S. W. de Leeuw, Rapid Free Energy Calculation of Peptide Self-Assembly by REMD Umbrella Sampling. *J. Phys. Chem. B*. **112**, 13493–13498 (2008).

55. D. B. Teplow *et al.*, Elucidating Amyloid β-Protein Folding and Assembly: A Multidisciplinary Approach. *Acc. Chem. Res.* **39**, 635–645 (2006).

56. T. J. Richmond, Solvent accessible surface area and excluded volume in proteins: Analytical equations for overlapping spheres and implications for the hydrophobic effect. *Journal of Molecular Biology*. **178**, 63–89 (1984).

57. P. Ren, J. W. Ponder, Polarizable Atomic Multipole Water Model for Molecular Mechanics Simulation. *J. Phys. Chem. B*. **107**, 5933–5947 (2003).

58. A. H. Windle, X-ray scattering measurements of order in non-crystalline polymers. *Pure Appl. Chem*. **57**, 1627–1638 (1985).

59. K. A. Houton *et al*., On Crystal versus Fiber Formation in Dipeptide Hydrogelator Systems. *Langmuir*. **28**, 9797–9806 (2012).

60. H.-G. Braun, A. Z. Cardoso, Self-assembly of Fmoc-diphenylalanine inside liquid marbles. *Colloids and Surfaces B: Biointerfaces*. **97**, 43–50 (2012).

61. E. Gazit, A possible role for π-stacking in the self-assembly of amyloid fibrils. *The FASEB Journal*. **16**, 77–83 (2002).

62. G. B. McGaughey, M. Gagné, A. K. Rappé, π-Stacking Interactions. *Journal of Biological Chemistry*. **273**, 15458–15463 (1998).

63. S. Sun, E. R. Bernstein, Aromatic van der Waals Clusters: Structure and Nonrigidity. *J. Phys. Chem*. **100**, 13348–13366 (1996).

64. R. Tycko, Insights into the Amyloid Folding Problem from Solid-State NMR. *Biochemistry*. **42**, 3151–3159 (2003).

65. J. C. C. Chan, N. A. Oyler, W.-M. Yau, R. Tycko, Parallel β-Sheets and Polar Zippers in Amyloid Fibrils Formed by Residues 10–39 of the Yeast Prion Protein Ure2p. *Biochemistry*. **44**, 10669–10680 (2005).

66. D. M. Ryan, S. B. Anderson, B. L. Nilsson, The influence of side-chain halogenation on the self-assembly and hydrogelation of Fmoc-phenylalanine derivatives. *Soft Matter*. **6**, 3220–3231 (2010).

67. Z. Yang *et al*., Enzymatic Formation of Supramolecular Hydrogels. *Advanced Materials*. **16**, 1440–1444 (2004).

68. S. Sutton *et al*., Controlled Release from Modified Amino Acid Hydrogels Governed by Molecular Size or Network Dynamics. *Langmuir*. **25**, 10285–10291 (2009).

69. M. Jackson, H. H. Mantsch, The Use and Misuse of FTIR Spectroscopy in the Determination of Protein Structure. *Critical Reviews in Biochemistry and Molecular Biology*. **30**, 95–120 (1995).

70. M. A. Bryan *et al*., FTIR Studies of Collagen Model Peptides: Complementary Experimental and Simulation Approaches to Conformation and Unfolding. *J. Am. Chem. Soc*. **129**, 7877–7884 (2007).

71. R. Lakshminarayanan, D. Fan, C. Du, J. Moradian-Oldak, The role of secondary structure in the entropically driven amelogenin self-assembly. *Biophys. J*. **93**, 3664–3674 (2007).

Chapter 4: β-sheets not required: combined experimental and computational studies of self-assembly and gelation of the ester-containing analogue of an Fmoc-dipeptide hydrogelator

4.0 FOREWORD

This chapter is adapted from a research paper we published in 2014.[2] It is a follow up study to the work described in the publication on which Chapter 3 is based. I am listed as a co-first-author with Xiaojia Mu, however my name appears first because the paper is weighted toward the experimental work, which I performed. I designed and performed experimental work and wrote the associated methods and results/discussion sections, and Xiaojia Mu designed and performed all computational simulations and wrote the associated methods and results/discussion sections. Marissa Ruehle was an undergraduate research assistant who helped perform wet-lab experiments. Profs. Laura Suggs and Pengyu Ren conceptualized the research and aided in research design.

4.1 INTRODUCTION

Peptide-based low molecular weight gelators (LMWG) hold great promise for use as biomaterials for tissue engineering. These short peptides, typically conjugated to an N-terminal hydrophobic protecting group, can be triggered to self-assemble into gel-forming nano-fibrillar structures via a pH change, solvent switch, and/or heating and subsequent cooling (*1*). Because of this ability to trigger their self-assembly, peptide-conjugate LMWGs may be ideal for placement by injection; many polymer gel systems previously proposed for use as biomaterials require photo-initiators for crosslinking by

[1] K. M. Eckes, X. Mu, M. A. Ruehle, P. Ren, L. J. Suggs, β Sheets Not Required: Combined Experimental and Computational Studies of Self-Assembly and Gelation of the Ester-Containing Analogue of an Fmoc-Dipeptide Hydrogelator. *Langmuir*. **30**, 5287–5296 (2014).

UV light, which is highly scattered by biological tissues. Peptides also have inherent sequence-specific biological activity, which may be easily leveraged to enhance therapeutic cell signaling or promote cell-biomaterial adhesion. Finally, with recent examples of these peptide-based LMWGs using naturally occurring hydrophobic N-protecting groups (such as DNA bases (*2*) or groups with known biocompatibility (such as ibuprofen (*3*) and naproxen (*4*), these materials are likely to be highly biocompatible and possibly even actively anti-bacterial and anti-inflammatory.

While peptide-based gels possess many properties favorable for use as biomaterials, they are not readily degradable by non-enzymatic means at physiological pH and temperature. For this reason, our group has been developing synthetic protocols for ester-containing depsipeptides that have side-chain functionality analogous to peptides. As esters have a half-life over 1000 times shorter than that of amide bonds (*5*), depsipeptides are prone to hydrolysis over a time scale relevant to wound healing and tissue remodeling processes. We have developed di-depsipeptide units (containing a single N-protected amino acid conjugated to an alpha-hydroxy acid via an ester linkage) that can be coupled to other amino acids or depsipeptide units using standard solid-phase peptide synthesis chemistries (*6*).

The general structure of a depsipeptide unit is almost identical to that of a fluorenylmethyloxycarbonyl (Fmoc)- protected dipeptide. Several Fmoc-dipeptides have been reported to self-assemble into nano-fibrillar structures to form hydrogels, and it has been hypothesized that β-sheet-like hydrogen bonding between amide bonds on adjacent molecules helps to drive self-assembly and stabilize the supramolecular nanostructures (*1*, *7*). We recently developed computational simulation techniques to model self-assembly of Fmoc-Ala-Ala (abbr. Fmoc-AA), a simple Fmoc-dipeptide with uniform side chain functionality, and we found that amide-amide hydrogen bonding comprises less

than 10% of the total number of hydrogen bonds between Fmoc-Ala-Ala molecules in a supramolecular assembly (*8*). Given these results, we hypothesized that Fmoc-depsipeptides may be able to self-assemble into gel-forming nanostructures under similar conditions as an analogous Fmoc-dipeptide.

A depsipeptide analogue of an Fmoc-dipeptide contains an ester bond in place of an amide bond. Because esters lack a hydrogen bond donor, they are unable to interact with adjacent ester bonds via hydrogen bonding. Therefore a depsipeptide analogue serves as an ideal model for testing whether or not β-sheet-like amide-amide hydrogen bonding is truly a requirement for self-assembly and gelation of N-terminal hydrophobic protected peptides. In this paper we show that Fmoc-Ala-Lac (abbr. Fmoc-ALac), the depsipeptide analogue of the known LMWG Fmoc-Ala-Ala, indeed undergoes self-assembly and gelation despite its inability to form specific β-sheet-like hydrogen bonds. Morphological characterization of the gels shows striking similarities, whereas spectroscopic and mechanical analysis reveal distinct differences in the two systems that are attributable *only* to differences in the extent of hydrogen bonding. We also performed computational simulations of the self-assembly process of these molecules to compare the features of Fmoc-Ala-Lac Fmoc-Ala-Ala that are not readily measurable by experimental means, including the number and nature of hydrogen bonds formed, intra-fibril stability, and fibril-fibril aggregation potential. When combined, the results of the experimental and computational work herein provide critical information needed for successful design of new degradable, injectable, and biologically active biomaterials based on modified peptides.

4.2 MATERIALS AND METHODS

4.2.1 Experimental Details

4.2.1.1 Fmoc-L-Ala-L-Ala-OH.

The N-protected dipeptide was purchased from Bachem, Inc. (Torrance, CA) and used without further purification.

4.2.1.2 Fmoc-L-Ala-L-Lac-OH Synthesis.

Fmoc-L-Ala-L-Lac-OH was synthesized using the general strategy for depsipeptide unit synthesis introduced by Nguyen et al (*6*). Synthesis and purification details as well as identification and purity analysis though NMR and HPLC-MS can be found in the **Appendix Section A.2** and **Figure A.3**.

4.2.1.3 Gel preparation.

All gels characterized in this study were prepared using a pH switch method. To a solution of either Fmoc-AA or Fmoc-ALac, 1 eq. 0.5 M NaOH was added in order to deprotonate and dissolve the molecules. This mixture was vortexed and sonicated just until clear, then immediately added to a small volume of 1 eq 0.1 M HCl in a separate vial to reduce gel inhomogeneity. Gelator solutions at high pH were always prepared fresh and gelled immediately to prevent Fmoc removal. Although related work would indicate that ester-containing Fmoc-ALac gels are relatively stable to hydrolysis over the time course of analysis experiments (*9*), to minimize these effects only freshly prepared gels were analyzed. For 5 mg/mL gels, the final pH of Fmoc-AA gels was between 3.1 and 3.5, and the final pH of Fmoc-ALac gels was between 3.2 and 3.4.

4.2.1.4 Transmission Electron Microscopy (TEM).

TEM samples were prepared using 5 mg/mL gels. Approximately 10 μL of gel was placed on the shiny side of a non-glow-discharged 300-mesh carbon coated copper grid (Electron Microscopy Sciences, Hatfield, PA) and allowed to adsorb for 2 minutes. Excess gel and water were wicked away using filter paper, and the grid was placed shiny side down on top of a 10 μL drop of DI water for 30 seconds to wash away any salts. After wicking the washing water with filter paper, grids were placed shiny side down on top of a 10 μL drop of 4% uranyl acetate in water for 1 minute. Finally, the uranyl acetate solution was wicked away using filter paper and the grids allowed to dry completely before imaging. Samples were imaged at the nanometer scale using a FEI Tecnai instrument with an acceleration voltage of 80 kV, and the AMT Advantage HR 1kX1k digital camera associated with the instrument was used to produce digital micrographs.

4.2.1.5 Wide Angle X-ray Scattering (WAXS).

All gel samples were prepared at 5 mg/mL as described above and allowed to dry slowly on single crystal quartz slides over 48 hours in a humid environment, then dried completely *in vacuo*. Dried gel films were subjected to x-rays operating at a wavelength of 1.54059 Å (Cu K-α1) on a Scintag X1 θ-θ powder diffractometer. Diffraction patterns were analyzed using Jade v9.1.1 (Materials Data, Inc.) software.

4.2.1.6 Fourier Transform Infrared Absorption (FTIR) spectroscopy.

Gel samples for FTIR were prepared at 5 mg/mL and were prepared by tightly sandwiching gels between two calcium fluoride (CaF_2) windows, which were then seated within a flow cell. Solution phase samples were prepared at 20 mg/ml in ethanol to ensure adequate signal and were loaded into a sample cell composed of two CaF_2 windows separated with 50 μm thick PET spacers. All samples were measured using a

transmission configuration. A Bruker Vertex 70 FTIR instrument equipped with a liquid nitrogen-cooled MCT detector collected and averaged 250 scans (4000 cm^{-1} to 400 cm^{-1}) of each sample spectrum at a 2 cm^{-1} resolution. The ethanol background spectrum was subtracted from all solution phase sample spectra, and an empty flow cell background spectrum was subtracted from all gel phase sample data.

4.2.1.7 Circular Dichroism (CD) spectroscopy.

A Jasco J-815 instrument was used to collect CD spectra. 5 mg/mL gels were placed in a cylindrical demountable quartz cuvette with a pathlength of 0.1 mm for analysis. Background scans consisted of water containing the same concentrations of NaOH and HCl used to induce gelation of Fmoc-AA and Fmoc-ALac, and all scans were performed at a scan speed of 200 nm/min with a data pitch of 0.5 nm and response time of 1 s. For each scan, three spectra were taken with background subtraction then averaged to give the final spectrum. Linear dichroism artifacts were characterized by rotating the cuvette 90, 180, and 270 degrees from the original orientation, but were found to be small for both Fmoc-AA and Fmoc-ALac gels.

4.2.1.8 Rheological characterization.

The storage and loss moduli of Fmoc-AA and Fmoc-ALac gels were determined using an Anton-Paar Physica MCR-101 rheometer with a parallel-plate geometry (top plate diameter of 8 mm). 5 mg/mL gels for rheological analysis (n = 4 for each system) were formed within polystyrene cloning cylinders (~8 mm inner diameter) adhered to a polystyrene petri dish with silicone grease. Each gel had a volume of 200 μL. For all tests the operating height of the top plate was 2.5 mm to ensure good contact with the gel's top surface, which was often concave due to the meniscus formed within the cloning cylinder during gelation. Because the gel diameter matched that of the top plate, gels were not

trimmed prior to analysis. The strain amplitude used in the tests was 1%, and the angular frequency was varied from 0.2 to 5 rad/s over 8 points. For each gel, the storage and loss moduli were calculated as the average of the 8 points.

4.2.2 Computational Details

4.2.2.1 Molecular dynamics (MD) simulations.

MD simulations were performed on Fmoc-AA and Fmoc-ALac fibrils. The simulated fibril structures were based on previous results derived for the Fmoc-AA fibril (100 molecules that had already gone a 160 ns simulation and were proven to be stable) (*8*). MD simulations were performed using GROMACS (version 4.5.4). The atomic force field parameters were transformed from OPLS-AA (*10*), OPLS-AA/L (*11*), MM3 (*12*), and our previous work (*8*). Molecular dynamics simulations were performed on the Texas Advanced Computing Center's "Lonestar" supercomputer. All simulations were applied periodic boxes with explicit TIP3P water molecules, and all were subjected to steepest descent energy minimizations with 5000 maximum steps to remove high-energy contacts. In order to keep the system stable at 300 K and 1 bar, a 100 ps NVT and a 100 ps NPT equilibration were applied respectively. The LINCS algorithm was applied to constrain bonds (*13*). Further details can be found in our previous paper (Chapter 3 of this dissertation) (*8*). Modeling parameters were derived from previous studies (*8*, *14*) and final simulated fibril structures in .pdb format are provided in the online Supporting Information for this publication.

4.2.2.2 Melting temperature simulations.

For DNA and similar materials stabilized largely by non-covalent intermolecular interactions, the measurement of a "melting temperature" can be used to quantify the

material's stability and predict sequence-dependent thermodynamic behavior (*15–17*). In this work, we simulated a similar melting procedure and obtained the melting curves to understand the effect of replacing the amide bond of Fmoc-AA with an ester bond. When the temperature is gradually increased to some point (the so-called "melting temperature" in this article), the non-covalent interactions between individual molecules within a fibril structure will be disrupted, and therefore the fibril structure breaks apart and the fraction of the molecular surface area exposed to solvent will increase. By measuring the solvent accessible surface area (SASA) with increasing temperature from 670-870K, we quantitatively estimated the effect of changing the terminal residue (Ala to Lac) on non-covalent intermolecular interactions between Fmoc-dipeptides within a self-assembled fibril structure. During the simulations, for each selected temperature window at least one 50 ns MD simulation was performed and the last 30 ns' SASA results were averaged to plot. The standard deviation for each point has been indicated as error bars in **Figure 4.5 A**.

4.2.2.3 Potential of mean force.

In our previous study (*8*) (also Chapter 3 of this dissertation), we have observed that the surface of fibril is composed of both hydrophobic and hydrophilic regions, which may lead to higher order aggregation behavior (*18*). Using a collective reaction coordinates between two fibrils surfaces, we described the assembly procedure via depicting the potential of mean force (PMF) profile (*19*). With the MD simulated fibril structure (each of which had undergone an MD simulation for 100 ns at least), for each Fmoc-dipeptide system, we investigated the PMF for fibril-fibril assembly. We harmonically restrained two fibrils at increasing center-of mass (COM) distances (so-called "sampling windows,") and therefore a series of configurations along a single

degree of freedom were achieved. With the weighted histogram analysis method (WHAM) (*20*), the inter-fibril PMF was constructed along the dissociation coordinates.

4.3 RESULTS AND DISCUSSION

4.3.1 Experimental analysis

One of the goals of this study was to better understand the role of amide-amide hydrogen bonding in the self-assembly of short, conjugated peptides. To eliminate the ability of Fmoc-AA to hydrogen bond via protein-like amide-amide hydrogen bonding interactions, we synthesized Fmoc-Ala-Lac (Fmoc-ALac), an ester-containing analogue of Fmoc-AA in which the terminal alanine residue is replaced by lactic acid. As lactic acid is the α-hydroxy acid side chain analogue of alanine, the use of lactic acid in place of alanine results in a change in the molecule at only one site—replacing the -NH group in the backbone with an oxygen atom, as illustrated in **Figure 4.1 A**. Because the resulting ester group contains no hydrogen atoms, it acts only as a hydrogen bond acceptor rather than a donor *and* acceptor. Ester groups are therefore unable to form hydrogen bonds with other ester groups on adjacent molecules. This short conjugated depsipeptide thus serves as an ideal system for assessing the importance of hydrogen bonding in the self-assembly of short aromatic N-protected peptides.

Despite the inability for neighboring ester bonds to interact via hydrogen bonding, Fmoc-ALac (**Figure 4.1 B, bottom**) self-assembles to form a self-supporting gel (as evidenced by the inverted vial test) under the exact same conditions as Fmoc-AA (**Figure 4.1 B, top**). Furthermore, upon inspection of the gels at the nano-scale by Transmission Electron Micrsocopy (TEM), we find that both Fmoc-AA and Fmoc-ALac gels consist of flat, ribbon-like structures. Fmoc-ALac nanostructures are wider and seemingly more

aggregated than Fmoc-AA ribbons. From a purely morphological standpoint both at the macro- and nano-scale, amide-amide hydrogen bonding (and specifically β-sheet like hydrogen bonding) appears not to be absolutely crucial for self-assembly of short peptides into nanofibrillar structures that entrap water to form gels, but the larger structure size and therefore reduced gel clarity in Fmoc-ALac systems are clearly a result of the chemical change.

Wide Angle X-ray Scattering (WAXS) experiments also reveal important similarities between the two systems. Dried films of Fmoc-AA and Fmoc-ALac were analyzed and found to have strikingly similar diffraction patterns in terms of reflection *d*-spacing and relative peak intensities (**Figure 4.1 C**). The majority of the peaks in each pattern are higher order reflections (presumably attributable to regular fibril stacking during drying) of the leftmost peak, which for Fmoc-AA corresponds to a *d*-spacing of 26.6 Å and for Fmoc-ALac, 26.0 Å. This dimension is thought to be the characteristic "unit cell" distance, which in this case would be the diameter of the supramolecular fibril structure that, when aggregated, gives rise to the ribbon structures seen in TEM (*7*, *21*). The absence of amide-amide hydrogen bonding, whether β-sheet like or not, therefore seems to have little impact on the characteristic dimensions of the smallest fibrils that form as a result of self-assembly.

Another crucial similarity is apparent. The diffraction patterns for *both* Fmoc-AA and Fmoc-ALac contain a unique (i.e. not a higher order) reflection corresponding to a *d*-spacing of 4.3-4.4 Å indicated by the green arrows. Similar dimensions have been previously attributed to the distance between adjacent peptide chains within anti-parallel β-sheets (*7*, *21*). Through a previous computational analysis of Fmoc-AA self-assembly we discovered that this dimension could also correspond to the predominant interaction distance between Fmoc-groups toward the center of the fibril (*8*). The direct experimental

evidence presented here supports our computational findings, since Fmoc-ALac molecules' ester residues preclude them from associating in a "conventional" β-sheet manner. It is still possible that this dimension corresponds to spacing between the backbones of adjacent molecules, but our system allows us to rule out this dimension seen in WAXS as *specific to* and *characteristic of* β-sheets in these supramolecular structures. It should be noted that Adams and colleagues have reported that the drying of gel films may cause supramolecular rearrangements unrepresentative of the gel phase structure (*22*). However, for the sake of comparison with previous studies in which dried gel films were subjected to powder x-ray diffraction to measure supramolecular structural dimensions, we opted to use this simple method.

Spectroscopic analysis of solutions and self-assembled gels of Fmoc-AA and Fmoc-ALac reveals distinct differences between the two systems attributable only to their backbone bond chemistry. For reference, structures of Fmoc-AA and Fmoc-ALac molecules are reproduced in **Figure 4.2 A** with bond chemistry and carbonyl bonds highlighted to aid in interpretation of FTIR spectra in **Figure 4.2 B**. FTIR spectra of the molecules in solution (20 mg/ml in ethanol, **Figure 4.2 B, top**) show a vibration present in both systems at 1707- 1709 cm^{-1} and similar shoulder peaks at ~1728 cm^{-1}. A spectrum of Fmoc-Ala-OH in ethanol was also included to aid in peak assignment, and in this spectrum we see the same peak at 1706 cm^{-1} and a shoulder between 1720 and 1733 cm^{-1}. Other readily apparent spectral features are an intense peak in the Fmoc-AA spectrum at 1670 cm^{-1}, and a broad shoulder peak unique to Fmoc-ALac at ~1750 cm^{-1}.

Similar feature overlap is also observed in the gel phase (5 mg/mL in D_2O, **Figure 4.2 B, bottom**), where the shared vibration occurs at 1687 cm^{-1}. Fmoc-AA's unique vibration occurs at 1646 cm^{-1}, and Fmoc-ALac's at 1740 cm^{-1}. Though the peaks are shifted likely due to solvent interactions, all of these vibrations fall within the carbonyl

stretching absorption band (1870-1540 cm^{-1}) (*23*). A reference spectrum of Fmoc-Ala-OH is not included in **Figure 4.2 B**, as this molecule precipitates and does not gel under the same conditions as Fmoc-AA and Fmoc-ALac. A non-normalized version of this plot is provided in the Appendix (**Figure A.4**).

It is well known that the amide I (C=O) absorption band is centered around 1650 cm^{-1}, and therefore we attribute Fmoc-AA's unique vibration at 1646 cm^{-1} in D_2O and 1670 cm^{-1} in ethanol (shaded in light blue in **Figure 4.2 A and B**) to its amide carbonyl stretch. Furthermore, Fmoc-ALac's unique absorption at 1740 cm^{-1} in D_2O and shoulder at ~1750 cm^{-1} in ethanol (shaded in light red) falls within the range for the carbonyl stretch of saturated aliphatic esters (1750-1735 cm^{-1}) (*23*), and therefore we attribute this absorption to the ester bond between alanine and lactic acid. We attribute the gray-shaded shoulder peak absorptions (shared between Fmoc-AA, Fmoc-ALac, and Fmoc-Ala-OH in the solution phase and Fmoc-AA and Fmoc-ALac in the gel phase) to the carboxylic acid carbonyl stretch, as this peak is misaligned only in the aqueous gel phase, indicating the effect of pH and potentially different protonation state. The stronger shared absorption (shaded in light purple) therefore must represent the carbamate carbonyl stretching absorption. The shared peak also corresponds to a frequency range consistent with previous demonstrations of the carbamate carbonyl stretching absorption (*24–26*).

Importantly, these data serve as unambiguous evidence to rule out the higher frequency (1687 cm^{-1} in D_2O) carbonyl absorption as an indicator of the presence of antiparallel β-sheets in supramolecular assemblies of Fmoc-dipeptides. In FTIR spectra of solutions of proteins with high antiparallel β-sheet content, two peaks between 1625-1640 cm^{-1} and 1675-1695 cm^{-1} are typically observed in the amide I range (*27*), and many papers from another group studying Fmoc-peptide self-assembly have put forth similar-looking spectra in argument of the presence of specific β-sheet like interactions within

self-assembled structures (*7*, *21*, *28*, *29*). As this peak near 1690 cm^{-1} is present in β-sheet-incapable Fmoc-ALac systems and overlaps the Fmoc-AA spectrum exactly in both sol and gel phase, one must conclude that this absorption is not due to specific β-sheet like modulation of the amide I carbonyl stretching frequency and should therefore no longer be assumed to indicate the presence of antiparallel β-sheet structures in Fmoc-dipeptide systems.

Fleming et al. independently discovered that this higher frequency peak arises from the carbamate carbonyl stretch by showing that the peak disappears from the IR spectrum when Fmoc is replaced with fluorenylmethylcarbonyl (Fmc), which is coupled to the peptide via an amide bond rather than a carbamate group (*30*). Both of these examples of small structural changes leading to greatly altered IR spectra illustrate that attempts to elucidate supramolecular structural features of short peptide conjugate systems using canonical protein spectroscopic data for comparison may be inappropriate.

CD spectroscopy also reveals important differences between the two systems. As shown in **Figure 4.2 C**, both Fmoc-AA and Fmoc-ALac systems exhibit marked dichroism in the gelled state (solid line) relative to the solution state (high pH, dotted line), confirming that both molecules self-assemble into nanostructures with supramolecular chirality. The most apparent difference between the two spectra is the feature above 280 nm. Similar fine structure is apparent in both spectra, but Fmoc-AA exhibits far less dichroism than Fmoc-ALac. Transitions in this range are often seen in aromatic amino acids placed in chiral environments (*31*) and Xu and co-workers previously assigned a peak at 304 nm as the π-π^* transition induced by interactions of fluorenyl groups within a supramolecular assembly of both D- and L- forms of Fmoc-AA (*32*). We hesitate to make specific structural conclusions from lower wavelength spectral

features, as we have argued in previous work that such assignments are often inappropriately based on data obtained from protein solutions (*8*).

Viscoelastic analysis by oscillatory rheometry (frequency sweep, **Figure 4.3 A**) shows a significant difference between the strength of Fmoc-AA and Fmoc-ALac hydrogels directly attributable to differences in the backbone chemistry of the two molecules and the resulting effect on self-assembly. **Figure 4.3 B** shows the average storage and loss moduli of small Fmoc-AA and Fmoc-ALac hydrogels at a concentration of 5 mg/mL. The storage modulus (G') of Fmoc-AA is roughly twice that of Fmoc-ALac. Owing to the presence of hydrogen bond-capable amide groups, Fmoc-AA assemblies are potentially held together by many more intermolecular interactions than ester-containing Fmoc-ALac structures. However, it is unclear how exactly this difference translates into differences in bulk mechanical properties. It may be that these self-assembled systems are similar to fibrin gel systems, in which gel strength is governed both by fiber size and network branchpoint density, two characteristics that are interconnected (*33*). Within the context of these findings, it seems that while Fmoc-AA assemblies form thinner fibers/ribbons, these structures are more extensively entangled (as shown in TEM), leading to stronger bulk gels. Under the same conditions, Fmoc-ALac assemblies tend to form larger aggregates that are necessarily less branched and therefore contribute less to overall gel strength.

Several studies in Fmoc-FF systems have found that final gel pH relative to apparent pKa is important in governing nanoscale feature size and mechanical properties (*21*, *34*). Generally speaking, Fmoc-FF forms gels just below its apparent pKa, and gels exhibit thicker fibers and enhanced mechanical strength as pH drops further below the apparent pKa (up to the point of precipitation). Fmoc-AA has a higher apparent pKa (~5.1) than does Fmoc-ALac (~4.3) (see titration data in **Appendix Figure A.5**), and all

else equal one would expect that at the same final pH (~3.1-3.5) Fmoc-AA would exhibit larger structure sizes than Fmoc-ALac. As this is opposite as what we have described, it appears that ester replacement has implications for higher-order aggregation beyond pH relative to apparent pKa. Indeed, Raeburn et al. have studied variability in reported mechanical properties of Fmoc-dipeptide gels and concluded that the gel formation method and kinetics seem to influence rheology as much as the final gel pH relative to the apparent pKa of the system (*35*). We have observed that self-assembly leading to gelation proceeds more slowly for Fmoc-ALac than Fmoc-AA under the same gelation conditions, as gelation occurs in mere seconds for Fmoc-AA and several minutes for Fmoc-ALac. Therefore, it is possible that kinetics alone may determine the difference in mechanical properties; however, to our knowledge no strong correlation between self-assembly kinetics and final gel modulus has been well-established, likely because gelation kinetics often depend upon the gelation method. It is therefore very difficult to predict and/or rationalize differences in mechanical properties between related gelator systems.

4.3.2 Computational simulations and analysis

In this work, we characterized the conformational features of self-assembled Fmoc-ALac and compared the results with our previous observations from molecular dynamics simulations of the Fmoc-AA self-assembly (*8*). Similar to what we previously observed in Fmoc-AA simulations, Fmoc-ALac molecules form a stable fibril structure, as demonstrated by the plateau of the fibril's total number of hydrogen bonds (includes H-bonds with water) per molecule (**Figure 4.4 A**) and solvent-accessible surface area (SASA, **Figure 4.4 B**) vs. time. The number of H-bonds (~3.3/molecule) and SASA

(~1.6 nm^2/molecule) of the Fmoc-ALac fibril converge to smaller values than the Fmoc-AA results (~4 H bonds/molecule and SASA ~1.7 nm^2/molecule); this result is consistent with our hypothesis that substituting lactic acid for alanine to result in an ester linkage would reduce hydrogen bonding between neighboring molecules within an assembly.

Radial distribution function (RDF) analysis of the fibril structures also indicates similar assembled structures between Fmoc-AA and Fmoc-ALac systems. **Figures 4.4 C** and **D** show the RDF of the peptide terminus - fibril center and the Fmoc-Fmoc centroid distance, respectively. The peak in the former RDF corresponds to the fibril radius. The fibril radius for Fmoc-ALac is virtually indistinguishable from that of Fmoc-AA by RDF analysis, confirming our experimental WAXS results that suggest a very similar fibril size between the two systems. Also, as suggested previously in the discussion of experimental results, the reappeared unique *d*-spacing of 4.3-4.4 Å in WAXS and predominant Fmoc-Fmoc and strand-strand distance (**Appendix Figure A.6**) of 4-5 Å from RDF analysis of computational results for Fmoc-ALac assemblies suggest that this dimension is likely not indicative specifically of β-sheet interactions. Rather, it appears that the strand-strand and Fmoc-Fmoc association distances are quite similar between the two systems and independent of the difference in propensity for hydrogen bonding between adjacent molecules.

Similar to the observations in our previous Fmoc-AA study, the distribution of backbone torsion (ϕ,ψ) angles (**Figures 4.4 E** and **F**, respectively) for the alanine residue in Fmoc-ALac suggests that polyproline II-like angles are predominant. Interestingly, the Ramachandran plot for the terminal Lac residues indicates that Lac predominantly adopts torsional angles within the α-helix secondary structure region, which had not been observed in the earlier Fmoc-AA study. Notably, in a previous study of depsipeptide conformational properties in solution, we observed that Lac did show a high population

in α-helix region when adjacent to glycine residues but not next to lysines, suggesting the Lac residue's conformation strongly depends on the chemistry of the adjacent residues (*14*). In the current study, the situation is more complicated; as the peptides aggregate, the environment (water and other peptide molecules) would also have an impact. Also, note that there are some Lac structures near the (-150, 0) region, which is a result of unique intramolecular interactions arising from the ester group (*14*). The Ramachandran plots (**Figures 4.4 E and F**) reflect average distributions of individual residues' torsion angles within the fibrils. Previous studies on free alanine dipeptides (*36*) and depsipeptides (*14*) in solution show similar Ramachandran patterns as those observed in this work, with dominant polyproline-II-like populations that are not present in gas-phase simulations. Thus, we reason that solvation by water is likely the main cause of the observed conformational distribution with some variation arising from the packing of molecules within the supramolecular assembly.

An ensemble of non-covalent forces including aromatic stacking, hydrogen bonding, electrostatic and van der Waals interactions drive the self-assembly of low molecular weight hydrogelators, including short peptides. These diverse forces stabilize the supramolecular structures resulting from Fmoc-dipeptide self-assembly and likely drive further assembly into higher order structures. To understand the extent and nature of non-covalent interactions in the Fmoc-AA and Fmoc-ALac systems, we performed melting temperature and potential of mean force (PMF) studies, computational tools to examine the relative stability of self-assembled fibrils upon modification of the peptide backbone chemistry (*37*, *38*). To investigate the strength of the intermolecular interaction between Fmoc-dipeptides within fibril aggregation, we computed "melting" curves for both Fmoc-AA and Fmoc-ALac, as shown in **Figure 4.5 A**. We increased temperatures from 400K to 850K and performed a 50 ns MD simulation at each selected temperature

window for Fmoc-AA and Fmoc-ALac separately. Note that computational "temperature" has no analogy to experimental values, as simulations were performed under high pressures and natural effects such as reaction and decomposition were not accounted for. While not directly experimentally relevant, the use of this technique provides us with a measure of relative stability between the two systems.

The fibril's SASA has been calculated as the measurement of melting. In the low temperature regime (<400K in **Figure 4.5 A**) the Fmoc-AA shows a larger SASA than Fmoc-ALac that persists during heating from 500 to 750K. At 800K or above, the assembly is completely "melted" (solvated in water), and thus Fmoc-AA and Fmoc-ALac reached the same SASA. The inflection points around 670-700K for both Fmoc-AA and Fmoc-ALac suggest a "melting temperature"; Fmoc-ALac's melting point at roughly 700 K is about 50 K higher than that of Fmoc-AA. This observation suggests the Fmoc-ALac fibril structure is slightly more stable than the Fmoc-AA fibril. Furthermore, the lower SASA values for Fmoc-ALac at most temperatures suggest a more "hydrophobic" character of the fibril, i.e. individual Fmoc-ALac molecules prefer co-aggregation over solvation in water to a greater degree than Fmoc-AA molecules.

We have noted in previous simulations the apparently amphiphilic nature of the surface of stable Fmoc-AA fibrils (*8*). In this work, we also observed that the simulated Fmoc-ALac fibril's surface was similarly amphiphilic. Hydrophobicity has been widely discussed as a multifaceted phenomenon observed in self-assembled systems (*39*). In our system the hydrophobic units exposed on the observed fibril's amphiphilic surface likely reduce the volume of available configuration space for hydrogen bonding with other fibrils or water but increase the possibility of forming hydrophobic assemblies with other fibrils. On the other hand, the hydrophilic components--mainly the hydroxyl group on terminal alanine or lactic acid -- affect the assembly between fibrils by rearranging the

adjacent water molecules' orientations, and such amphiphilic assembly has already been widely discussed in studies including micelle formation (*39*, *40*).

In this work, to further determine the potential effects of presenting an amphiphilic surface, we first derived the inter-fibril association energy from the potential of mean force (PMF) between two fibrils, as shown in **Figure 4.5 B**. In our simulations, we harmonically restrained two fibrils (each of which had undergone an MD simulation for 100 ns at least to reach a stable structure) at increasing center-of mass (COM) distances (so-called "sampling windows,") using an umbrella biasing potential, with the defined reaction coordinate sampled by multiple windows. The inter-fibril interaction energies were computed along the dissociation coordinates using WHAM (see ***Potential of Mean Force*** in the **Computational Details** section). Interestingly, the interaction energy minimum occurred at a COM distance of 3.25-3.5 nm, which is in good agreement with fibril diameters we determined by WAXS experiments and RDF calculations, and which also indicates an energetic preference for fibril-fibril surface contact, i.e. aggregation. As predicted by the PMF calculations, with no covalent bonds breaking or forming, the dissociation energies between two fibrils differ: the Fmoc-AA two-fibril system has a less favorable dissociation energy (or lower barrier to break the association) than the analogous Fmoc-ALac system, indicating that Fmoc-ALac fibrils tend to aggregate more easily. Taken with the melting temperature calculations, this observation indicates that both the intra- and inter-fibril interactions in Fmoc-ALac are somewhat stronger than in Fmoc-AA assemblies.

In order to examine the effect of Ala vs. Lac within simulated fibril systems more closely, we calculated the residue- and bond-specific solvent accessible surface area, as well as the number and specific connectivity of H-bonds formed between Fmoc-AA or Fmoc-ALac molecules and water at the solvent interface of the fibril. As suggested in the

discussion of the melting temperature and PMF results, Fmoc-ALac fibrils appear to form tighter aggregates than Fmoc-AA fibrils. The SASA and H-bonding values calculated here support that observation and are presented in **Tables 4.1 and 4.2**, respectively.

From these calculations, we observed that the substitution of the amide group with an ester from Fmoc-AA to Fmoc-ALac: 1) leads to a decreased total SASA and therefore fewer H-bonds with water molecules; 2) reduces the middle alanine carbonyl group's H-bonding ability with water while only slightly reducing the SASA; and 3) slightly enhances the hydrophobic Fmoc groups' exposure on the surface; and 4) reduces the exposure to water of the between-residue bond, which in the case of Fmoc-AA is an amide bond capable of acting as an H-bond donor. Therefore, the replacement of Ala with Lac leads to a decreased overall fibril hydrophilicity by decreasing the SASA and H-bonding with the solvent (water). Remarkably, the average total number of hydrogen bonds between the Fmoc-AA fibril and water is 23% higher than the Fmoc-ALac fibril. This result suggests that Fmoc-AA structures are more hydrated than Fmoc-ALac fibrils. Combined with the melting and PMF studies, these results corroborate well our TEM images that suggest that under the same gelation conditions, Fmoc-ALac gels contain larger structures that result from an increased aggregation of fibrils relative to Fmoc-AA fibrils. As discussed earlier, it is possible that the consequence of this behavior on the macro scale is that Fmoc-ALac forms larger fibrils at the expense of network branchpoint density, resulting in its reduced bulk mechanical strength relative to Fmoc-AA, as indicated in **Figure 4.3**.

Taken together, these experimental and computational results provide a new perspective of the role of the amide bond in the self-assembly of short peptide-based gelator systems. Whereas previously it was hypothesized that extensive amide-amide hydrogen bonding helped stabilize self-assembled structures, our results suggest that the

amide bond plays less of a role in forming and stabilizing the single fibril structure and a greater role in determining the nature of the higher-order aggregation of intermediate fibrils. The idea that different fibril amphiphilicity impacts higher-order self-assembly is not a new concept; in 2001, Aggeli et al. suggested that beyond initially assembled β-sheet-like tapes of peptide monomers, such tapes' amphiphilicity can further drive their formation into higher order structures, a process the authors referred to as "hierarchical self-assembly" (*18*). Indeed, many sophisticated functional materials are created through a hierarchical self-assembly process mediated by the balance between hydrophobicity and hydrophilicity of intermediate structures (*41–45*). In nature, virus capsids are hierarchically assembled from protomers, pentamers or hexamers (*46*). In the study of amyloid fibril formation, with the ability to determine the atomic-resolution structure, researchers proved that amyloids can assemble hierarchically into higher dimensional structures including protofilaments, filaments, and mature fibrils (*44*, *47*, *48*).

Following the above discussion, we summarize our findings as such in **Figure 4.6**: Fmoc-dipeptides are of amphiphilic character, which enable them to initially self-assemble into a fibril structure (diameter ~3nm). Owing to the amphiphilic nature of the fibril surfaces exposed to water, fibrils further aggregate into higher order supramolecular aggregates (width ~20-200 nm), such as fiber- and ribbon-like structures observed in TEM. The amide-to-ester modification we have made here seems to have little effect in the first stage of the process, but greater implications in the second stage of the hierarchical assembly process leading to observable differences in nanostructure morphology and bulk properties.

4.4 CONCLUSIONS

We have demonstrated here experimentally what we hypothesized in our previous study: that β-sheet specific hydrogen bonding between adjacent molecules within a supramolecular structure is likely not as important as hydrophobic or aromatic-aromatic interactions in driving and stabilizing self-assembly of Fmoc-dipeptides. However, while the initial self-assembly may not be completely affected by a chemical change resulting in different hydrogen bonding capability (as in the Ala to Lac change), resulting intermediate fibrils may have different surface-solvent interface properties that result in different propensities of fibrils to associate and form higher-order supramolecular aggregates.

Through the combination of experimental and computational molecular dynamics simulations, it is clear that the inclusion of the ester bond (and thereby lack of extensive amide-amide hydrogen bonding) in this simple Fmoc-dipeptide system still leads to gelation under the same experimental conditions but also has implications for the amphiphilic nature of the self-assembled fibril units, the nature of their higher order assembly, and ultimately the bulk mechanical properties of the gel. These considerations must be taken into account when designing more structurally complex and potentially bioactive peptide-based gelator systems for use in tissue engineering and regenerative medicine applications.

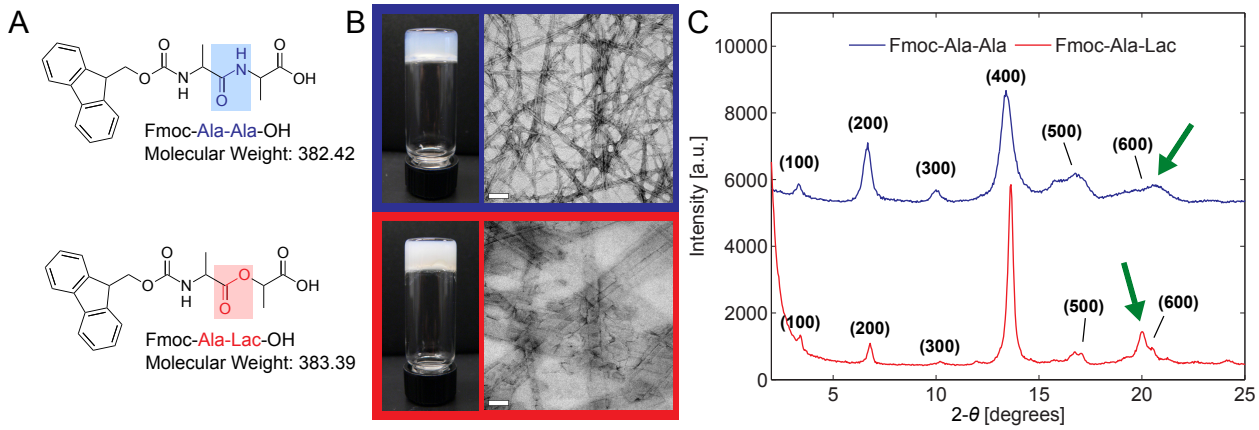

Figure 4.1 Both Fmoc-Ala-Ala (A, top) and Fmoc-Ala-Lac (A, bottom) self-assemble upon a pH change to form hydrogels (B, left) composed of fibrillar structures seen in TEM micrographs (B, right). Scale bar = 100 nm. X-ray diffraction patterns obtained from dried gel films (C) show similar peak positions and intensity, indicating that characteristic dimensions (such as fibril diameter) are similar between the two systems. The green arrows point out a unique, non-higher order reflection in each diffraction pattern that may correspond to different Fmoc-Fmoc or strand-strand spacing in each system.

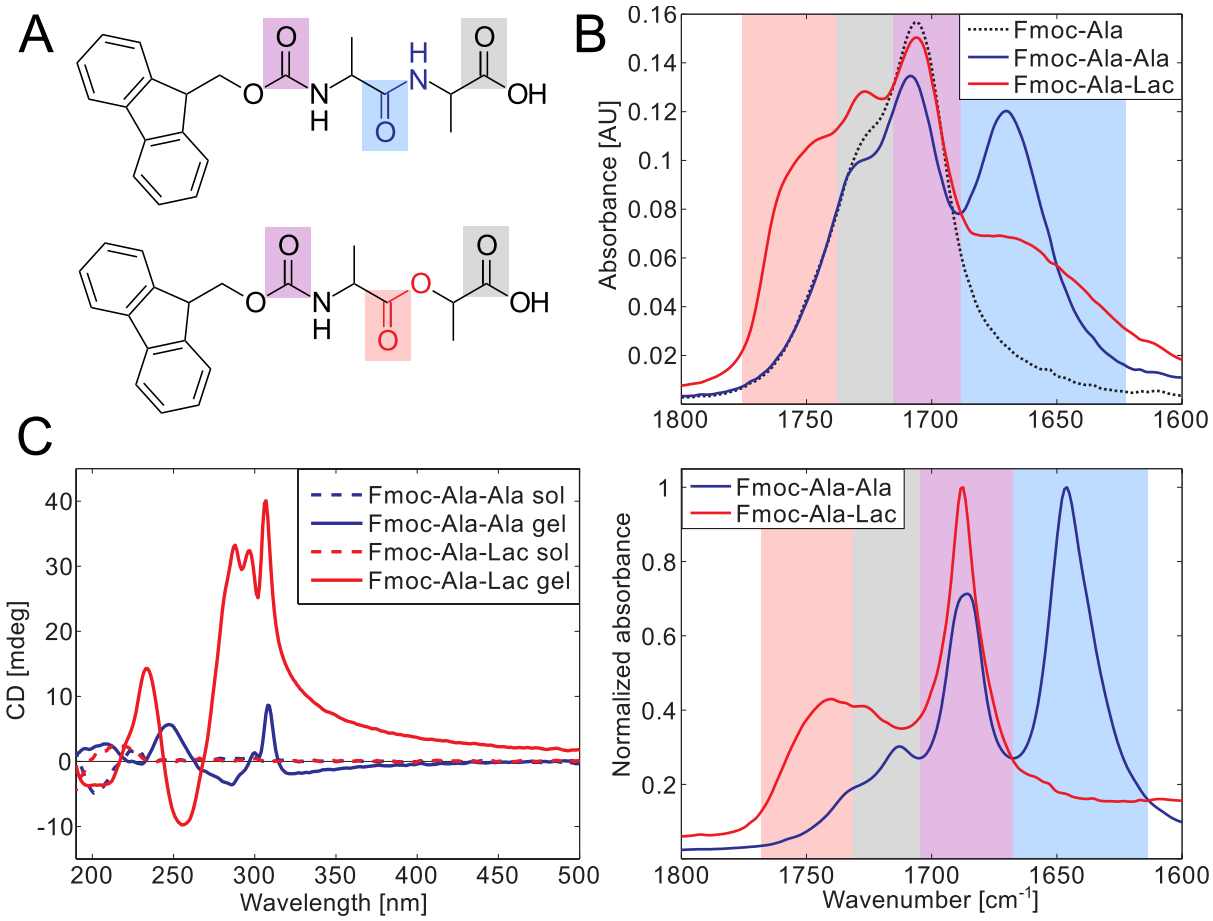

Figure 4.2 Fmoc-Ala-Ala and Fmoc-Ala-Lac are spectrally distinct in both their gelled and non-gelled forms. Carbonyl bonds are highlighted in the chemical structures of Fmoc-Ala-Ala (A, top) and Fmoc-Ala-Lac (A, bottom), and the resonant stretching frequencies of these particular bonds are highlighted in the same color in IR spectra of solutions in ethanol (B, top) and gels in water (B, bottom). Spectral overlap can be correlated with carbonyl features, with the carbamate linker's carbonyl stretching (purple) and the terminal carboxylic acid carbonyl (gray) common to Fmoc-Ala-Ala, Fmoc-Ala-Lac, and Fmoc-Ala (structure not shown). CD spectra (C) show marked increase in dichroism in the gelled state (solid lines) relative to the solution state (high pH, dashed lines) in both Fmoc-Ala-Ala and Fmoc-Ala-Lac, indicating induced chirality as a result of self-assembly. Large peaks above 280 nm indicate interaction of aromatic Fmoc groups within a chiral assembly.

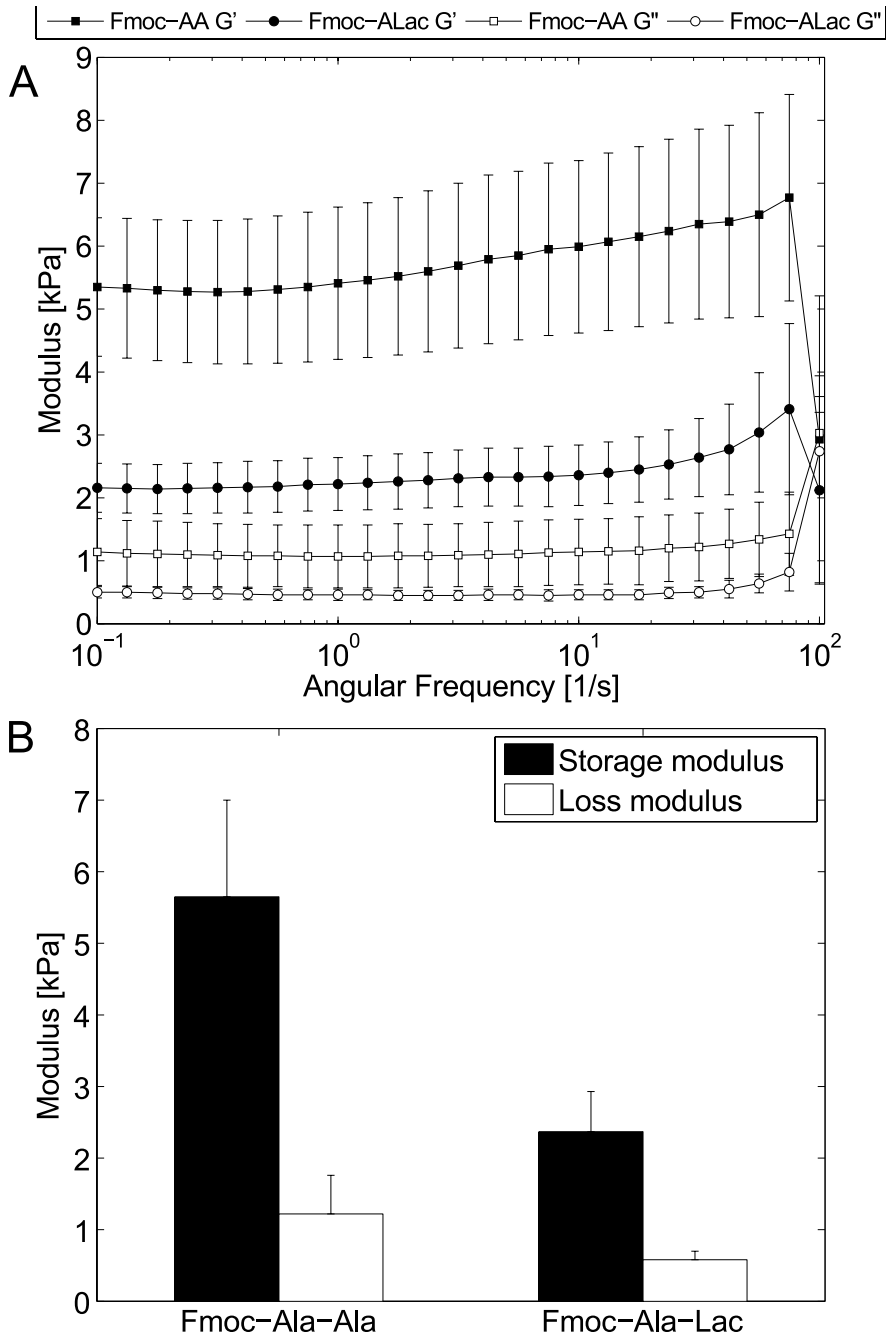

Figure 4.3 Fmoc-Ala-Ala gels are stiffer than Fmoc-Ala-Lac gels, as evidenced by frequency sweeps (A) in parallel plate rheometry. When averaged, both the storage and loss moduli of Fmoc-Ala-Ala gels are greater than Fmoc-Ala-Lac gels but within the same order of magnitude (B).

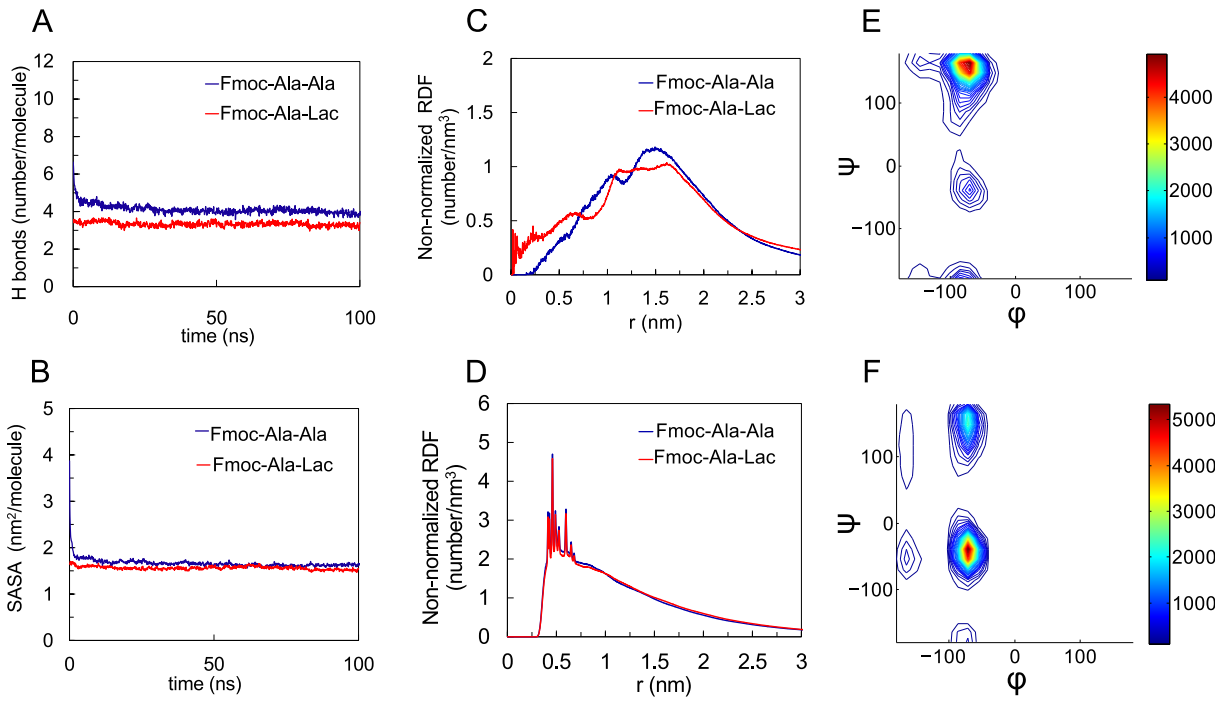

Figure 4.4 Computational results characterizing the structural properties of Fmoc-Ala-Ala compared to Fmoc-Ala-Lac. In both systems, the number of hydrogen bonds per molecule (A) and solvent-accessible surface area (SASA) (B) converge, indicating fibril stability. Non-normalized radial distribution function (RDF) plots of the last 50 ns of each simulation for the distance between the terminal residue's hydroxyl hydrogen and fibril axis (approximating the radius) (C), and the distance between fluorenyl rings (D) show feature size similarity between Fmoc-Ala-Ala and Fmoc-Ala-Lac systems. For the Fmoc-Ala-Lac fibril assembly, a Ramachandran plot for the alanine (E) during the last 50 ns of simulation shows a large population at $\phi,\psi = (-70°, 164°)$ (indicative of polyproline-II conformation) and a minor population at $\phi,\psi = (-70°, -39°)$. The Ramachandran plot for the terminal Lac residue (F) in Fmoc-Ala-Lac during the last 50 ns of simulation shows a large population at $\phi,\psi = (-70°, -39°)$ (indicative of α-helix-like conformation) and a minor population at $\phi,\psi = (-70°, 148°)$.

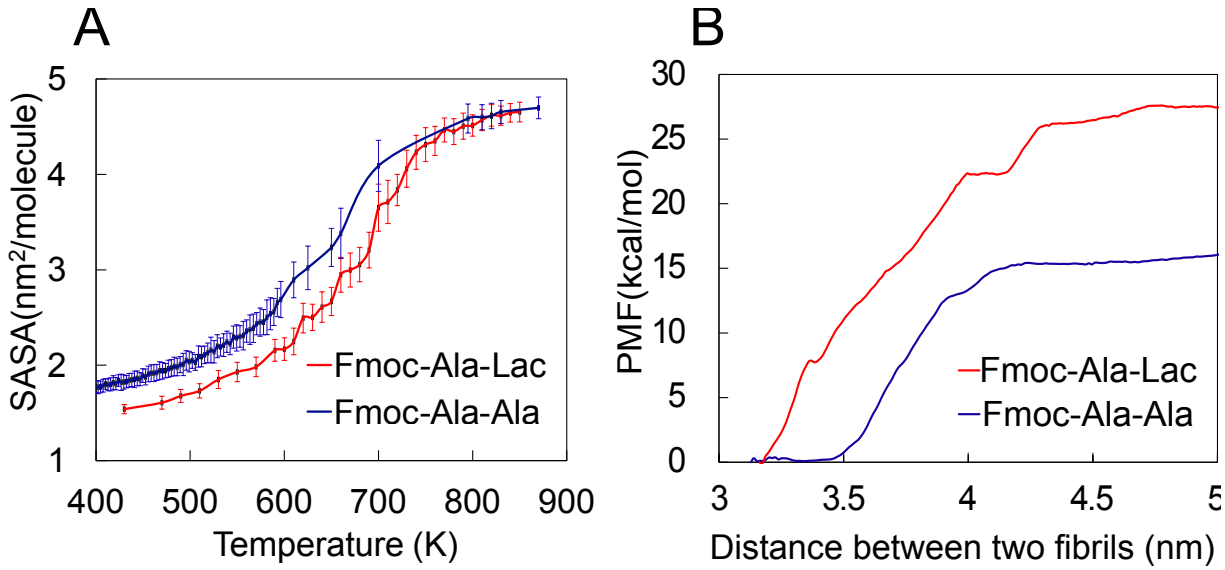

Figure 4.5 Computational study of interaction energy between Fmoc-dipeptides and fibrils. Melting curves (A) show that Fmoc-Ala-Lac fibril assemblies are slightly more stable than Fmoc-AA firbils. Potential of mean force (PMF) calculated at varying fibril-fibril separation distances shows that Fmoc-Ala-Lac fibrils require more force to "pull apart," or tend to aggregate more readily than Fmoc-Ala-Ala fibrils.

Table 4.1 The total and partially decomposed SASA of Fmoc-dipeptides. *

Fmoc-AA		Total	Fmoc	Ala-mid-C=O	Ala-term-COOH	Ala-mid-NH	Ala-term-NH
	nm^2	165.3	58.5	9.2	33.1	1.4	2.5
	Percentage	100.0	35.4	5.5	20.0	0.9	1.5
Fmoc-ALac		Total	Fmoc	Ala-C=O (ester)	Lac-COOH	Ala-NH	Lac-O(ester)
	nm^2	155.7	55.9	8.1	37.5	1.9	1.1
	Percentage	100.0	35.9	5.2	24.1	1.2	0.7

* "Ala-mid" refers to the N-terminal alanine, and "Ala-term" refers to the C-terminal alanine. Percentages do not add up to 100% because the hydrophobic and hydrophilic groups of interest listed here do not comprise the entire surface area of the fibril.

Table 4.2 H-bonds between residues on Fmoc-dipeptides and water molecules. *

Fmoc-AA		Total	Fmoc	Ala-mid-C=O	Ala-term-COOH	Ala-mid-NH	Ala-term-NH
	Number	408.1	100.9	70.5	168.9	20.7	47.1
	Percentage	100.0	24.7	17.3	41.4	5.1	11.6
Fmoc-ALac		Total	Fmoc	Ala-C=O (ester)	Lac-COOH	Ala-NH	Lac-O (ester)
	Number	331.3	93.9	44.1	165.1	26.4	1.8
	Percentage	100.0	28.4	13.3	49.8	8.0	0.5

*Hydrogen bonds were calculated as interactions between water molecules and groups of interest, with an donor-acceptor distance of ≤3.5 A˚ and an interaction angle of ≤30°.

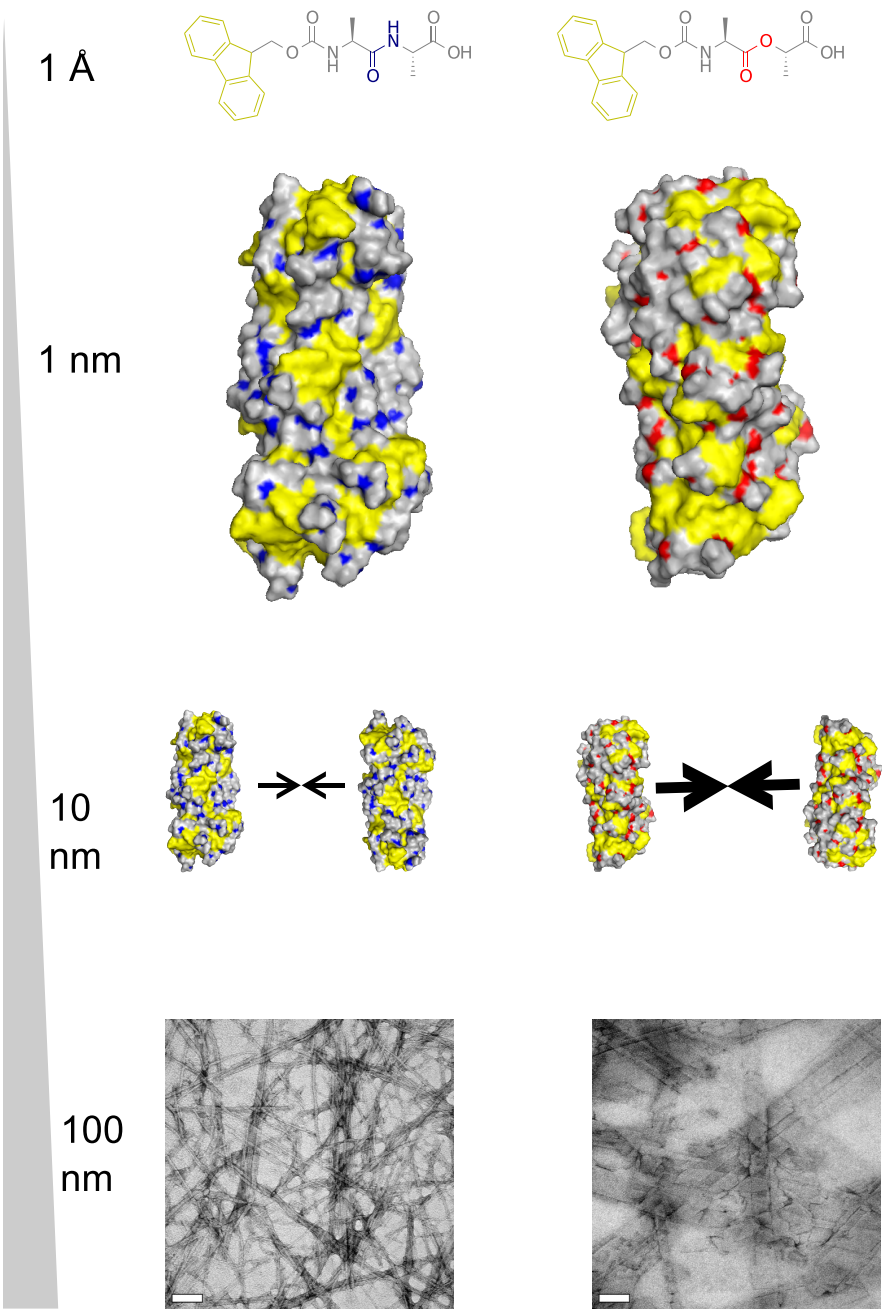

Figure 4.6 Schematic of hierarchical assembly of Fmoc-AA and Fmoc-ALac. Both systems self-assemble into similar intermediate single fibrils, but differences in the amphiphilicity of fibrils cause Fmoc-ALac fibrils to associate more strongly and extensively, giving rise to larger nanoscale structures observed in TEM.

4.5 REFERENCES

1. D. J. Adams, Dipeptide and Tripeptide Conjugates as Low-Molecular-Weight Hydrogelators. *Macromol. Biosci.* **11**, 160–173 (2011).
2. X. Li, Y. Kuang, B. Xu, "Molecular trinity" for soft nanomaterials: integrating nucleobases, amino acids, and glycosides to construct multifunctional hydrogelators. *Soft Matter.* **8**, 2801–2806 (2012).
3. S. Bhuniya, Y. J. Seo, B. H. Kim, (S)-(+)-Ibuprofen-based hydrogelators: an approach toward anti-inflammatory drug delivery. *Tetrahedron Letters.* **47**, 7153–7156 (2006).
4. J. Li *et al.*, The conjugation of nonsteroidal anti-inflammatory drugs (NSAID) to small peptides for generating multifunctional supramolecular nanofibers/hydrogels. *Beilstein Journal of Organic Chemistry.* **9**, 908–917 (2013).
5. W. Mabey, T. Mill, Critical review of hydrolysis of organic compounds in water under environmental conditions. *Journal of Physical and Chemical Reference Data.* **7**, 383–415 (1978).
6. M. M. Nguyen, N. Ong, L. Suggs, A general solid phase method for the synthesis of depsipeptides. *Organic & Biomolecular Chemistry.* **11**, 1167 (2013).
7. A. M. Smith *et al.*, Fmoc-Diphenylalanine Self Assembles to a Hydrogel via a Novel Architecture Based on π–π Interlocked β-Sheets. *Advanced Materials.* **20**, 37–41 (2008).
8. X. Mu, K. M. Eckes, M. M. Nguyen, L. J. Suggs, P. Ren, Experimental and Computational Studies Reveal an Alternative Supramolecular Structure for Fmoc-Dipeptide Self-Assembly. *Biomacromolecules.* **13**, 3562–3571 (2012).
9. M. M. Nguyen, K. M. Eckes, L. J. Suggs, Charge and sequence effects on the self-assembly and subsequent hydrogelation of Fmoc-depsipeptides. *Soft Matter.* **10**, 2693 (2014).
10. W. L. Jorgensen, J. M. Briggs, J. Gao, A priori calculations of pKa's for organic compounds in water. The pKa of ethane. *Journal of the American Chemical Society.* **109**, 6857–6858 (1987).
11. W. L. Jorgensen, P. Schyman, Treatment of Halogen Bonding in the OPLS-AA Force Field: Application to Potent Anti-HIV Agents. *Journal of Chemical Theory and Computation.* **8**, 3895–3901 (2012).
12. N. L. Allinger, Y. H. Yuh, J. H. Lii, Molecular mechanics. The MM3 force field for hydrocarbons. 1. *Journal of the American Chemical Society.* **111**, 8551–8566 (1989).

13. B. Hess, H. Bekker, H. J. C. Berendsen, J. G. E. M. Fraaije, LINCS: A linear constraint solver for molecular simulations. *Journal of Computational Chemistry*. **18**, 1463–1472 (1997).

14. J. Zhang, M. King, L. Suggs, P. Ren, Molecular Modeling of Conformational Properties of Oligodepsipeptides. *Biomacromolecules*. **8**, 3015–3024 (2007).

15. R. D. Blake *et al*., Statistical mechanical simulation of polymeric DNA melting with MELTSIM. *Bioinformatics*. **15**, 370–375 (1999).

16. N. Le Novère, MELTING, computing the melting temperature of nucleic acid duplex. *Bioinformatics*. **17**, 1226–1227 (2001).

17. G. Khandelwal, J. Bhyravabhotla, A Phenomenological Model for Predicting Melting Temperatures of DNA Sequences. *PLoS ONE*. **5**, e12433 (2010).

18. A. Aggeli *et al*., Hierarchical self-assembly of chiral rod-like molecules as a model for peptide β-sheet tapes, ribbons, fibrils, and fibers. *Proc Natl Acad Sci U S A*. **98**, 11857–11862 (2001).

19. J. A. Lemkul, D. R. Bevan, Assessing the Stability of Alzheimer's Amyloid Protofibrils Using Molecular Dynamics. *The Journal of Physical Chemistry B*. **114**, 1652–1660 (2010).

20. S. Kumar, J. M. Rosenberg, D. Bouzida, R. H. Swendsen, P. A. Kollman, THE weighted histogram analysis method for free-energy calculations on biomolecules. I. The method. *Journal of Computational Chemistry*. **13**, 1011–1021 (1992).

21. C. Tang, A. M. Smith, R. F. Collins, R. V. Ulijn, A. Saiani, Fmoc-Diphenylalanine Self-Assembly Mechanism Induces Apparent pKa Shifts. *Langmuir*. **25**, 9447–9453 (2009).

22. K. A. Houton *et al*., On Crystal versus Fiber Formation in Dipeptide Hydrogelator Systems. *Langmuir*. **28**, 9797–9806 (2012).

23. R. M. Silverstein, *Spectrometric identification of organic compounds* (Wiley, New York, 5th ed., 1991).

24. L. Xu, C. Li, K. Y. S. Ng, In-Situ Monitoring of Urethane Formation by FTIR and Raman Spectroscopy. *The Journal of Physical Chemistry A*. **104**, 3952–3957 (2000).

25. Y. Wu *et al*., An FTIR–ATR investigation of in vivo poly (ether urethane) degradation. *Journal of applied polymer science*. **46**, 201–211 (1992).

26. Y. Ni, F. Becquart, J. Chen, M. Taha, Polyurea–Urethane Supramolecular Thermo-Reversible Networks. *Macromolecules*. **46**, 1066–1074 (2013).

27. M. Jackson, H. H. Mantsch, The Use and Misuse of FTIR Spectroscopy in the Determination of Protein Structure. *Critical Reviews in Biochemistry and Molecular Biology*. **30**, 95–120 (1995).

28. M. Zhou *et al*., Self-assembled peptide-based hydrogels as scaffolds for anchorage-dependent cells. *Biomaterials*. **30**, 2523–2530 (2009).

29. V. Jayawarna *et al*., Introducing chemical functionality in Fmoc-peptide gels for cell culture. *Acta Biomater*. **5**, 934–943 (2009).

30. S. Fleming *et al*., Assessing the Utility of Infrared Spectroscopy as a Structural Diagnostic Tool for β-Sheets in Self-Assembling Aromatic Peptide Amphiphiles. *Langmuir*. **29**, 9510–9515 (2013).

31. B. Nordén, A. Rodger, T. Dafforn, *Linear Dichroism and Circular Dichroism: A Textbook on Polarized-Light Spectroscopy* (Royal Society of Chemistry, 2010).

32. Y. Zhang, H. Gu, Z. Yang, B. Xu, Supramolecular Hydrogels Respond to Ligand–Receptor Interaction. *J. Am. Chem. Soc*. **125**, 13680–13681 (2003).

33. E. A. Ryan, L. F. Mockros, J. W. Weisel, L. Lorand, Structural Origins of Fibrin Clot Rheology. *Biophysical Journal*. **77**, 2813–2826 (1999).

34. J. Raeburn *et al*., Fmoc-diphenylalanine hydrogels: understanding the variability in reported mechanical properties. *Soft Matter*. **8**, 1168–1174 (2012).

35. J. Raeburn, A. Z. Cardoso, D. J. Adams, The importance of the self-assembly process to control mechanical properties of low molecular weight hydrogels. *Chem. Soc. Rev*. **42**, 5143–5156 (2013).

36. V. Parchaňský, J. Kapitán, J. Kaminský, J. Šebestík, P. Bouř, Ramachandran Plot for Alanine Dipeptide as Determined from Raman Optical Activity. *J. Phys. Chem. Lett*. **4**, 2763–2768 (2013).

37. T. Yu, O.-S. Lee, G. C. Schatz, Steered Molecular Dynamics Studies of the Potential of Mean Force for Peptide Amphiphile Self-Assembly into Cylindrical Nanofibers. *The Journal of Physical Chemistry A*. **117**, 7453–7460 (2013).

38. T. Yu, G. C. Schatz, Free Energy Profile and Mechanism of Self-Assembly of Peptide Amphiphiles Based on a Collective Assembly Coordinate. *The Journal of Physical Chemistry B*. **117**, 9004–9013 (2013).

39. D. Chandler, Interfaces and the driving force of hydrophobic assembly. *Nature*. **437**, 640–647 (2005).

40. F. Stillinger, Structure in aqueous solutions of nonpolar solutes from the standpoint of scaled-particle theory. *J Solution Chem*. **2**, 141–158 (1973).

41. G. M. Whitesides, B. Grzybowski, Self-Assembly at All Scales. *Science*. **295**, 2418–2421 (2002).

42. M. J. Buehler, T. Ackbarow, Nanomechanical strength mechanisms of hierarchical biological materials and tissues. *Computer Methods in Biomechanics and Biomedical Engineering*. **11**, 595–607 (2008).

43. M. J. Buehler, Y. C. Yung, Deformation and failure of protein materials in physiologically extreme conditions and disease. *Nat Mater*. **8**, 175–188 (2009).

44. T. P. J. Knowles, T. W. Oppenheim, A. K. Buell, D. Y. Chirgadze, M. E. Welland, Nanostructured films from hierarchical self-assembly of amyloidogenic proteins. *Nat Nano*. **5**, 204–207 (2010).

45. P. Ortoleva, A. Singharoy, S. Pankavich, Hierarchical multiscale modeling of macromolecules and their assemblies. *Soft Matter*. **9**, 4319–4335 (2013).

46. J. Baschek, H. R Klein, U. Schwarz, Stochastic dynamics of virus capsid formation: direct versus hierarchical self-assembly. *BMC Biophysics*. **5**, 22 (2012).

47. A. W. P. Fitzpatrick *et al*., Atomic structure and hierarchical assembly of a cross-β amyloid fibril. *Proceedings of the National Academy of Sciences*. **110**, 5468–5473 (2013).

48. S.-Y. Qin, Y. Pei, X.-J. Liu, R.-X. Zhuo, X.-Z. Zhang, Hierarchical self-assembly of a [small beta]-amyloid peptide derivative. *Journal of Materials Chemistry B*. **1**, 668–675 (2013).

Chapter 5: Assessing the self-assembly and integrin-binding activity of a depsipeptide RGD analog

5.0 FOREWORD

The previous two chapters of this dissertation discussed two published studies analyzing the self-assembly and subsequent hydrogelation of a simple Fmoc-protected dipeptide and its depsipeptide analog. We showed that, at least in this simple system, a specific mode of amide-amide hydrogen bonding between adjacent peptide bonds in a supramolecular assembly is not an absolute requirement for hierarchical self-assembly that leads to gelation in aqueous solution. In this chapter, we investigate a system with biomedical relevance. Described herein are the development and synthesis of an Fmoc-protected, self-assembling depsipeptide analogue of the cell adhesion motif, Arginine-Glycine-Aspartic acid (RGD), and fundamental studies to evaluate the integrin-binding capability of the RGD analogue and its potential effect on cell adhesion and spreading.

5.1 INTRODUCTION

Self-assembled short peptides continue to be explored as the basis for new, *in situ* forming hydrogel materials for biomedical applications. Oligomeric self-complementary peptides, such as the RAD16 peptide first described by Zhang et al. (*1*, *2*), have been utilized in a number of different tissue engineering approaches, including regeneration of cardiac, nerve, and bone tissue. In many cases, these materials displayed good biocompatibility, cell ingrowth, and functional improvement (*3–6*). Peptide amphiphiles, pioneered by Samuel Stupp's group, have also been applied in a vast array of different tissue engineering and drug delivery experiments (*7–10*), with several particularly notable functional improvements in murine *in vivo* models including rats recovering hind

limb function after paralysis-inducing spinal cord compression (*11*). A newer class of materials based on peptides with N-terminal aromatic protecting groups has recently been evaluated for cell-supporting ability and the Ulijn group has spun off a company called Biogelx to manufacture these materials specifically for the purpose of 3D *in vitro* cell culture.

Peptide-based self-assembling materials clearly show great promise for biomedical applications, but little work has been done to demonstrate their long-term biocompatibility and biodegradation. FDA approval of any device for *in vivo* use requires full characterization of the safety of the device and its constituent material, and this will likely include studies that show degradation kinetics and biodistribution of the intact or degraded material. There is also a possibility that such materials may not be easily degraded by the body—indeed, the level of matrix-degrading protease expression varies with tissue and cell type, thus frequently remodeled tissues (e.g. skin) likely have much greater protease activity than tissue with low turnover (e.g. nerve) (*12*, *13*). Moreover, specific protease types act on different ECM components e.g. collagen, fibronectin, etc., so for peptide-based materials to be enzymatically degradable, protease-specific sequences may need to be incorporated into the peptide chain according to the tissue application. This level of sequence specificity required may ultimately make peptide-based materials less generally applicable and more expensive to develop.

Recent work by our group and others suggests that it may be possible to engineer non-enzyme-specific degradability into self-assembling peptides while still retaining their self-assembly capability and potential bioactivity. Previously, we synthesized and characterized the self-assembly capability of a depsipeptide analogue of the simple gelator Fluorenylmethoxycarbonyl-dialanine (Fmoc-AA) (*14*). The analogue, Fmoc-Ala-Lac, has side chain identity and stereochemistry exactly identical to that of Fmoc-AA but

contains an ester bond where Fmoc-AA contains an amide (peptide) bond. Ester bonds are electrically and conformationally similar to amide bonds but are several orders of magnitude more susceptible to non-enzymatic degradation by alkaline or acidic hydrolysis (*15*). Importantly, ester bonds contain no hydrogen bond donor, and thus esters are not able to interact with other esters via hydrogen bonding. β-sheet-like amide-amide hydrogen bonding was previously thought to be crucial in stabilizing assemblies of short Fmoc-protected peptides (*16*), thus it was unclear initially whether the amide-deficient Fmoc-Ala-Lac would be capable of self-assembly similar to that seen for Fmoc-AA. We found, however, that under similar triggering conditions (solvent exchange and pH switch) both Fmoc-AA and Fmoc-Ala-Lac are capable of self-assembly leading to gelation. Our results and computational analyses suggested also that the self-assembled fibril structures were largely similar in size and structure and supramolecular assemblies were mainly formed and stabilized through hydrophobic and aromatic π-π interactions rather than β-sheet-like hydrogen bonding interactions.

Recent work by Tian et al. involved the incorporation of a single ester bond into the backbone of an 11-residue acetyl-capped peptide previously developed in Collier's lab (*17*). Perhaps unsurprisingly in this case, the peptides retained self-assembly capability, as only one of ten bonds between residues was replaced by an ester. However, the authors were able to demonstrate convincingly through HPLC analysis, TEM, and gel rheometry that ester incorporation conferred non-enzymatic degradability to the otherwise stable peptide. Importantly, they also showed that the degradation rate could be controlled through selection of the α-hydroxy acid side chain group proximal to the ester group; sterically bulkier side chains (e.g. phenyl, isopropyl) tended to cause slower hydrolysis than small side chains (e.g. hydrogen, methyl).

Another study by our group investigated the self-assembly of longer Fmoc-depsipeptides with charged side chains (*18*). In this study we found that side chain charge and sequence were the primary determinants of self-assembly and that the presence of ions in the solution had a dramatic effect on the rate of self-assembly and the onset of gelation. We also demonstrated that a molecule's overall hydrophobicity plays a role in speed of self-assembly and the time to gelation; when the C-terminal alanine residue of a 3-day gelling depsipeptide was replaced with a phenylalanine residue, the time to gelation was reduced to mere minutes. Based on these results it is clear that even multi-ester depsipeptides are quite capable of self-assembly beyond a simple, two-residue system.

In this paper, we describe a self-assembling depsipeptide based on a sequence with great relevance to biomedical applications, the Arginine-Glycine-Aspartic acid sequence. This sequence is found in several ECM proteins and is known to bind to a number of cell surface integrin variants to mediate cell adhesion to the ECM (*19*). RGD and RGD-containing peptides have been incorporated into many synthetic hydrogel systems in order to encourage cell interaction with otherwise completely non-bioactive materials. Cell-adhesive sequences also allow cells to interrogate the substrate material's mechanical properties. This process, known as mechanosensing, has been shown to be extremely important for directing cell behavior, migration, and more recently stem cell differentiation (*20–23*). For these reasons and the fact that the RGD sequence is one of the shortest known biomolecular recognition sequences we chose to develop RGD-mimicking depsipeptides as the basis for self-assembling degradable materials with the potential for peptide-like bioactivity. We were particularly interested in using the system to study the role that backbone hydrogen bonding plays in the binding of RGD peptides to an integrin protein. While ester-modified peptides have been used previously to

elucidate the role of backbone hydrogen bonding in protein folding (*24–27*), β-amyloid formation (*28*, *29*) and other peptide-protein interactions (*30*, *31*), to our knowledge there have been no studies investigating the importance of such interactions in mediating biomechanically important peptide-protein interactions such as integrin-RGD binding.

5.2 MATERIALS AND METHODS

5.2.1 Synthesis and purification of peptides and depsipeptides.

5.2.1.1 Solution phase synthesis of depsipeptide unit (Fmoc-R-Glc)

Depsipeptides were synthesized using a combinatorial solution- and solid phase synthesis approach previously developed by our lab (*32*). Through this approach, Fmoc-protected depsipeptide units of a specific amino- and α-hydroxy- acid combination can be incorporated into peptides synthesized on solid resin support using well-established coupling chemistries and automated peptide synthesizing instruments (**Figure 5.1**). For the present study, we synthesized a Fmoc-Arg(Pbf)-Glc (Fmoc-R-Glc) unit in solution. Glycolic acid (Acros Organics) was first carboxyl-protected by the method of Fan et al. (*33*). Glycolic acid and 1.5 equiv benzyl chloride (Sigma Aldrich) were dissolved in a minimal volume of ethyl acetate, then 1.5 equiv triethylamine (TEA, Acros Organics) was added. The mixture was refluxed at 85 °C overnight then filtered to remove TEA-chloride salts and then distilled to remove excess benzyl chloride. Excess benzyl chloride was removed from the mixture by vacuum distillation to yield the pure benzyl glycolate (Glc-Bn). Glc-Bn was then dissolved in dichloromethane (DCM) with 1.2 equiv Fmoc-Arg(Pbf)-OH (Novabiochem) and 0.01 equiv dimethylaminopyridine (DMAP) and the mixture was chilled on ice. To the chilled mixture was added 1.2 equiv dicyclohexylcarbodiimide (DCC). The reaction was allowed to warm to room

temperature overnight, after which the mixture was filtered to remove dicyclohexylurea (DCU) crystals, and concentrated *in vacuo*. The carboxyl-protected Fmoc-depsipeptide product, Fmoc-R-Glc-Bn, was then purified by flash chromatography (avg. yield ~85-90%) and concentrated *in vacuo*. Pure Fmoc-R-Glc-Bn was benzyl-deprotected by catalytic hydrogenolysis following the general method described by Bajwa (*34*). Fmoc-R-Glc-Bn was dissolved in a minimal volume of absolute ethanol with DCM added to aid dissolution. To this mixture, 10 equiv 1,4-cyclohexadiene (Acros Organics) was added, followed by a mass of palladium on carbon (Pd/C, 10% Pd, Acros Organics) equivalent to the mass of the Fmoc-R-Glc-Bn. This mixture was stirred at room temperature for at least three hours, and the reaction was monitored by thin layer chromatography (TLC). The mixture was then filtered *in vacuo* through a celite pad and triturated with hot ethanol and hot DCM, then reconcentrated *in vacuo*. The crude product was then dissolved in <10 mL of DMSO and purified by reverse phase flash chromatography using a RediSep Gold C18 column on a Combiflash instrument (Teledyne Isco) with a 45 minute linear gradient of 0-95% acetonitrile in water. The pure Fmoc-R-Glc product was then lyophilized from a concentrated solution in acetonitrile and stored as a powder at -20 °C for future use.

5.2.1.2 Solid phase coupling and purification of Fmoc-peptides and Fmoc-depsipeptides

All peptides and depsipeptides were coupled on solid phase using diisopropylcarbodiimide (DIC) / OxymaPure (ethyl 2-cyano-2-(hydroxyimino)acetate) amide coupling chemistry. Depending on the desired sequence, either Fmoc-Asp(OtBu)-Wang resin or Fmoc-Glu(0tBu)-Wang resin were swelled in DCM in a fritted, capped syringe for 20 minutes. The resin was rinsed with DMF and then Fmoc groups were

removed with 20% piperidine in DMF (5 mL). After addition to the resin, the capped syringe was placed in a BioWave scientific microwave oven (Ted Pella, Inc.) operating at ~100 watts and subjected to microwave energy in 30 second increments for a total of 2 minutes. At the end of each 30-second increment, the mixture was vortexed. This process was repeated twice more with fresh piperidine solution to ensure completely Fmoc removal. The resin was then washed (vortexed 4 x 15 mL DMF followed by 4 x 15 mL DCM) and a coupling solution containing the next Fmoc-amino acid was added to the resin. Coupling solutions consisted of 3 equiv of the Fmoc-amino acid and 3 equiv of OxymaPure in less than 10 mL of DMF to which 3 equiv of DIC was added. The mixture was allowed to pre-activate for at least 10 minutes before adding to resin (for most amino acids a yellow color develops upon DIC addition). After microwaving (5 minutes at ~100 W with mixing every 30 seconds), the resin was washed (vortexed 4 x 15 mL DMF followed by 4 x 15 mL DCM). Subsequent coupling steps followed the same Fmoc-deprotection, washing, and coupling methods. For coupling solution-synthesized Fmoc-R-Glc units, a similar protocol was used, with a slight difference. For the coupling solution, only 2 equiv of Fmoc-R-Glc was used in an effort to conserve the material.

Upon completion of coupling, the peptide (or depsipeptide) was cleaved from the resin and side chains were simultaneously deprotected by adding 5 mL of a solution of 95:2.5:2.5 trifluoroacetic acid:water:triisopropylsilane (TFA:H_2O:TIPS) and mixing for 1.5-2 hours. The mixture was then collected in a clean round bottom flask, and subsequent resin washes (1 x 5 mL TFA:H2O:TIPS and 5 x 10 mL DCM) were added to the flask before concentrating *in vacuo* on a rotary evaporator. Excess TFA and H_2O were removed by repeatedly adding acetone or DCM and reconcentrating. The resulting oil was dissolved in < 5 mL DMF and the product was precipitated with cold diethyl ether to form a white product. The mixture was split into separate centrifuge tubes, centrifuged

and triturated and vortexed with cold ether, then recombined into a single tube followed by three subsequent rounds of centrifugation and trituration/vortexing to remove excess TFA and scavenged side chain protecting groups. After drying the product under a gentle stream of N_2, the product was redissolved in DMF or DMSO and purified by reversed phase- (RP-) HPLC (0% H2O initially for 10-15 minutes to remove excess DMF/DMSO, followed by a 30-40 minute linear gradient of 0-90% acetonitrile in water). Pure product fractions were collected and lyophilized in a low temperature (-100 °C collector) for 2 days.

5.2.2 Preparation of peptide-functionalized glass surfaces for cell adhesion/spreading studies

5.2.2.1 Covalent functionalization of glass coverslips with amine-terminated PEG

Glass surfaces were functionalized with RGD peptides or R-Glc-D depsipeptides to assess cell adhesion and spreading in a system that facilitates imaging and quantitative assessment. Functionalization was accomplished using the methods described by Piehler et al. and Todd et al (*35*, *36*). Circular glass coverslips (18 mm diameter, thickness "2") were cleaned by sonicating for 10 minutes in acetone followed by rinsing with deonized (DI) water. Coverslips were then submerged in 3 M NaOH for 5 minutes, rinsed with DI water, and submerged in a piranha solution (30% v/v concentrated sulfuric acid, 70% v/v hydrogen peroxide). After 1 hour, coverslips were removed and rinsed in a large excess of DI water and air dried completely. An epoxide-terminated silane, (3-glycidyloxipropyl)trimethoxysilane (GOPTS, Sigma Aldrich), was pipetted onto the surface of half the coverslips, and the remaining coverslips were placed on top of the GOPTS to reduce air exposure. The sandwiched coverslips were then placed in an oven

at 37 °C for at least 2 hours, after which the coverslips were washed with dry acetone and dried under N_2. Immediately following, homobifunctional diamino-polyethylene glycol (H_2N-PEG-NH_2) in dry powder form was placed directly on the silane-functionalized surface of half of the coverslips, which were then placed in an oven at ~75 °C. The PEG powder melted into a semi-viscous liquid, and while still in the oven the remaining coverslips were placed on top of the PEG-covered coverslips with the silane side facing down. The coverslip-PEG assemblies were incubated at 75 °C for 48 hours in order to provide sufficient time for complete coupling of the PEG-terminal amine groups to the epoxide groups on the silanated glass. After incubation, coverslips were disassembled while still hot (in order to prevent PEG recrystallization/hardening) and were rinsed with a large excess of DI water. Coverslips were then marked to indicate the non-PEGylated side.

5.2.2.2 Peptide synthesis on glass substrates

For solid-phase synthesis of peptides on PEG-ylated glass substrates, coverslips were immersed in pre-activated coupling solutions and subjected to microwave energy. Coupling solutions were similar to those prepared for normal resin-bound peptide synthesis, with 0.2 – 0.8 mmol Fmoc-amino acid and 2 equiv of OxymaPure dissolved in ~ 6 mL of DMF, followed by addition of 2 equiv of DIC and 10 minutes of pre-activation prior to coupling. For each amino acid coupling step, 2 mL of coupling solution was added to a glass petri dish containing several coverslips with the PEGylated side facing up, and the coverslips were microwaved for 3 minutes at 250 watts (very little heating was observed). This process was repeated two more times with fresh coupling solution each time. Coverslips were then washed thoroughly with DMF. To remove Fmoc groups, ~2 mL 20% piperidine in DMF was added to the petri dish and the dish was microwaved

for 2 minutes. This process was repeated two more time with fresh piperidine solution, then coverslips were washing thoroughly wish DMF. Subsequent Fmoc-amino acid or Fmoc-depsipeptide couplings were performed as described above until the full peptide was completed. Solid-state fluorescence spectroscopy was used to confirm the coupling of peptides to PEG-glass surfaces through the fluorescence of the Fmoc group (*37*) at an excitation wavelength of 270 nm and emission spectrum from 290-360 nm. Finally, to cleave peptide side chain protecting groups but leave the peptide C-terminus attached to the PEG-glass, a 95:2.5:2.5 TFA:H2O:TIPS mixture was applied to the coverslips and allowed to incubate at room temperature for 2 hours, followed by thorough washing with DMF, DCM, and water. Coverslips were sterilized by soaking in ethanol prior to seeding with cells.

5.2.3 Cell culture and spreading assessment on functionalized glass

NIH 3T3 fibroblasts were cultured from frozen stock in standard tissue culture flasks and passaged at least twice before experimental use. For adhesion and spreading on glass substrates, cells were trypsinized, centrifuged, and resuspended in serum-free medium. Peptide-functionalized glass substrates were placed in separate wells of 12 well plates and washed 2x with phosphate-buffered saline (PBS). Cell suspensions were added at a seeding density of ~6500 cells/cm^2 and incubated for 4-5 hours. Non-adherent cells were washed away with PBS and adherent cells were fixed with 4% formalin in PBS for 10 minutes.

5.2.4 Fluorescent staining and microscopy

After fixation, coverslips were washed with PBS and cells were permeabilized with a 0.1% Triton X-100 solution. After washing 3X with PBS, cell actin filaments were stained with Alexa Fluor® 488 phalloidin (Life Technologies) according to the

manufacturer's protocol and incubated for 30 minutes. The solution was removed, and a DAPI nuclear stain (5 μg/mL) was applied and allowed to incubate for 10 minutes. After washing 3X with PBS, coverslips were removed from wells, mounted on glass microscope slides, and imaged on a microscope with fluorescence excitation using DAPI and FITC filter cubes.

5.2.5 Cell number/shape quantification

Images were analyzed using ImageJ. Cell number in 15 10X images was assessed by automated counting of DAPI-stained nuclei through the use of a custom thresholding and particle counting macro. Cell area, perimeter, and circularity were measured using the ImageJ trace and measure tool on 10 randomly selected cells from images at 40X magnification. The pixel-to-distance relationship used to calculate actual distance and area metrics in μm was established by taking a photograph of a hemocytometer grid at 40X using the same microscope and attached camera used for cell imaging. Statistical analysis was performed using GraphPad Prism 6. A one-way ANOVA was performed, followed by Tukey's test for multiple comparisons. Corrected p-values are reported.

5.2.6 Cytotoxicity assays

The cytotoxicity of leached material from Fmoc-FRGD and Fmoc-F-R-Glc-D gels was assessed by forming gels within well plate inserts with μm scale membrane pore sizes and placing the inserts in wells pre-seeded with cells. NIH 3T3 fibroblasts were seeded in 24 well plates at a density of 5000 cells/cm^2 the day prior to beginning the experiment. Gels (150 μL) were also formed a day prior to the experiment via a pH switch (high to low) at a concentration of 2.5 mg/ml (~3.5 mM). After gels had formed (< 1 hour), the inserts were placed in a well plate containing serum-free cell medium and allowed to equilibrate to physiological pH overnight. On the day of the experiment, gel-

containing inserts were placed in cell-containing well plates and allowed to incubate at 37 °C. For assays involving glycolic acid, sterile-filtered solutions (150 μL) of glycolic acid at varying concentrations (1.75 mM, 3.5 mM, 7 mM, and 14 mM) in medium were added directly to cell-containing wells. At specified time points, inserts were removed, cells were washed with PBS and a tetrazolium-based cell metabolic assay (MTS, CellTiter 96®, Promega Corp.) was performed according to the manufacturer protocol. Color change according to cell number/viability was quantified by measuring the absorbance at 490 nm on a plate reader.

5.3 RESULTS AND DISCUSSION

5.3.1 Gelator synthesis, mechanical properties, and degradation characteristics

Initial efforts to synthesize an RGD analogue focused on the development of Fmoc-R-Glc-D, which is the depsipeptide of Fmoc-RGD, a molecule previously reported to be capable of self-assembly leading to gelation, as well as enhanced cell attachment and spreading (*38*). Following these methods, we found that pure Fmoc-R-Glc-D (**Figure 5.2 A**) at a concentration of ~15 mg/mL self assembles over the course of 2-3 days to form gels both in PBS and in DI water with 50 mM NaCl added. Gelation was demonstrated by the inverted vial test (**Figure 5.2 B**). However, the slow speed of self-assembly and gelation limited the utility of Fmoc-R-Glc-D for functional tests of cell adhesion and spreading. In part due to the work of Gazit and coworkers demonstrating the self-assembly of Fmoc-FRGD (*39*) and also our own previous work with longer, charged depsipeptides (*18*), we hypothesized that adding a phenylalanine residue to Fmoc-R-Glc-D would dramatically decrease the time to gelation. To test this hypothesis more generally prior to full synthesis and purification of Fmoc-F-R-Glc-D, we

synthesized several structure analogs of Fmoc-F-R-Glc-D and assessed their gelation capability (**Table 5.1**) as crude products. All of these phenylalanine-containing di- or tri-peptides were capable of self-assembly leading to gelation, and nearly all formed gels within a matter of seconds and often by several gelation-triggering methods. These results indicated that adding phenylalanine to our R-Glc-D sequence would likely result in robust, flexible, and fast self-assembly behavior.

Fmoc-F-R-Glc-D was readily synthesized using the methods described above. Crude purity was excellent (>90%, **Figure 5.3 A**), with the major impurity (Fmoc-FRD, likely resulting from generation of Fmoc-R by accidental hydrogenolysis of the ester bond during C-terminal debenzylation) being largely removed by subsequent semi-preparative RP-HPLC. In anticipation of needing appropriate controls for functional experiments for integrin- and cell binding, we also synthesized Fmoc-FRGD and Fmoc-FRGE as positive and negative control hydrogelators, respectively. Structures of all are shown in **Figure 5.3 B**. All were capable of self-assembly leading to gelation, as shown in **Figure 5.3 C**. both by pH switch (Solution of 1 equiv 0.5 M NaOH with 1 equiv Fmoc-FRGD, Fmoc-FRGE, or Fmoc-F-R-Glc-D added to 1 equiv 0.1 M HCl) and solvent exchange (100 mg/ml solution of gelator in DMSO diluted 20x to 5 mg/ml with DI water). Interestingly, and only in the case of the solvent exchange method, self-assembly of Fmoc-F-R-Glc-D resulted in gelation only with input of ultrasonic energy by a sonicator or ultrasound probe (SoniGene), whereas Fmoc-FRGD and Fmoc-FRGE formed gels within a few minutes. With a pH switch trigger, all molecules formed gels within 15-20 minutes without the need for input of ultrasound energy. We hypothesize that this apparent discrepancy is due to the ability of residual DMSO in solvent exchange systems stabilizing intermediate micellar structures that, in the absence of DMSO, fairly rapidly convert to fibrous, hydrogel forming structures. In the presence of DMSO,

ultrasound energy provides energy sufficient to overcome the local energy minimum represented by the micelle state and re-assemble into a lower-energy local minimum represented by the fibrous/gel state. Once self-assembled and formed into a hydrogel, Fmoc-F-R-Glc-D, Fmoc-FRGD, and Fmoc-FRGE have remarkably similar rheological properties (**Figure 5.3 D**) with all storage moduli well within the same order of magnitude. Based on our previous work showing that Fmoc-Ala-Lac, the ester analogue of Fmoc-Ala-Ala, was significantly less stiff than Fmoc-Ala-Ala, one might expect that Fmoc-F-R-Glc-D should also be less stiff than Fmoc-FRGD. However, because Fmoc-F-R-Glc-D contains only one ester bond but retains two amide bonds relative to Fmoc-FRGD's three amide bonds, the remaining amide bonds may participate extensively in hydrogen bonding interactions similar to those in Fmoc-FRGD. As a result, the nanostructures and higher order fiber characteristics that contribute to gel rheology may only be slightly dissimilar.

We also assessed the degradation characteristics of Fmoc-F-R-Glc-D gels. Fmoc-FRGD and Fmoc-F-R-Glc-D gels were formed in microcentrifuge tubes at a final concentration of 5 mg/ml (7 mM) via solvent exchange from DMSO followed by sonication. Gels were placed in a 37 °C incubator, and at specified time points 10 μL of gel was dissolved in 490 μL of HPLC-grade methanol and of this mixture 10 μL was analyzed by HPLC (**Figures 5.4 A and B**). Peak area percentages were calculated from peak integrations and plotted as a function of time, as shown in **Figures 5.4 C and D**. Fmoc-F-R-Glc-D gels clearly degraded over a five week period; a new peak in the chromatogram, corresponding to Fmoc-FR released as a result of ester hydrolysis, grew in fractional area over time while the starting product peak decreased. Moreover, this change in peak area was highly linear ($R^2 = 0.98$, least squares method) over the 5-week period. Gels were still fairly intact at the end of the experiment, suggesting that remaining

starting material is still self-assembled and stable in these supramolecular assemblies. It is unclear whether degradation products (chiefly Fmoc-FR and Glc-D) are retained in a self-assembled state, but given the propensity of Fmoc-FR to form hydrogels it may remain mostly incorporated in fibrous nanostructures and contribute to stability after ester cleavage.

5.3.2 Cell spreading and adhesion on gels, and gel cytotoxicity

With gelation ability established, it was possible to use gels for functional tests involving cells. First, we performed simple, short-term experiments to assess cell adhesion and spreading on Fmoc-FRGD gels. Lower concentration gels (5 mg/ml) promoted NIH 3T3 fibroblast attachment and spreading (as determined by phase contrast and fluorescence microscopy) perhaps due to somewhat thin gels allowing for cells to "feel" the underlying glass substrate. Higher concentration gels (10-15 mg/ml) seemed to promote cell attachment but did not cause cells to spread, possibly because the higher RGD density combined with the compliant nature of the gel prevented cells from needing to "reach" as far to make sufficient integrin-RGD contacts (*40*). However, in all cases, use of gels to assess cell adhesion and spreading was technically difficult, as gels tended to fall apart during washing steps and excessive background staining was observed with fluorescent phalloidin and DAPI stains. The DAPI excitement filter cube also caused large background signal even in non-DAPI stained gel samples likely due to the Fmoc group's large intrinsic fluorescence.

Cytotoxicity assays of leached materials from self-assembled gels also gave interesting but potentially problematic results. In various independent cytotoxicitiy experiments, we observed that after 24 hours (day 1), Fmoc-FRGD was more cytotoxic

than Fmoc-F-R-Glc-D (**Figures 5.5 A and C**). However, the remaining cells in Fmoc-FRGD-containing wells seem to recover, showing greater metabolic activity relative to positive controls on day 2 (**Figure 5.5 A**). The reason for this "bounce back" is not understood, though one explanation could be that Fmoc-FRGD molecules are in high enough concentrations on day 1 to competitively interfere with integrin binding to media serum proteins adsorbed to the surface of the well, thereby reducing cell attachment and giving a falsely lowered MTS absorbance. After the day 1 MTS assay is performed, cells are washed (and thus much of the leached Fmoc-FRGD is washed away), and by day 2 the remaining attached cells have proliferated, showing increased absorbance in the day 2 MTS assay. An alternate explanation is that free Fmoc-FRGD molecules are themselves toxic due to the Fmoc group or Fmoc-FR feature, and that by day 2 most of the free molecules that are not incorporated into a fibril assembly have been leached (and then washed) away.

In contrast to cells in Fmoc-FRGD wells, the viability of cells in Fmoc-F-R-Glc-D wells continued to decline, and on day 2 near-zero levels of metabolic activity were observed. If this decline in viability is related to the greater degradability of Fmoc-F-R-Glc-D relative to Fmoc-FRGD, the release of glycolic acid seems not to be the cause—indeed, up to 4X the normal (~3.5 mM) concentration of glycolic did not induce a significant decrease in cell viability (**Figure 5.5 B**). We hypothesized that a more likely degradation product and cause of cytotoxicity would be the Fmoc-FR unit released due to ester hydrolysis. Fmoc-FR (purchased from Bachem, Inc.) was found to be quite cytotoxic, to the same degree as both Fmoc-FRGD and Fmoc-F-R-Glc-D (**Figure 5.5 C**). It therefore is likely that either the Fmoc-group, or the Fmoc-F or Fmoc-FR combination is cytotoxic, even when incorporated into a longer peptide.

5.3.3 Cell spreading and adhesion on peptide- or depsipeptide-modified glass substrates

In order to circumvent the complications of using high-background, potentially cytotoxic gels for measuring the cell interaction with an ester-modified RGD peptide, we opted to assess cell attachment and spreading in 2-D on specially prepared RGD- or R-Glc-D presenting PEGylated glass surfaces. These surfaces were prepared according to the procedure described above, which is summarized in **Figure 5.6 A**. Successful coupling of Fmoc-amino acids to amino-PEG-glass was confirmed by checking for fluorescence of the Fmoc group using a fluorimeter with a solid state sample holder. Excitation was at 270 nm, and emission spectra were recorded from 290-360 nm in 1-nm increments. Fmoc-R(Pbf)-OH coupled directly to amino-PEG-glass resulted in a fluorescent surface (**Figure 5.6 B and C**) even with no background correction. After removal of the Fmoc group by piperidine, the surface is once again non-fluorescent. Given the high efficiency of amide coupling under microwave conditions (*41*), these results were taken to indicate that high-density amino acid coupling had taken place.

RGD- and R-Glc-D, and RGE peptides were then built step by step on amino-PEGylated glass surfaces using identical coupling conditions. NIH 3T3 cells were cultured on these substrates for four hours, then fixed and stained with Alexa Fluor 488®-phalloidin and DAPI and imaged. Fluorescent images (**Figure 5.7, top**) demonstrate significantly increased cell adhesion on RGD-presenting surfaces relative to all other groups (**Figure 5.7, bottom**); R-Glc-D surfaces were not statistically different from PEG-only and RGE surfaces in terms of cell attachment. Cell spreading was assessed by measuring area and perimeter of attached cells in 40x microscope images, and cells on RGD surfaces were significantly greater than cells on all other surfaces for both metrics. Cell circularity, a shape parameter to describe roundness, was also calculated for each

measured cell. Cells on RGD surfaces tended to be less circular due to spreading and extension of pseudo- and filo-podia, presumably due to the strong affinity of their surface integrin proteins for the peptide surface. Finally, upon examination of micrographs it is clear that actin filaments within cells on RGD surfaces are bundled into stress fibers, whereas on non-RGD surfaces actin staining is diffuse and largely delocalized. Stress fibers are characteristic of cells generating traction forces on a surface (*42*), and as they are not observed in cells on PEG, RGE, and R-Glc-D surfaces, we infer that cells are likely not interacting strongly or specifically with these molecules. In other words, these non-adhesive surfaces do not induce intracellular signaling pathways initiated by integrin-binding and/or focal adhesion complex formation that ultimately result in cytoskeletal organization and stress fiber formation. From these results, it appears that hydrogen bonding by backbone amide groups within the RGD sequence may be as critical as side chain identity and sequence in mediating specific and functional binding with cell surface integrin proteins.

5.4 CONCLUSIONS

In this chapter we demonstrated the synthesis and gelation of an N-protected depsipeptide with side chain analogy to the RGD cell adhesion sequence. The inclusion of the ester bond did not appear to disrupt self-assembly and gelation, although under solvent exchange conditions the input of ultrasound energy was required to completely induce gel formation. Degradation of the depsipeptide RGD mimic at physiological temperature was steadily linear with original mass loss of nearly 50% over five weeks, whereas the analogous peptide remained completely intact during the same amount of time. Depsipeptide analogs of RGD were also built on specially modified amino-PEG

glass in order to assess cell adhesion and spreading in 2D, and we found that fibroblasts did not adhere or spread on R-Glc-D surfaces to the same degree as on RGD surfaces. However, given the known context dependence of peptide backbone mutations on disrupting peptide-protein interactions, this result is not likely to be broadly applicable to many other such interactions. Finally, *both* RGD and R-Glc-D gelators were found to be highly cytotoxic over 24 hours, likely due to the presence of non-biological Fmoc protecting group. Further development of self-assembling depsipeptides should therefore focus on replacement of the Fmoc group with a more biocompatible or even biologically-derived aromatic/hydrophobic moiety, with perhaps less emphasis on sequence analogy to bioactive peptides.

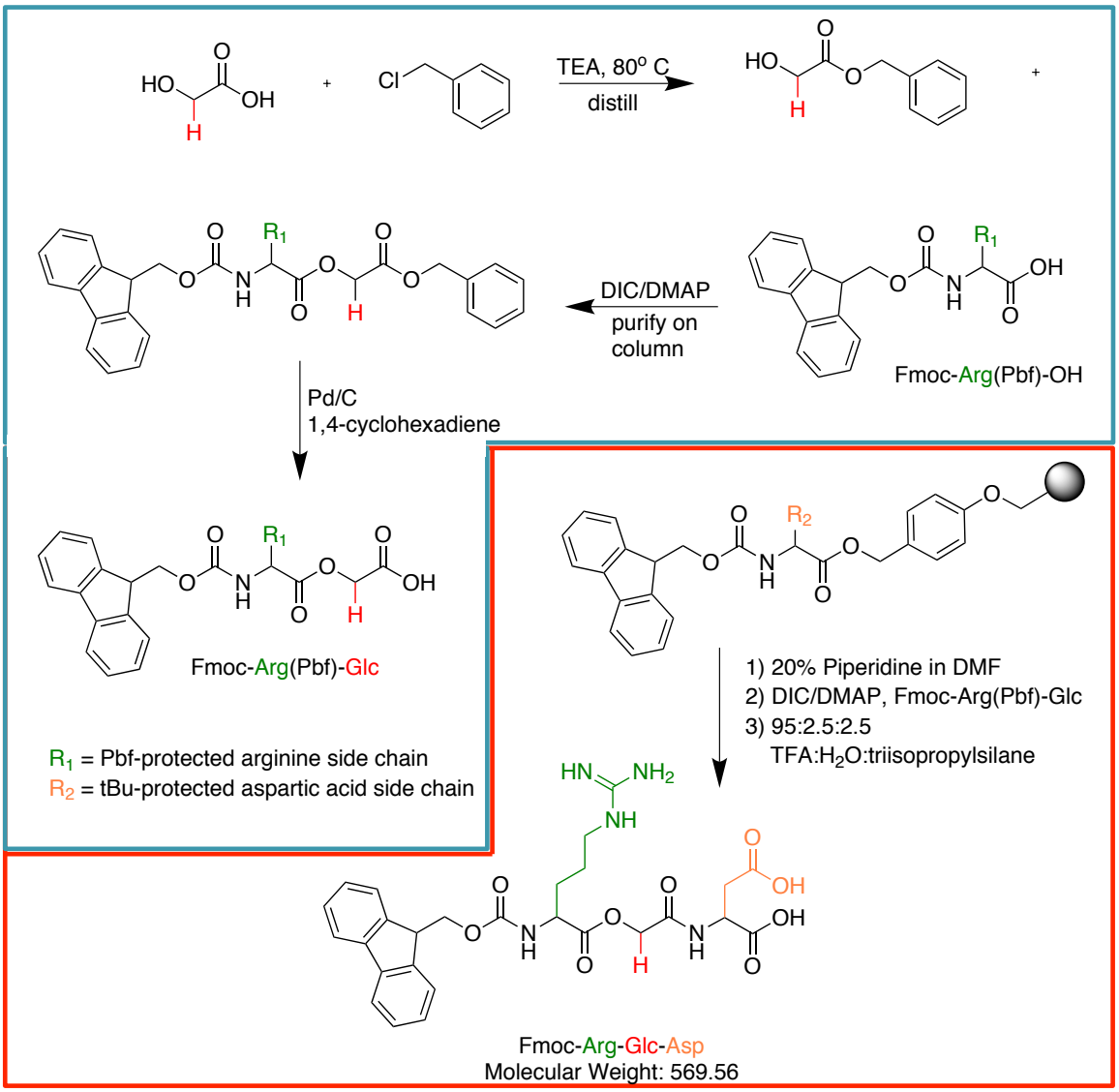

Figure 5.1 Example synthesis scheme for depsipeptides. Here, the final product is a simple Fmoc-R-Glc-D (Glc = glycolic acid) composed of a solution-synthesized (blue outline) Fmoc-R-Glc unit coupled on solid phase (red outline) to resin pre-coupled with aspartic acid. This method is generalizable both in the composition of solution-synthesized depsipeptide units and the solid-phase sequence.

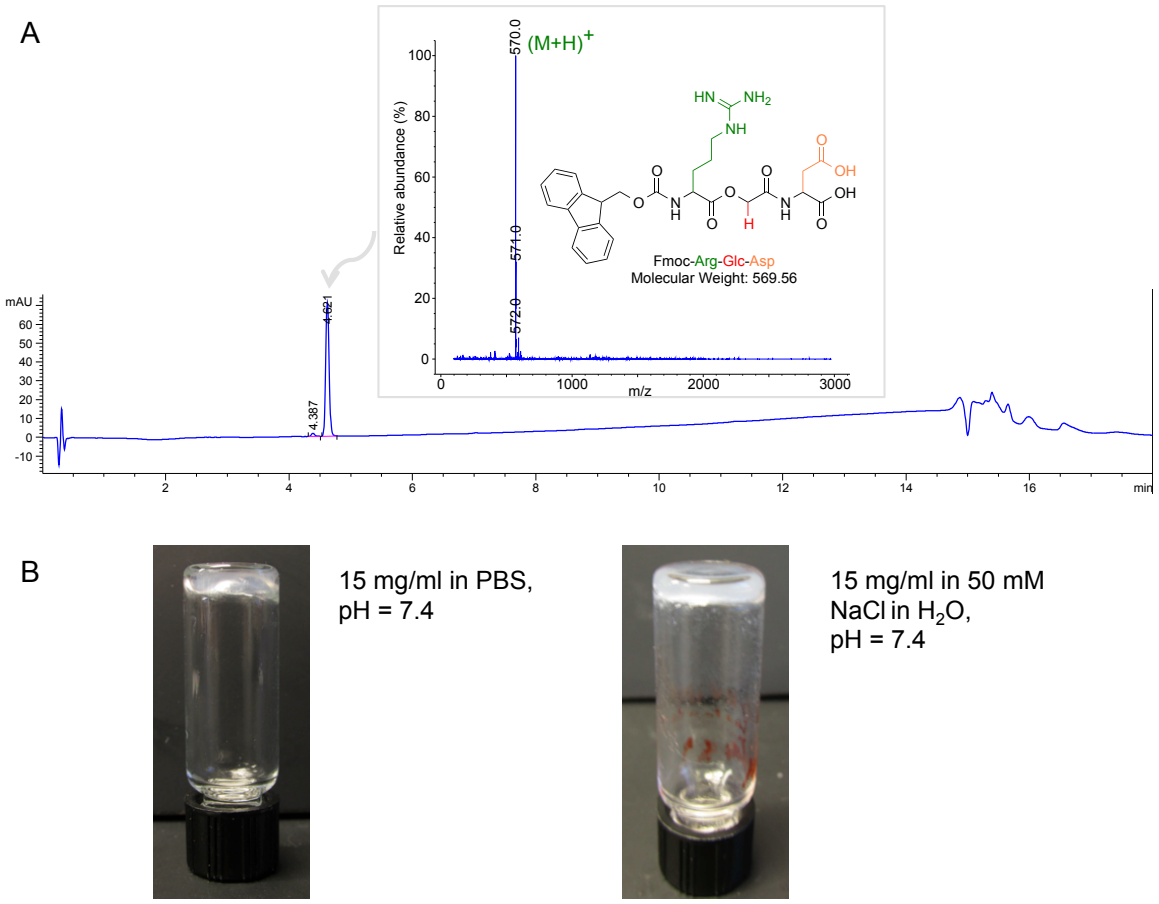

Figure 5.2 Fmoc-R-Glc-D is capable of self-assembly leading to gelation. The purity and identity of the purified compound were assessed using HPLC-MS (A, inset) and gelation was assessed by the inverted vial test (B). Gels were formed over the course of 2-3 days at a gelator concentration of 15 mg/ml (1.5 wt%) both in PBS and DI water with 50 mM NaCl.

Table 5.1 Structure and gelation capability of several phenylalanine-containing di- and tri-peptides with structural analogy to Fmoc-F-R-Glc-D.

Name	Structure	Gelation trigger	Vial photograph
Fmoc-FD	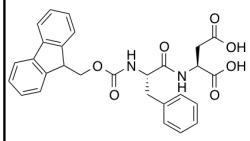	Solvent switch (MeOH→ excess H2O) pH switch (high to low)	
palm-FD	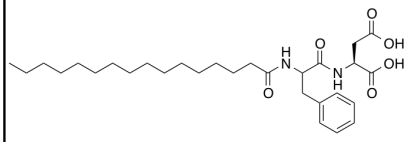	pH switch (high to low)	
Fmoc-FRD	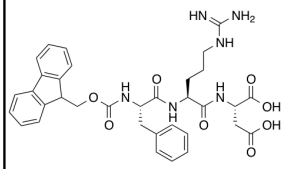	Solvent switch (DMF → excess H2O) pH switch (high to low)	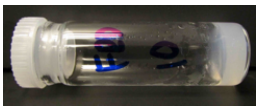
Fmoc-FR	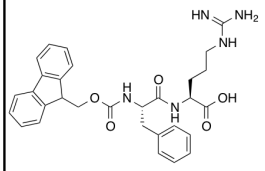	Solvent switch (DMF→ excess H2O) pH switch (high to low) pH switch (only acid added)	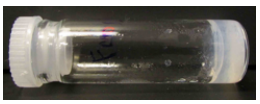

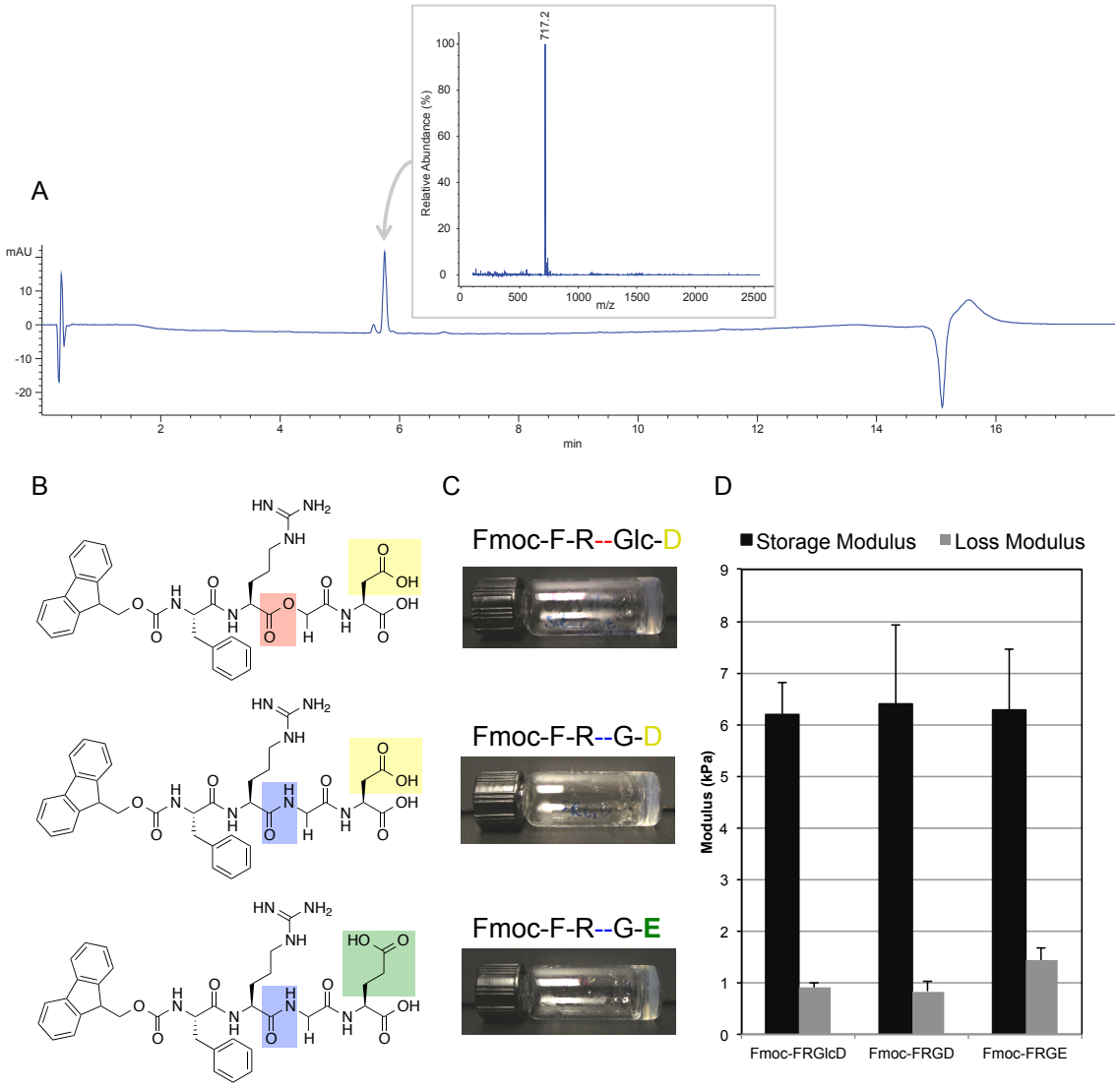

Figure 5.3 Fmoc-F-R-Glc-D synthesis yields a >90% pure crude product (A) with the large peak corresponding to the product (mass spectrum inset). Fmoc-F-R-Glc-D, Fmoc-FRGD, and Fmoc-FRGE (structures in B) all are capable of self-assembly leading to gel formation (C) with similar mechanical properties (D).

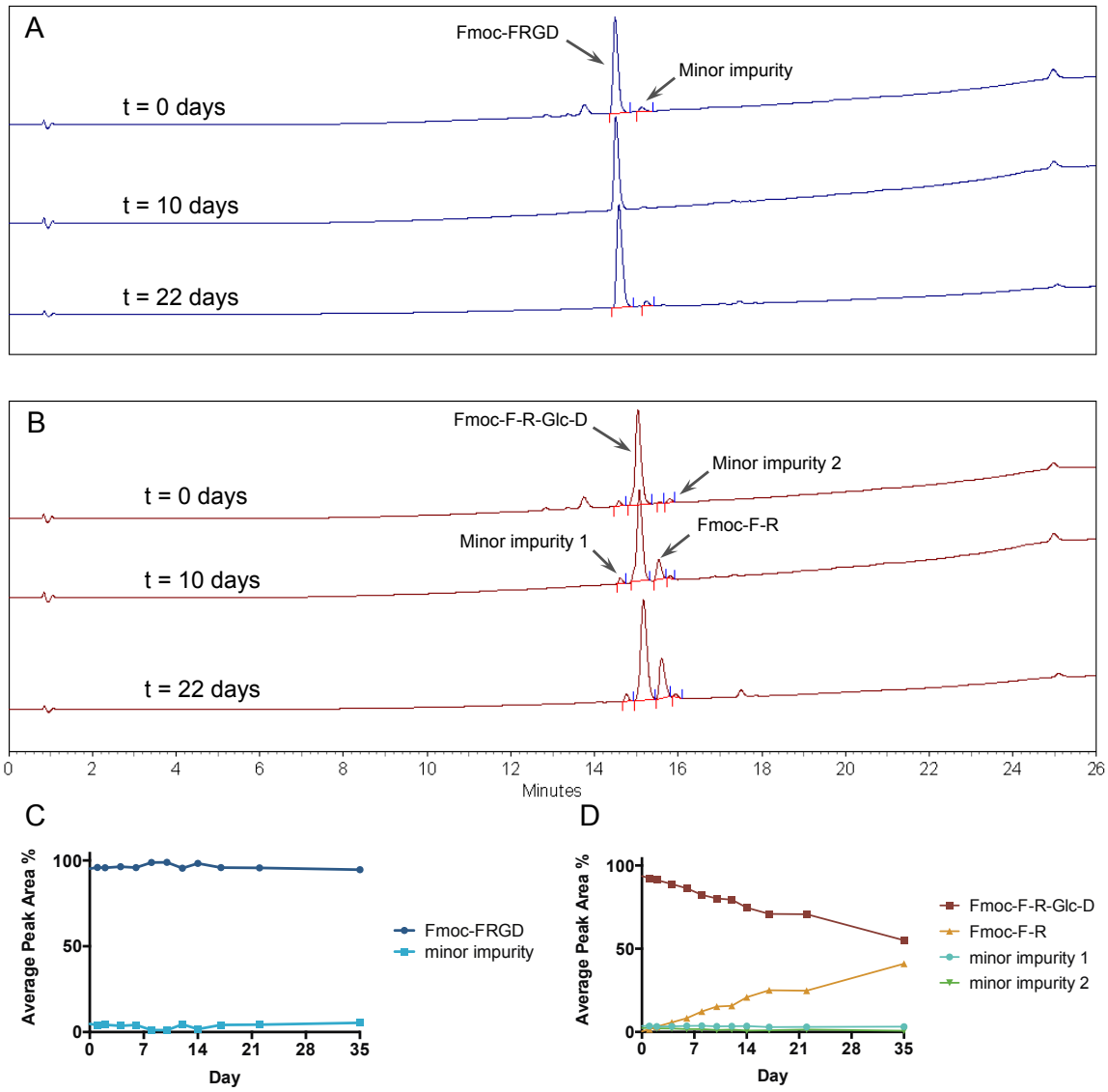

Figure 5.4 Degradation of Fmoc-FRGD and Fmoc-F-R-Glc-D at 37 °C. Representative chromatograms of Fmoc-FRGD (A) and Fmoc-F-R-Glc-D (B) show that over the course of several weeks, Fmoc-F-R-Glc-D degrades via ester hydrolysis whereas Fmoc-FRGD is intact. Integrating peaks and comparing the average percent area (C and D) illustrates that Fmoc-F-R-Glc-D degrades linearly ($R^2 = 0.98$) over five weeks, and Fmoc-FRGD does not degrade significantly.

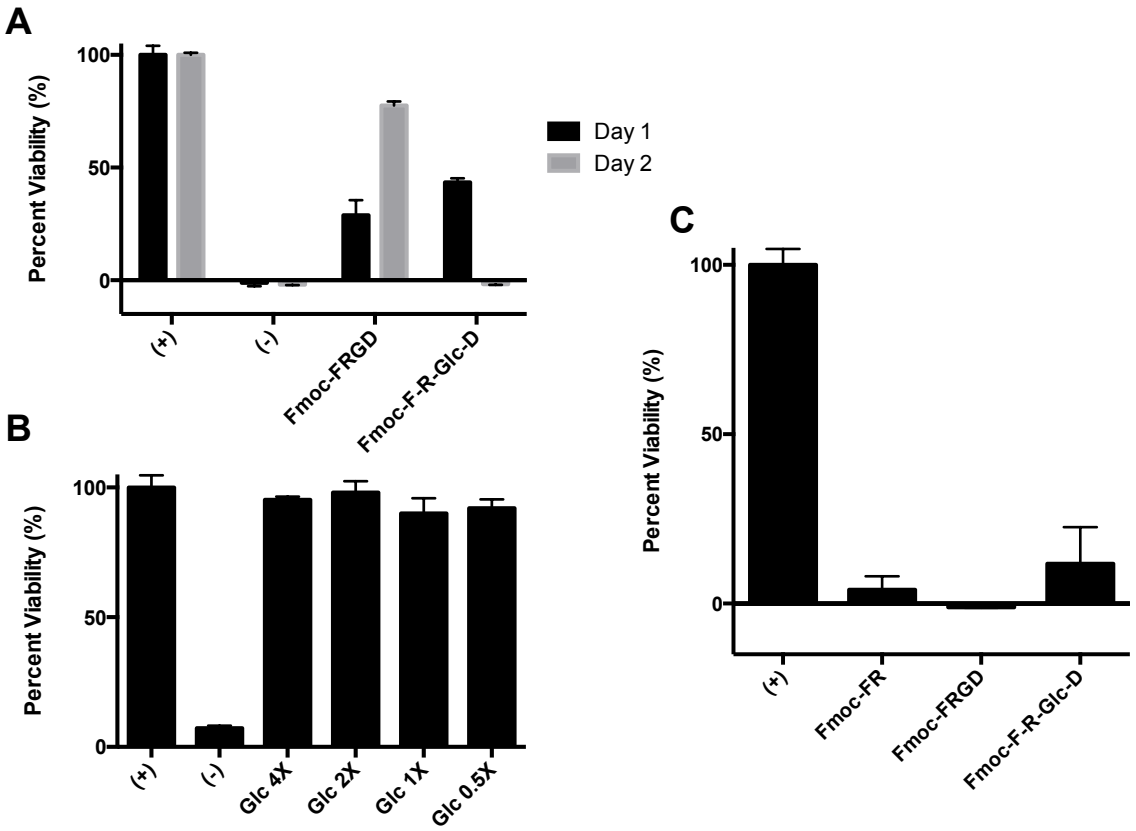

Figure 5.5 Cytoxicity of Fmoc-FRGD and Fmoc-F-R-Glc-D gels with 3T3 cells over days 1 and 2 of culture with gels formed in well inserts. Potential degradation product glycolic acid (Glc) was found to be non-toxic even when added to culture at 4X the molar concentration of gelator in other trials (B). Fmoc-FR, another degradation product of Fmoc-F-R-Glc-D ester hydrolysis, was shown to be as toxic as both gelators (C), indicating that the Fmoc group of Fmoc-FR unit may be directly responsible for observed toxicity in gel trials. (Data is displayed as mean + S.D. for error bars)

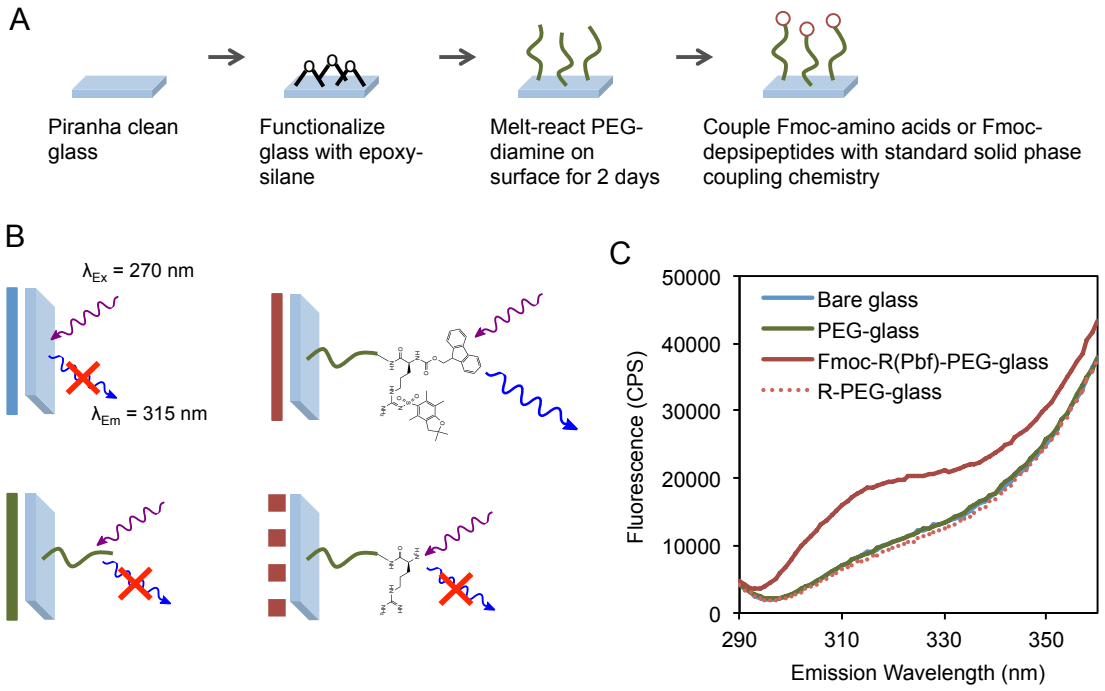

Figure 5.6 Process of functionalizing glass substrates for 2-D cell adhesion and spreading studies (A). To determine if amino acid coupling was successful, Fmoc-mediated fluorescence could be measured in the solid state (B). Indeed, only when Fmoc groups were present on coupled amino acids was a fluorescence signal above background seen (C, no background subtraction).

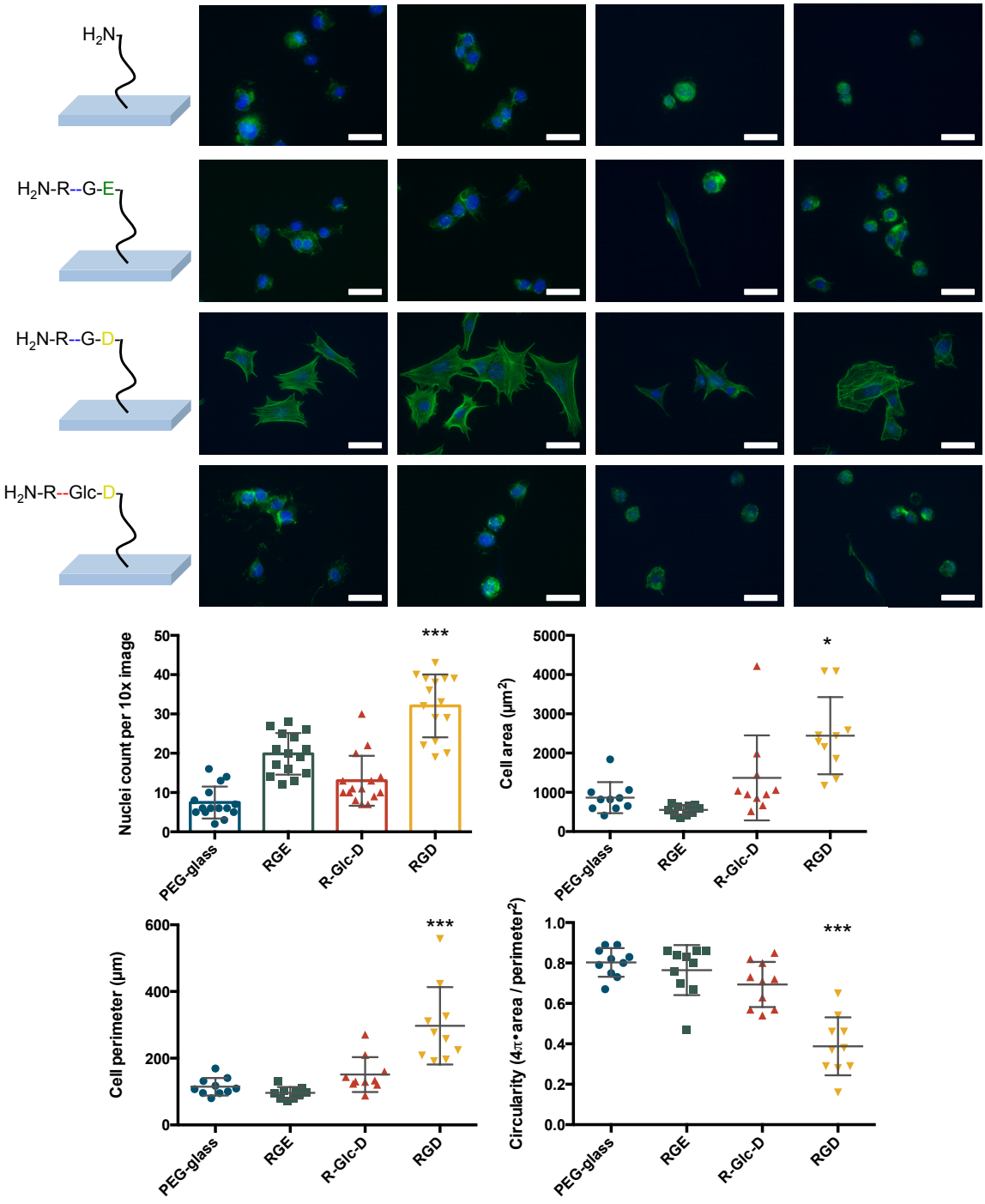

Figure 5.7 Fluorescence images of NIH 3T3 cells on peptide- or depsipeptide-presenting glass surfaces (top, scale bar = 50 μm). Cell attachment and spreading metrics (bottom) are significantly different for RGD presenting surfaces (* indicates $p < 0.05$, *** indicates $p < 0.001$).

5.5 REFERENCES

1. S. Zhang, T. Holmes, C. Lockshin, A. Rich, Spontaneous assembly of a self-complementary oligopeptide to form a stable macroscopic membrane. *Proceedings of the National Academy of Sciences*. **90**, 3334 –3338 (1993).
2. S. Zhang *et al*., Self-complementary oligopeptide matrices support mammalian cell attachment. *Biomaterials*. **16**, 1385–1393 (1995).
3. M. E. Davis *et al*., Injectable Self-Assembling Peptide Nanofibers Create Intramyocardial Microenvironments for Endothelial Cells. *Circulation*. **111**, 442 – 450 (2005).
4. M. E. Davis *et al*., Local myocardial insulin-like growth factor 1 (IGF-1) delivery with biotinylated peptide nanofibers improves cell therapy for myocardial infarction. *Proceedings of the National Academy of Sciences*. **103**, 8155–8160 (2006).
5. F. Gelain, D. Bottai, A. Vescovi, S. Zhang, Designer Self-Assembling Peptide Nanofiber Scaffolds for Adult Mouse Neural Stem Cell 3-Dimensional Cultures. *PLoS ONE*. **1**, e119 (2006).
6. D. A. Narmoneva *et al*., Self-assembling short oligopeptides and the promotion of angiogenesis. *Biomaterials*. **26**, 4837–4846 (2005).
7. N. L. Angeloni *et al*., Regeneration of the cavernous nerve by Sonic hedgehog using aligned peptide amphiphile nanofibers. *Biomaterials*. **32**, 1091–1101 (2011).
8. S. Ghanaati *et al*., Dynamic in vivo biocompatibility of angiogenic peptide amphiphile nanofibers. *Biomaterials*. **30**, 6202–6212 (2009).
9. G. A. Silva *et al*., Selective Differentiation of Neural Progenitor Cells by High-Epitope Density Nanofibers. *Science*. **303**, 1352 –1355 (2004).
10. M. J. Webber *et al*., Supramolecular nanostructures that mimic VEGF as a strategy for ischemic tissue repair. *Proceedings of the National Academy of Sciences*. **108**, 13438 –13443 (2011).
11. V. M. Tysseling-Mattiace *et al*., Self-Assembling Nanofibers Inhibit Glial Scar Formation and Promote Axon Elongation after Spinal Cord Injury. *Journal of Neuroscience*. **28**, 3814–3823 (2008).
12. A. Page-McCaw, A. J. Ewald, Z. Werb, Matrix metalloproteinases and the regulation of tissue remodelling. *Nat Rev Mol Cell Biol*. **8**, 221–233 (2007).
13. B. Sekton, Matrix metalloproteinases - an overview. *Research and Reports in Biology*, 1 (2010).

14. K. M. Eckes, X. Mu, M. A. Ruehle, P. Ren, L. J. Suggs, β Sheets Not Required: Combined Experimental and Computational Studies of Self-Assembly and Gelation of the Ester-Containing Analogue of an Fmoc-Dipeptide Hydrogelator. *Langmuir*. **30**, 5287–5296 (2014).

15. W. Mabey, T. Mill, Critical review of hydrolysis of organic compounds in water under environmental conditions. *Journal of Physical and Chemical Reference Data*. **7**, 383–415 (1978).

16. A. M. Smith *et al*., Fmoc-Diphenylalanine Self Assembles to a Hydrogel via a Novel Architecture Based on π–π Interlocked β-Sheets. *Advanced Materials*. **20**, 37–41 (2008).

17. Y. F. Tian, G. A. Hudalla, H. Han, J. H. Collier, Controllably degradable β-sheet nanofibers and gels from self-assembling depsipeptides. *Biomaterials Science*. **1**, 1037 (2013).

18. M. M. Nguyen, K. M. Eckes, L. J. Suggs, Charge and sequence effects on the self-assembly and subsequent hydrogelation of Fmoc-depsipeptides. *Soft Matter*. **10**, 2693 (2014).

19. E. Ruoslahti, M. D. Pierschbacher, Arg-Gly-Asp: a versatile cell recognition signal. *Cell*. **44**, 517–518 (1986).

20. R. J. Pelham, Y. Wang, Cell locomotion and focal adhesions are regulated by substrate flexibility. *PNAS*. **94**, 13661–13665 (1997).

21. G. Maheshwari, G. Brown, D. A. Lauffenburger, A. Wells, L. G. Griffith, Cell adhesion and motility depend on nanoscale RGD clustering. *J Cell Sci*. **113**, 1677–1686 (2000).

22. A. J. Engler, S. Sen, H. L. Sweeney, D. E. Discher, Matrix Elasticity Directs Stem Cell Lineage Specification. *Cell*. **126**, 677–689 (2006).

23. N. Huebsch *et al*., Harnessing traction-mediated manipulation of the cell/matrix interface to control stem-cell fate. *Nat Mater*. **9**, 518–526 (2010).

24. G. S. Beligere, P. E. Dawson, Design, Synthesis, and Characterization of 4-Ester CI2, a Model for Backbone Hydrogen Bonding in Protein α-Helices. *Journal of the American Chemical Society*. **122**, 12079–12082 (2000).

25. C. L. Jenkins, M. M. Vasbinder, S. J. Miller, R. T. Raines, Peptide Bond Isosteres: Ester or (*E*)-Alkene in the Backbone of the Collagen Triple Helix. *Organic Letters*. **7**, 2619–2622 (2005).

26. J. T. Koh, V. W. Cornish, P. G. Schultz, An Experimental Approach to Evaluating the Role of Backbone Interactions in Proteins Using Unnatural Amino Acid Mutagenesis†. *Biochemistry*. **36**, 11314–11322 (1997).

27. S. Deechongkit *et al*., Context-dependent contributions of backbone hydrogen bonding to β-sheet folding energetics. *Nature*. **430**, 101–105 (2004).

28. D. J. Gordon, S. C. Meredith, Probing the Role of Backbone Hydrogen Bonding in β-Amyloid Fibrils with Inhibitor Peptides Containing Ester Bonds at Alternate Positions. *Biochemistry*. **42**, 475–485 (2003).

29. R. C. Elgersma, T. Meijneke, G. Posthuma, D. T. S. Rijkers, R. M. J. Liskamp, Self-Assembly of Amylin(20–29) Amide-Bond Derivatives into Helical Ribbons and Peptide Nanotubes rather than Fibrils. *Chemistry - A European Journal*. **12**, 3714–3725 (2006).

30. J. N. N. Eildal *et al*., Probing the Role of Backbone Hydrogen Bonds in Protein–Peptide Interactions by Amide-to-Ester Mutations. *Journal of the American Chemical Society*. **135**, 12998–13007 (2013).

31. S. W. Pedersen *et al*., Probing backbone hydrogen bonding in PDZ/ligand interactions by protein amide-to-ester mutations. *Nat Commun*. **5** (2014), doi:10.1038/ncomms4215.

32. M. M. Nguyen, N. Ong, L. Suggs, A general solid phase method for the synthesis of depsipeptides. *Organic & Biomolecular Chemistry*. **11**, 1167 (2013).

33. W. Fan, X. Li, S. Qian, S. Wang, Y. Wu, Enhanced Brain Targeting of Tegafur Using Novel Lactyl Cholesterol Liposome as a Carrier. *Letters in Drug Design & Discovery*. **6**, 542–547 (2009).

34. J. S. Bajwa, Chemoselective deprotection of benzyl esters in the presence of benzyl ethers, benzyloxymethyl ethers and n-benzyl groups by catalytic transfer hydrogenation. *Tetrahedron Letters*. **33**, 2299–2302 (1992).

35. J. Piehler, A. Brecht, R. Valiokas, B. Liedberg, G. Gauglitz, A high-density poly(ethylene glycol) polymer brush for immobilization on glass-type surfaces. *Biosensors and Bioelectronics*. **15**, 473–481 (2000).

36. S. J. Todd, D. J. Scurr, J. E. Gough, M. R. Alexander, R. V. Ulijn, Enzyme-Activated RGD Ligands on Functionalized Poly(ethylene glycol) Monolayers: Surface Analysis and Cellular Response. *Langmuir*. **25**, 7533–7539 (2009).

37. M. Zelzer, D. J. Scurr, M. R. Alexander, R. V. Ulijn, Development and Validation of a Fluorescence Method to Follow the Build-up of Short Peptide Sequences on Solid 2D Surfaces. *ACS Appl. Mater. Interfaces*. **4**, 53–58 (2012).

38. G. Cheng, V. Castelletto, R. R. Jones, C. J. Connon, I. W. Hamley, Hydrogelation of self-assembling RGD-based peptides. *Soft Matter*. **7**, 1326–1333 (2010).

39. R. Orbach *et al*., Self-Assembled Fmoc-Peptides as a Platform for the Formation of Nanostructures and Hydrogels. *Biomacromolecules*. **10**, 2646–2651 (2009).

40. A. Engler *et al*., Substrate Compliance versus Ligand Density in Cell on Gel Responses. *Biophysical Journal*. **86**, 617–628 (2004).

41. C. O. Kappe, Controlled Microwave Heating in Modern Organic Synthesis. *Angewandte Chemie International Edition*. **43**, 6250–6284 (2004).

42. S. Pellegrin, H. Mellor, Actin stress fibres. *Journal of Cell Science*. **120**, 3491–3499 (2007).

Chapter 6: Conclusions and Future Directions

6.1 Conclusions

The purpose of this research project was to characterize the self-assembly and bioactivity of small, N-terminal protected peptides containing ester bond modifications to the amide bond backbone. Through a strong collaboration with Dr. Pengyu Ren's computational molecular modeling group, we performed experimental and computational tests with results suggesting that, at least in the case of small Fmoc-dipeptides, previously hypothesized models for self-assembled structures of Fmoc-dipeptides were highly energetically unfavorable. The same results also indicated that a strict repeating pattern of amide-amide hydrogen bonding in a β-sheet manner was not likely to be the prevalent mode of intermolecular interaction in self-assembled structures of Fmoc-dipeptides and therefore was likely not a strict requirement for self-assembly leading to gelation in water. Based on these results, we hypothesized that an ester-containing analogue of a well-characterized Fmoc-dipeptide hydrogelator should similarly self-assemble into hydrogel-forming nanostructures. To test this hypothesis, we synthesized and purified the depsipeptide analogue of the Fmoc-dipeptide hydrogelator, and found that the Fmoc-depsipeptide was indeed capable of pH- and solvent exchange-triggered self-assembly and gelation. While similar at the level of the basic fibril unit, these systems had important differences in both nano- to micro-scale morphology and macro-scale mechanical properties that could only be attributed to the effect of the ester replacement on higher-order self-assembly of fibril units.

In order to apply these interesting results to a system with greater relevance to biomaterials research and to understand the potential for depsipeptide-protein binding with functional outcomes, we developed a self-assembling depsipeptide RGD analogue.

The analogue, Fmoc-F-R-Glc-D, was capable of self-assembly similar to Fmoc-FRGD, and as hypothesized, Fmoc-F-R-Glc-D also displayed steady, linear degradation over time. We also developed a 2D culture system to determine the propensity of cells to interact with RGD or R-Glc-D tethered to a glass surface, and found that R-Glc-D did not promote cell adhesion and spreading at a level similar to that of RGD. Fibroblasts on R-Glc-D surfaces behaved more similarly to cells on negative control (RGE) surfaces, indicating perhaps that the amide bond between residues R (arginine) and G (glycine) within the RGD peptide participates in hydrogen bonding vital to the RGD-integrin interaction. Furthermore, neither Fmoc-FRGD nor Fmoc-F-R-Glc-D appeared to be suitable as *in vitro* research biomaterials, as we found both to be quite cytotoxic. We attributed the cytotoxicity to the Fmoc group or Fmoc-FR feature, as Fmoc-F-R-Glc-D showed higher cytotoxicity after two days presumably due to release of Fmoc-F-R during degradation. Despite the apparently functional failure of Fmoc-F-R-Glc-D specifically, the work we have performed has contributed to the general scientific community fundamental knowledge about the design requirements for small, peptide-based hydrogelators. We have also demonstrated at a cellular level the importance of backbone-mediated hydrogen bonding in the RGD-integrin interaction. These results indicate that the strengths of depsipeptide-based materials are their self-assembly capability, useful degradation characteristics and natural degradation product, but not necessarily their capability for specific protein binding-mediated bioactivity.

6.2 FUTURE DIRECTIONS

6.2.1 Alternate N-terminal protecting groups for depsipeptides as biocompatible biomaterials

The cytotoxicity of Fmoc-F-R-Glc-D, demonstrated in Chapter 5, is likely not due to the backbone ester substitution, as Fmoc-FRGD was found to be nearly as cytotoxic at the same concentrations. Indeed, even investigations into up to fourfold higher concentrations of glycolic acid alone (a possible degradation product) showed nearly no effect on cell metabolic activity, whereas Fmoc-FR (a definite product of degradation by ester hydrolysis) was cytotoxic at a level similar to both Fmoc-F-R-Glc-D and Fmoc-FRGD. These data point to the culprit for cytotoxicity as the Fmoc group or the Fmoc-FR combination, and this finding is in fairly good agreement with another report of the cytotoxicity of Fmoc-FRGD in the literature (*1*). Yet other reports of fibroblast cells cultured in or on Fmoc-peptide gels have also showed decreasing viability of cells over several days (*2*), however, some show good viability if a RGD sequence is present (*3*). Perhaps unsurprisingly, as they are known to be particularly hardy, only chondrocytes have thus far been shown to have excellent viability within Fmoc-dipeptide hydrogels over longer periods (*4*, *5*). The viability of cells in Fmoc-peptide gels, therefore, seems to be mostly dependent on the cell type used.

We would like our depsipeptide materials to be broadly applicable to a number of different tissue types. For this ideal to be realized, these materials and their constituents must have minimal cytotoxicity to most cell types. As amino acids and many α-hydroxy acids are naturally occurring, the apparent molecular feature to target for optimizing biocompatibility and minimizing cytotoxicity is the N-protecting group. The Fmoc group should be replaced with a nearly equally hydrophobic group that is known to be non-toxic. Due to their current use within peptide amphiphiles, fatty acid chains are an

obvious choice. Non-steroidal anti-inflammatory drugs are inexpensive and have been used as N-terminal protecting groups to drive peptide self-assembly (*6*, *7*). It is also probable that with careful sequence design to include alternating hydrophobic and hydrophilic side chains, N-terminal protecting groups may be completely eliminated while retaining self-assembly capability.

6.2.2 In-depth characterization of depsipeptide degradability

We demonstrated in Chapter 5 that Fmoc-F-R-Glc-D displayed a linear degradation profile over time, whereas Fmoc-FRGD did not degrade appreciably over the same five-week period. Tian et al. have recently demonstrated that the degradation rate of single-ester, 11-residue depsipeptides was highly dependent on pH, temperature, and the steric bulk of the side chain group directly adjacent to the ester bond (*8*), with degradation occurring faster at higher temperatures, slower with bulkier side chain groups, and faster at slightly basic pH (7.4) relative to slightly acidic pH (6.5). We also demonstrated in a previous work that longer, charged depsipeptides capable of self-assembly were slower to degrade when in a diffusion-restricted gel form, and faster to degrade in the presence of salt ions in solution (*9*). These data are from different systems, so experiments could be designed to elucidate which parameter has the greatest effect on degradation within a single, uniform system. However, when designing for biomedical applications in which temperature, pH, and ion concentration are nearly constant, tuning ester-adjacent side chain identity and/or the number of esters would be most interesting. These same parameters could be varied to investigate the impact on mechanical properties as well; indeed, it has been shown that side chain hydrophobicity appears to be roughly correlated with mechanical strength in Fmoc-dipeptide systems (*10*).

Furthermore, experiments could be designed to understand if it is possible to decouple the effects of side chain steric bulk and hydrophobicity on degradation rate and gel mechanical strength. These results would allow for elucidation of the design parameters for depsipeptide-based gels, thereby not only contributing structure-property knowledge about depsipeptides to the scientific canon but also enabling optimization of properties for specific biomedical applications, such as drug- or therapeutic peptide-eluting materials.

6.2.3 Non-gelling depsipeptides for DNA delivery

Our group has already undertaken preliminary work to understand if polycationic, micelle-forming Fmoc-depsipeptides are capable of binding DNA for non-viral delivery to cells as part of a new gene therapy strategy. We hypothesize that nanostructured polycationic carriers, as opposed to polymers like poly(L-lysine) (PLL) and polyethyleneimine (PEI), may be more efficiently taken up by cells. Furthermore, we believe that non-specifically degradable carriers would more readily release DNA in the environment of the endosome, enhancing the efficiency of DNA delivery to the nucleus. This hypothesized process is summarized in **Illustration 6.1**.

Our previous work showed that micelle-like structures could be formed by non-gel-forming depsipeptides in aqueous solution (*9*). We have recently determined that a polycationic depsipeptide, Fmoc-(K-Lac)$_3$-K-A, is capable of forming nano-scale particles that can be observed by TEM. We also found that the presence of Fmoc-(K-Lac)$_3$-K-A in solution with plasmid DNA retarded the migration of DNA during gel electrophoresis, suggesting that complexes of DNA and Fmoc-(K-Lac)$_3$-K-A nanoparticles form and are too large to pass through agarose gel pores. Importantly, we

also found that Fmoc-(K-Lac)$_3$-K-A was only as cytotoxic as PLL and *less* cytotoxic than PEI. Further development of polycationic depsipeptides could result in self-assembling nanoparticulate DNA carriers that have minimal or no apparent cytotoxicity. Unlike current non-viral carriers for DNA delivery, the flexibility of the depsipeptide synthesis technique allows for optimization of a sequence to enhance nanostructure size and perhaps DNA binding affinity. With tunable properties such as these, self-assembled depsipeptides may act as efficient gene delivery vehicles that circumvent many of the complications, toxicity, and efficiency problems associated with both viral- and polymer-assisted DNA delivery to cells.

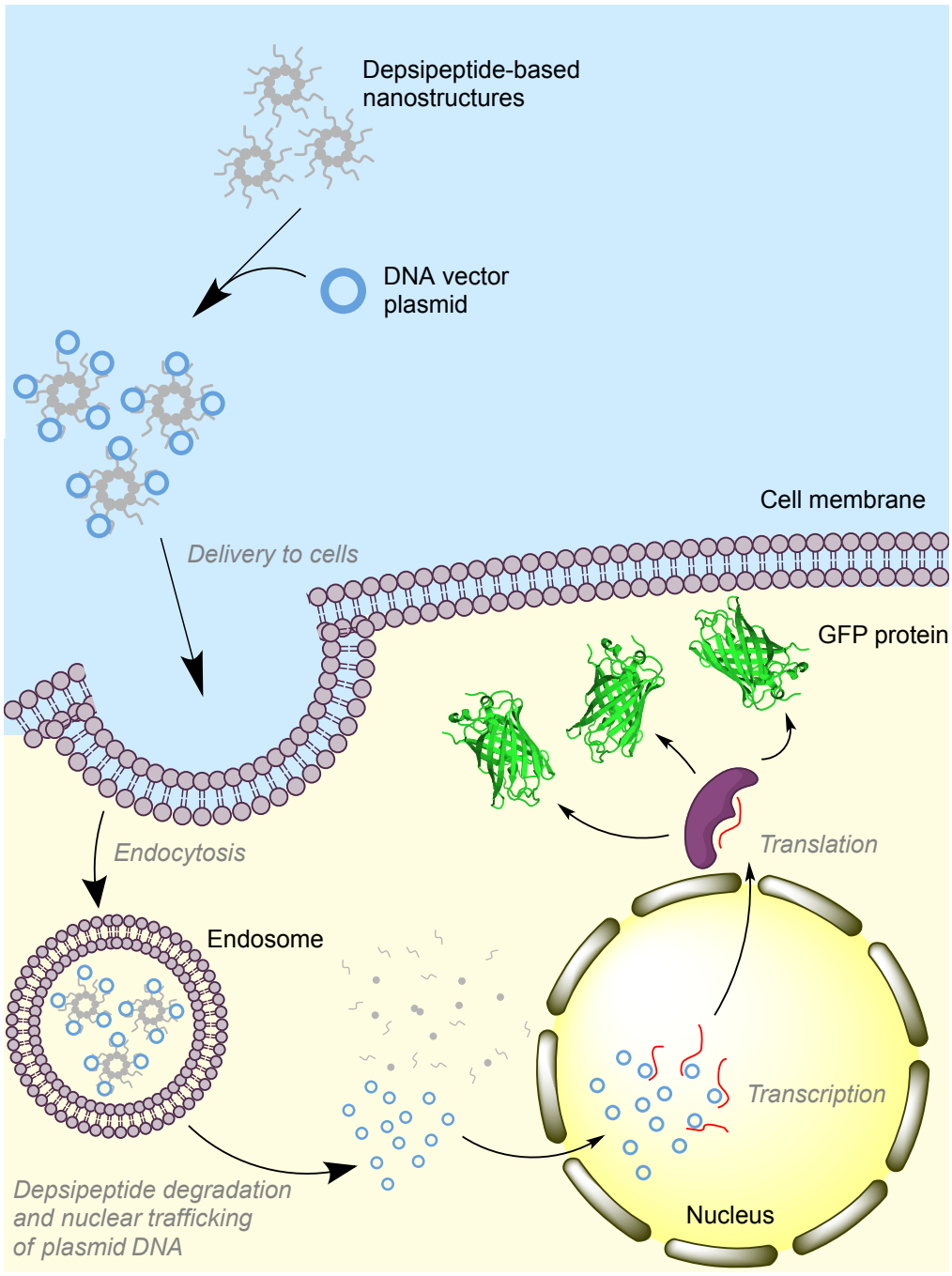

Illustration 6.1 Hypothesized mechanism of degradable depsipeptide nanostructure-mediated gene delivery.

6.3 REFERENCES

1. R. Orbach *et al*., Self-Assembled Fmoc-Peptides as a Platform for the Formation of Nanostructures and Hydrogels. *Biomacromolecules*. **10**, 2646–2651 (2009).
2. M. Zhou *et al*., Self-assembled peptide-based hydrogels as scaffolds for anchorage-dependent cells. *Biomaterials*. **30**, 2523–2530 (2009).
3. V. N. Modepalli *et al*., In vitro response to functionalized self-assembled peptide scaffolds for three-dimensional cell culture. *Biopolymers*. **102**, 197–205 (2014).
4. T. Liebmann, S. Rydholm, V. Akpe, H. Brismar, Self-assembling Fmoc dipeptide hydrogel for in situ 3D cell culturing. *BMC Biotechnology*. **7**, 88 (2007).
5. V. Jayawarna *et al*., Introducing chemical functionality in Fmoc-peptide gels for cell culture. *Acta Biomater*. **5**, 934–943 (2009).
6. J. Li *et al*., The conjugation of nonsteroidal anti-inflammatory drugs (NSAID) to small peptides for generating multifunctional supramolecular nanofibers/hydrogels. *Beilstein Journal of Organic Chemistry*. **9**, 908–917 (2013).
7. S. Bhuniya, Y. J. Seo, B. H. Kim, (S)-(+)-Ibuprofen-based hydrogelators: an approach toward anti-inflammatory drug delivery. *Tetrahedron Letters*. **47**, 7153–7156 (2006).
8. Y. F. Tian, G. A. Hudalla, H. Han, J. H. Collier, Controllably degradable β-sheet nanofibers and gels from self-assembling depsipeptides. *Biomaterials Science*. **1**, 1037 (2013).
9. M. M. Nguyen, K. M. Eckes, L. J. Suggs, Charge and sequence effects on the self-assembly and subsequent hydrogelation of Fmoc-depsipeptides. *Soft Matter*. **10**, 2693 (2014).
10. D. J. Adams, L. M. Mullen, M. Berta, L. Chen, W. J. Frith, Relationship between molecular structure, gelation behaviour and gel properties of Fmoc-dipeptides. *Soft Matter*. **6**, 1971–1980 (2010).

Appendix

A.1 Supplementary Information for Chapter 3

A.1.1 Preliminary 300 ns simulation of Fmoc-AA fibril

A fibril proposed by Smith *et al*. (*1*) was used as the starting structure for our Fmoc-AA self-assembly preliminary simulation. However, the center hollow was not maintained and the tube shrunk into a more compact aggregate after 300 ns simulation, as shown in **Figure A.1**.

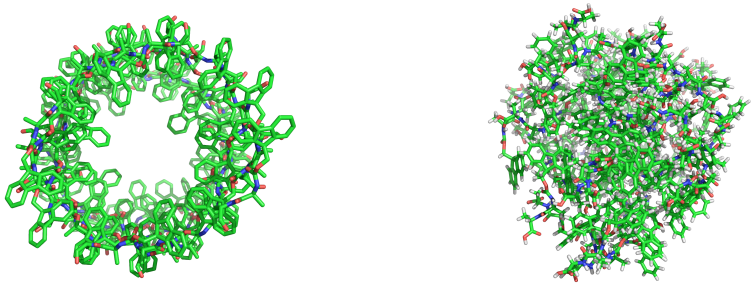

(A) Starting structure (B) After 300 ns simulation

(hydrogens are not shown)

Figure A.1 "Top down" views of Fmoc-AA fibril structure before and after preliminary simulation.

A.1.2 Analysis of GdL hydrolysis by Circular Dichroism

To slow down the process of gelation so that time course measurements of gels could be made easily using circular dichroism, we acidified solutions of Fmoc-AA with 1

eq NaOH using ~2.5 eq glucono-δ-lactone (GdL), after Adams et al. (*2*) GdL is a lactone ring that hydrolyzes in solution to yield gluconic acid, which then acidifes the solution. To understand what extent the hydrolysis of GdL contributed to the overall increase in dichroism during the gelation process, we took CD spectra of a GdL solution. A hypothetical concentration of 5 mg/ml Fmoc-AA was used to calculate the total solution volume (3 mL), the volume of 1 eq NaOH (78.5 μL), and the mass of ~2.5 eq GdL (16.2 mg). The NaOH was added to DI water, and a spectrum was obtained. Then the GdL was added, and the solution was vortexed and a small amount placed in a cylindrical quartz cuvette with a path length of 0.1 mm. Spectra were taken every 10 minutes, as shown in **Figure A.2** below. Interestingly, the magnitude of dichroism decreases slightly over time due to hydrolysis of GdL. Therefore, the increase in dichroism seen in Fmoc-AA solutions acidified with GdL must be due to the self-assembly process and not the hydrolysis of GdL to gluconic acid.

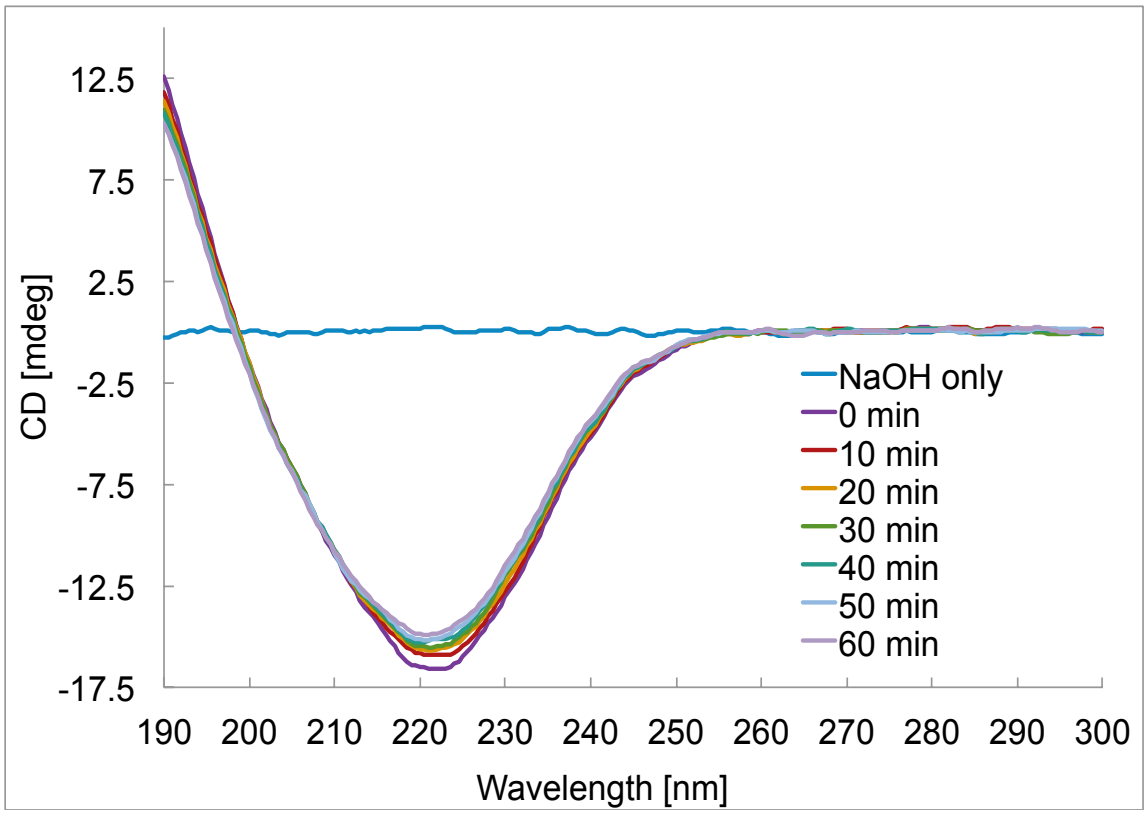

Figure A.2 Time course CD spectra of glucono-δ-lactone. Note that peak intensity decreases over time as hydrolysis proceeds.

A.1.3 References for Chapter 3 Supplementary Information

1. A. M. Smith *et al*., Fmoc-Diphenylalanine Self Assembles to a Hydrogel via a Novel Architecture Based on π–π Interlocked β-Sheets. *Advanced Materials*. **20**, 37–41 (2008).
2. D. J. Adams *et al*., A new method for maintaining homogeneity during liquid–hydrogel transitions using low molecular weight hydrogelators. *Soft Matter*. **5**, 1856 (2009).

A.2 SUPPLEMENTAL METHODS AND INFORMATION FOR CHAPTER 4

A.2.1 Fmoc-L-Ala-L-Lac synthesis and purification

The carboxyl terminus of lactic acid was benzyl-protected using the method of Fan et al (*1*). After purification by distillation, the benzyl-lactate product was dissolved in dichloromethane (DCM) with 1.5 equivalents of Fmoc-L-Ala-OH (EMD Chemicals, Gibbstown, NJ), and the mixture was chilled to 0° C, at which time 1.5 equiv dicyclohexylcarbodiimide (DCC) and 0.01 equiv 4-dimethylaminopyridine (DMAP) were added to initiate the esterification reaction. The reaction was allowed to slowly warm to room temperature and was stirred overnight. The crude mixture was filtered to remove dicyclohexylurea (DCU) crystals, then concentrated *in vacuo* and redissolved in ethyl acetate for aqueous washes (2x 0.1 M HCl, 2x DI water, 1x brine). The organic layer was dried over $MgSO_4$, filtered, and then purified via silica column chromatography using 20% ethyl acetate in hexane as the mobile phase. Fmoc-Ala-Lac-Bn was recovered with a yield of 80-90%.

Fmoc-Ala-Lac-Bn was benzyl-deprotected using the transfer hydrogenolysis method of Bajwa, et al (*2*). Fmoc-Ala-Lac-Bn was dissolved in dry methanol and a small amount of dry DCM, and a 1:1 mass ratio Pd/C (10 wt% Pd) was added to the mixture. The mixture was stirred vigorously and 10 equiv of 1,4-cyclohexadiene was added to the

mixture. After four hours the mixture was filtered over Celite and triturated with dry DCM, then concentrated *in vacuo*. The crude product was purified by silica column chromatography using a 1-5% methanol in DCM gradient. The pure Fmoc-Ala-Lac-OH was lyophilized and recovered at a 30-40% yield. Purity was assessed using LC-MS and NMR and was determined to be > 96%. An ^{1}H NMR spectrum and HPLC chromatogram of the purified product are provided in **Figure A.3**.

^{1}H NMR (500 MHz, DMSO-d_6, δ): 7.89 (d, J = 7.6 Hz, 2H, H_{Ar}), 7.85 (d, J = 7.32, 1H, -N*H*CHCH$_3$), 7.73 (t, J = 6.7 Hz, 2H, H_{Ar}), 7.42 (t, J = 7.4 Hz, 2H, H_{Ar}), 7.34 (t, J = 7.4 Hz, 2H, H_{Ar}), 4.96 (q, J = 7.0 Hz, 1H, -OC*H*CH$_3$), 4.35-4.27 (m, 2H, CHC*H*$_2$), 4.24 (t, J = 6.8 Hz, 1H, -C*H*CH$_2$), 4.17 (quin, J = 7.3, 1H, -NHC*H*CH$_3$), 1.41 (d, J = 7.1 Hz, 3H, -OCHC*H*$_3$), 1.36 (d, J = 7.3 Hz, 3H, -NHCHC*H*$_3$).

^{13}C NMR (500 MHz, DMSO-d_6, δ): 172.43 (1C, -CH(*C*=O)O or –CH$_3$(*C*=O)OH), 171.57 (1C, -CH(*C*=O)O or –CH$_3$(*C*=O)OH), 155.79 (1C, -O(*C*=O)NH), 143.73 (2C, $C_{Ar,\ quaternary}$), 140.66 (2C, $C_{Ar,\ quaternary}$), 127.57 (2C, $C_{Ar,5}$), 127.01 (2C, $C_{Ar,6}$), 125.15 (2C, $C_{Ar,7}$), 120.04 (2C, $C_{Ar,1}$), 68.59 (1C, -O*C*HCH$_3$), 65.62 (1C, CH*C*H$_2$), 48.99 (1C, -NH*C*HCH$_3$), 46.54 (1C, -*C*HCH$_2$), 16.68 (1C, -NHCH*C*H$_3$), 16.64 (1C, -OCH*C*H$_3$).

ESI MS (*m/z*): [M+H]$^+$ calculated for $C_{21}H_{21}NO_6$, 384.14; found, 384.0.

A.2.2 References for Chapter 4 Supplementary Information

1. W. Fan, X. Li, S. Qian, S. Wang, Y. Wu, Enhanced Brain Targeting of Tegafur Using Novel Lactyl Cholesterol Liposome as a Carrier. *Letters in Drug Design & Discovery*. **6**, 542–547 (2009).

2. J. S. Bajwa, Chemoselective deprotection of benzyl esters in the presence of benzyl ethers, benzyloxymethyl ethers and n-benzyl groups by catalytic transfer hydrogenation. *Tetrahedron Letters*. **33**, 2299–2302 (1992).

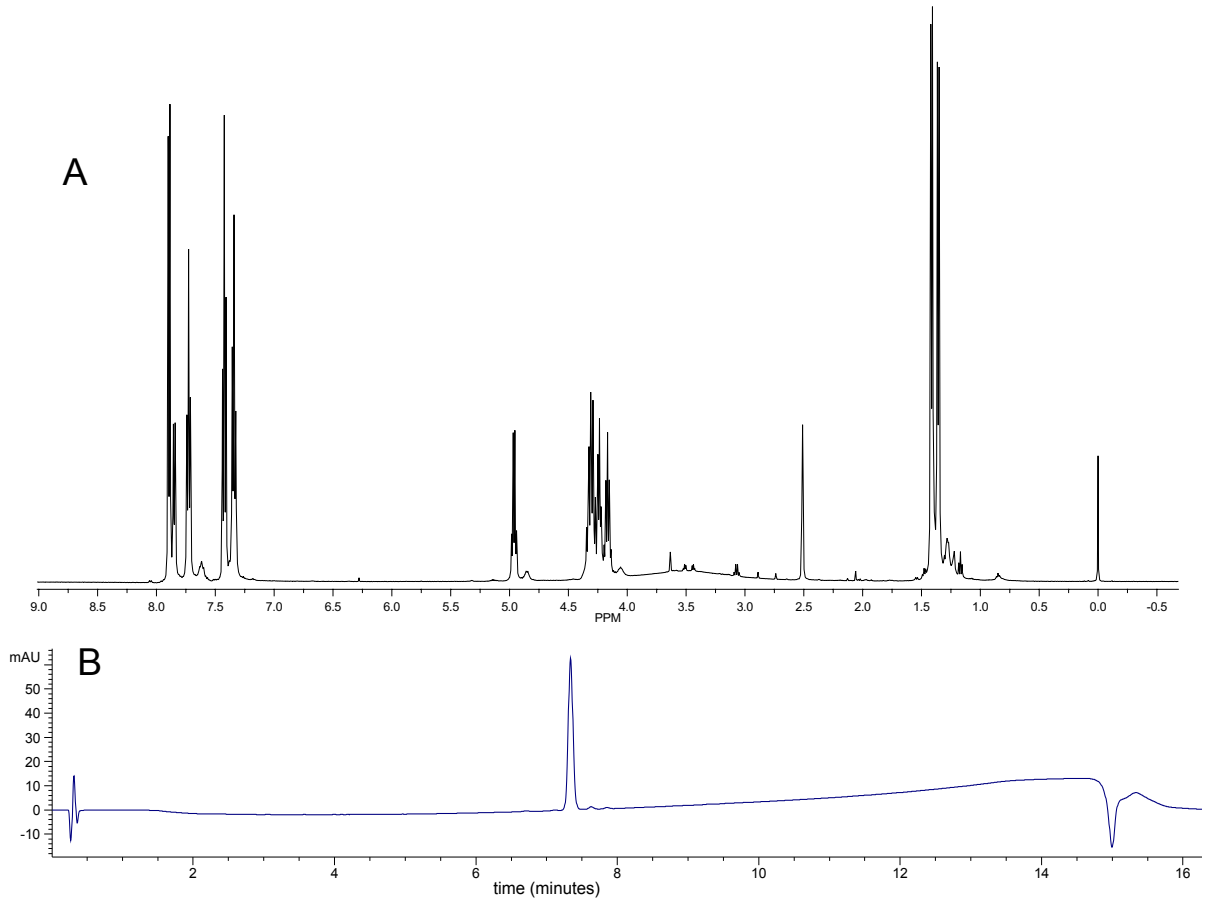

Figure A.3 NMR spectrum (a) and HPLC-MS trace (b) of column-purified Fmoc-Ala-Lac sample. Percent area of product peak (7.4 min) is >98%.

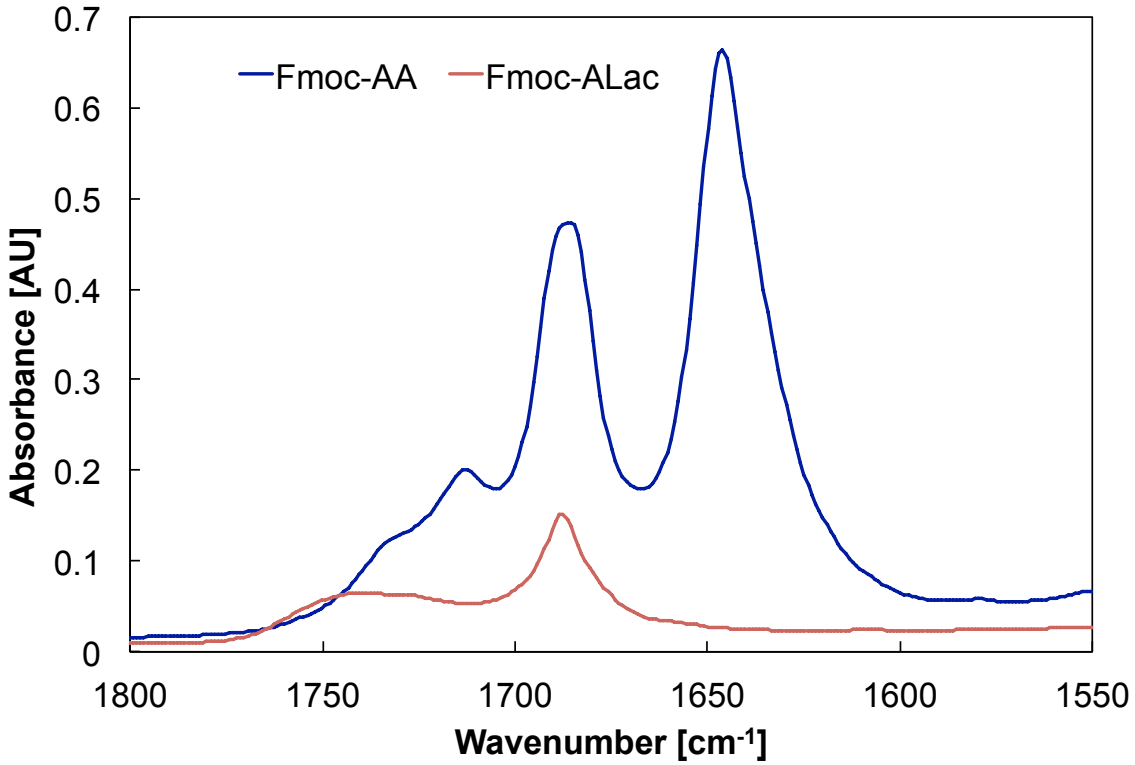

Figure A.4 Non-normalized version of bottom plot in Figure 4.2 B.

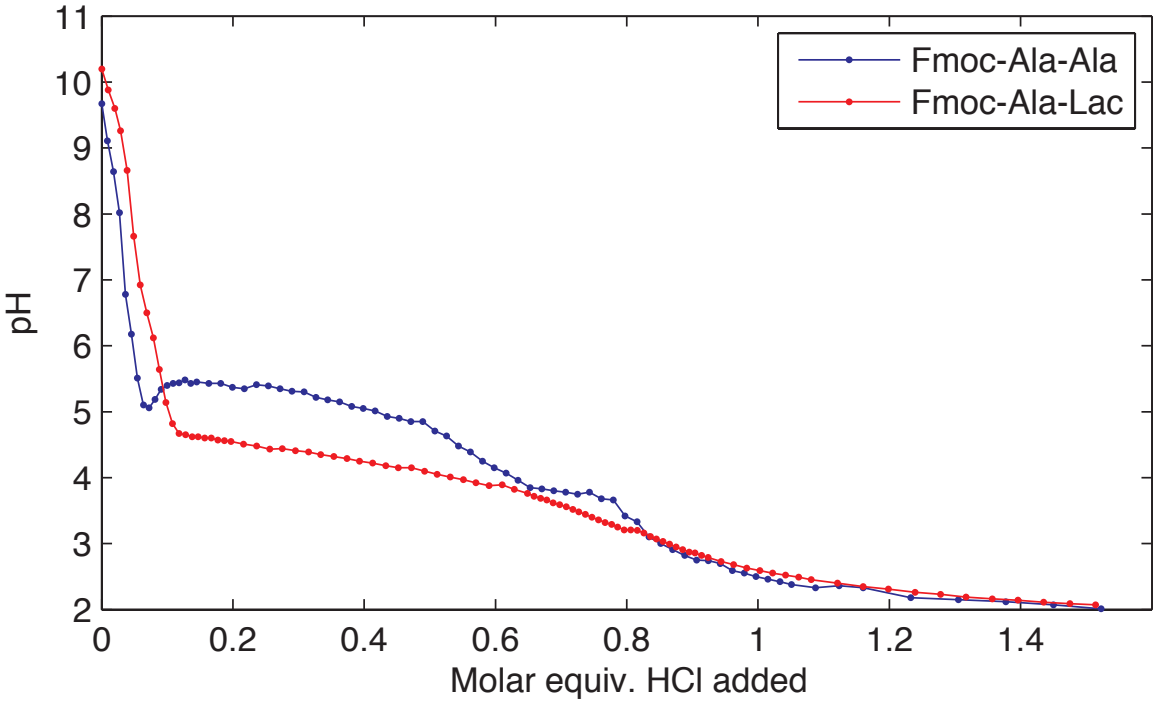

Figure A.5 Titration curves show that Fmoc-Ala-Ala has a higher apparent pKa (~5.1) (indicated by midpoint of the buffering region between ~0.1 – 0.5 eq HCl) than Fmoc-Ala-Lac (pKa ~4.3).

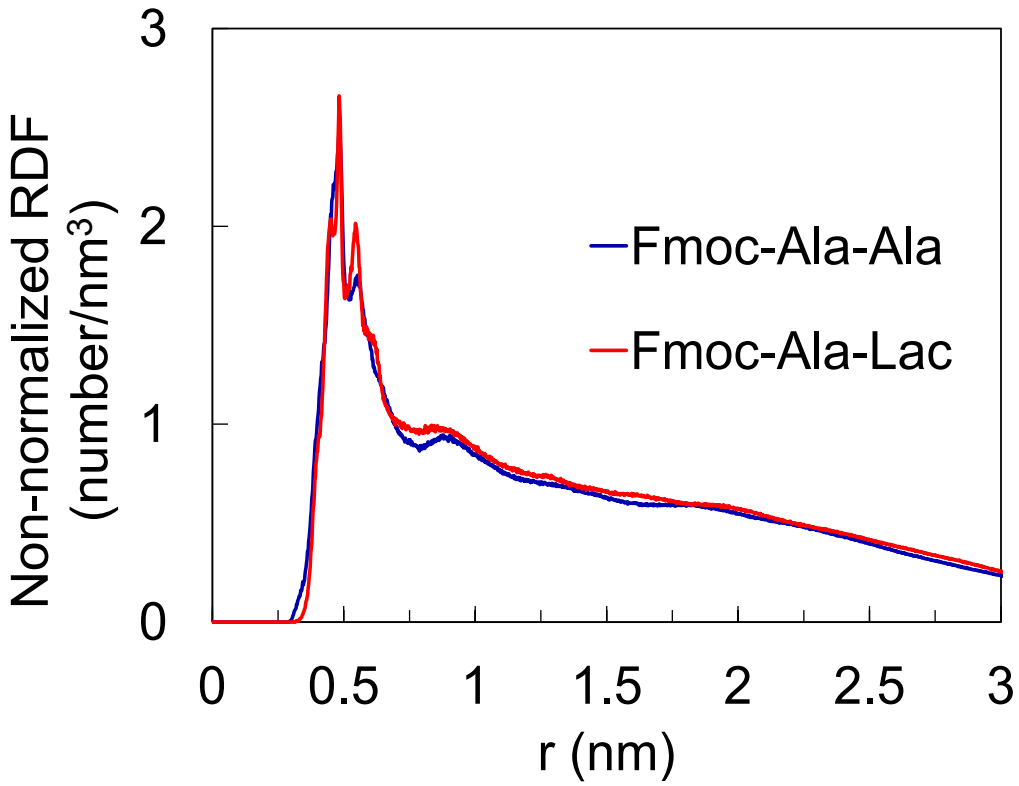

Figure A.6 Radial distribution function (RDF) plot for strand-to-strand (where strand refers to peptide backbone) distance in simulated fibrils of Fmoc-Ala-Ala and Fmoc-Ala-Lac shows marked overlap, indicating similar interaction distances independent of amide-amide hydrogen bonding ability.

Bibliography

Adams, D. J. (2011). Dipeptide and Tripeptide Conjugates as Low-Molecular-Weight Hydrogelators. *Macromol. Biosci.*, *11*(2), 160–173. http://doi.org/10.1002/mabi.201000316

Adams, D. J., Butler, M. F., Frith, W. J., Kirkland, M., Mullen, L., & Sanderson, P. (2009). A new method for maintaining homogeneity during liquid–hydrogel transitions using low molecular weight hydrogelators. *Soft Matter*, *5*(9), 1856. http://doi.org/10.1039/b901556f

Adams, D. J., Morris, K., Chen, L., Serpell, L. C., Bacsa, J., & Day, G. M. (2010). The delicate balance between gelation and crystallisation: structural and computational investigations. *Soft Matter*, *6*(17), 4144–4156. http://doi.org/10.1039/C0SM00409J

Adams, D. J., Mullen, L. M., Berta, M., Chen, L., & Frith, W. J. (2010). Relationship between molecular structure, gelation behaviour and gel properties of Fmoc-dipeptides. *Soft Matter*, *6*(9), 1971–1980. http://doi.org/10.1039/B921863G

Adams, D. J., & Topham, P. D. (2010). Peptide conjugate hydrogelators. *Soft Matter*, *6*(16), 3707–3721. http://doi.org/10.1039/C000813C

Adhikari, B., & Banerjee, A. (2010). Short-Peptide-Based Hydrogel: A Template for the In Situ Synthesis of Fluorescent Silver Nanoclusters by Using Sunlight. *Chemistry – A European Journal*, *16*(46), 13698–13705. http://doi.org/10.1002/chem.201001240

Adhikari, B., & Banerjee, A. (2011). Short peptide based hydrogels: incorporation of graphene into the hydrogel. *Soft Matter*, *7*(19), 9259–9266. http://doi.org/10.1039/C1SM06330H

Aggeli, A., Nyrkova, I. A., Bell, M., Harding, R., Carrick, L., McLeish, T. C. B., … Boden, N. (2001). Hierarchical self-assembly of chiral rod-like molecules as a model for peptide β-sheet tapes, ribbons, fibrils, and fibers. *Proceedings of the National Academy of Sciences of the United States of America*, *98*(21), 11857–11862. http://doi.org/10.1073/pnas.191250198

Ahn, J.-M., Boyle, N. A., MacDonald, M. T., & Janda, K. D. (2002). Peptidomimetics and peptide backbone modifications. *Mini Reviews in Medicinal Chemistry*, *2*(5), 463–473.

A. H. Windle. (1985). X-ray scattering measurements of order in non-crystalline polymers. *Pure Appl. Chem.*, *57*(11), 1627–1638. http://doi.org/10.1351/pac198557111627

Allinger, N. L., Yuh, Y. H., & Lii, J. H. (1989). Molecular mechanics. The MM3 force field for hydrocarbons. 1. *Journal of the American Chemical Society*, *111*, 8551–8566. http://doi.org/10.1021/ja00205a001

Alwan, A., & World Health Organization. (2011). *Global status report on noncommunicable diseases 2010*. Geneva, Switzerland: World Health Organization.

Anderson, J. M., Patterson, J. L., Vines, J. B., Javed, A., Gilbert, S. R., & Jun, H.-W. (2011). Biphasic Peptide Amphiphile Nanomatrix Embedded with Hydroxyapatite Nanoparticles for Stimulated Osteoinductive Response. *ACS Nano*. http://doi.org/10.1021/nn203247m

Anderson, J. M., Vines, J. B., Patterson, J. L., Chen, H., Javed, A., & Jun, H.-W. (2011). Osteogenic differentiation of human mesenchymal stem cells synergistically enhanced by biomimetic peptide amphiphiles combined with conditioned medium. *Acta Biomaterialia*, *7*(2), 675–682. http://doi.org/10.1016/j.actbio.2010.08.016

Angeloni, N. L., Bond, C. W., Tang, Y., Harrington, D. A., Zhang, S., Stupp, S. I., … Podlasek, C. A. (2011). Regeneration of the cavernous nerve by Sonic hedgehog using aligned peptide amphiphile nanofibers. *Biomaterials*, *32*(4), 1091–1101. http://doi.org/10.1016/j.biomaterials.2010.10.003

Bajwa, J. S. (1992). Chemoselective deprotection of benzyl esters in the presence of benzyl ethers, benzyloxymethyl ethers and n-benzyl groups by catalytic transfer hydrogenation. *Tetrahedron Letters*, *33*(17), 2299–2302. http://doi.org/10.1016/S0040-4039(00)74195-5

Baschek, J., R Klein, H., & Schwarz, U. (2012). Stochastic dynamics of virus capsid formation: direct versus hierarchical self-assembly. *BMC Biophysics*, *5*, 22.

Beligere, G. S., & Dawson, P. E. (2000). Design, Synthesis, and Characterization of 4-Ester CI2, a Model for Backbone Hydrogen Bonding in Protein α-Helices. *Journal of the American Chemical Society*, *122*(49), 12079–12082. http://doi.org/10.1021/ja001648e

Bhuniya, S., Seo, Y. J., & Kim, B. H. (2006). (S)-(+)-Ibuprofen-based hydrogelators: an approach toward anti-inflammatory drug delivery. *Tetrahedron Letters*, *47*(40), 7153–7156. http://doi.org/10.1016/j.tetlet.2006.08.002

Biogelx - Pushing Forward BIO-INSPIRED Applications. (2015). Retrieved February 26, 2015, from http://www.biogelx.com

Blake, R. D., Bizzaro, J. W., Blake, J. D., Day, G. R., Delcourt, S. G., Knowles, J., … SantaLucia, J. (1999). Statistical mechanical simulation of polymeric DNA melting with MELTSIM. *Bioinformatics*, *15*, 370–375. http://doi.org/10.1093/bioinformatics/15.5.370

Braun, H.-G., & Cardoso, A. Z. (2012). Self-assembly of Fmoc-diphenylalanine inside liquid marbles. *Colloids and Surfaces B: Biointerfaces*, *97*(0), 43–50. http://doi.org/10.1016/j.colsurfb.2012.03.028

Bryan, M. A., Brauner, J. W., Anderle, G., Flach, C. R., Brodsky, B., & Mendelsohn, R. (2007). FTIR Studies of Collagen Model Peptides: Complementary Experimental and Simulation Approaches to Conformation and Unfolding. *J. Am. Chem. Soc.*, *129*(25), 7877–7884. http://doi.org/10.1021/ja071154i

Buehler, M. J., & Ackbarow, T. (2008). Nanomechanical strength mechanisms of hierarchical biological materials and tissues. *Computer Methods in Biomechanics and Biomedical Engineering*, *11*, 595–607. http://doi.org/10.1080/10255840802078030

Buehler, M. J., & Yung, Y. C. (2009). Deformation and failure of protein materials in physiologically extreme conditions and disease. *Nat Mater*, *8*, 175–188. http://doi.org/10.1038/nmat2387

Bulut, S., Erkal, T. S., Toksoz, S., Tekinay, A. B., Tekinay, T., & Guler, M. O. (2011). Slow Release and Delivery of Antisense Oligonucleotide Drug by Self-Assembled Peptide Amphiphile Nanofibers. *Biomacromolecules*, *12*(8), 3007–3014. http://doi.org/10.1021/bm200641e

Bussi, G., Donadio, D., & Parrinello, M. (2007). Canonical sampling through velocity rescaling. *The Journal of Chemical Physics*, *126*(1), 014101–7.

Castelletto, V., Moulton, C. M., Cheng, G., Hamley, I. W., Hicks, M. R., Rodger, A., … Alemán, C. (2011). Self-assembly of Fmoc-tetrapeptides based on the RGDS cell adhesion motif. *Soft Matter*, *7*(24), 11405. http://doi.org/10.1039/c1sm06550e

Chandler, D. (2005). Interfaces and the driving force of hydrophobic assembly. *Nature*, *437*, 640–647. http://doi.org/10.1038/nature04162

Chandrakumar, N. S., Yonan, P. K., Stapelfeld, A., Savage, M., Rorbacher, E., Contreras, P. C., & Hammond, D. (1992). Preparation and opioid activity of analogs of the analgesic dipeptide 2,6-dimethyl-L-tyrosyl-N-(3-phenylpropyl)-D-alaninamide. *Journal of Medicinal Chemistry*, *35*(2), 223–233. http://doi.org/10.1021/jm00080a005

Chan, J. C. C., Oyler, N. A., Yau, W.-M., & Tycko, R. (2005). Parallel β-Sheets and Polar Zippers in Amyloid Fibrils Formed by Residues 10–39 of the Yeast Prion Protein Ure2p. *Biochemistry*, *44*(31), 10669–10680. http://doi.org/10.1021/bi050724t

Chapman, E., Thorson, J. S., & Schultz, P. G. (1997). Mutational analysis of backbone hydrogen bonds in staphylococcal nuclease. *Journal of the American Chemical Society*, *119*(30), 7151–7152.

Cheng, G., Castelletto, V., Jones, R. R., Connon, C. J., & Hamley, I. W. (2010). Hydrogelation of self-assembling RGD-based peptides. *Soft Matter*, *7*(4), 1326–1333.

Chen, L., Morris, K., Laybourn, A., Elias, D., Hicks, M. R., Rodger, A., … Adams, D. J. (2009). Self-Assembly Mechanism for a Naphthalene–Dipeptide Leading to Hydrogelation. *Langmuir*, *26*(7), 5232–5242. http://doi.org/10.1021/la903694a

Chen, L., Revel, S., Morris, K., C. Serpell, L., & Adams, D. J. (2010). Effect of Molecular Structure on the Properties of Naphthalene–Dipeptide Hydrogelators. *Langmuir*, *26*(16), 13466–13471. http://doi.org/10.1021/la102059x

Christman, K. L., Fok, H. H., Sievers, R. E., Fang, Q., & Lee, R. J. (2004). Fibrin Glue Alone and Skeletal Myoblasts in a Fibrin Scaffold Preserve Cardiac Function after Myocardial Infarction. *Tissue Engineering*, *10*(3-4), 403–409. http://doi.org/10.1089/107632704323061762

Christman, K. L., & Lee, R. J. (2006). Biomaterials for the Treatment of Myocardial Infarction. *Journal of the American College of Cardiology*, *48*(5), 907–913. http://doi.org/10.1016/j.jacc.2006.06.005

Christman, K. L., Vardanian, A. J., Fang, Q., Sievers, R. E., Fok, H. H., & Lee, R. J. (2004). Injectable Fibrin Scaffold Improves Cell Transplant Survival, Reduces Infarct Expansion, and Induces Neovasculature Formation in Ischemic Myocardium. *Journal of the American College of Cardiology*, *44*(3), 654–660. http://doi.org/10.1016/j.jacc.2004.04.040

Clinical Trials. (2014). Retrieved February 26, 2015, from http://www.puramatrix.com/clinical_trials.html

Cui, H., Webber, M. J., & Stupp, S. I. (2010). Self-assembly of peptide amphiphiles: From molecules to nanostructures to biomaterials. *Peptide Science*, *94*(1), 1–18. http://doi.org/10.1002/bip.21328

Darden, T., York, D., & Pedersen, L. (1993). Particle mesh Ewald: An N [center-dot] log(N) method for Ewald sums in large systems. *The Journal of Chemical Physics*, *98*(12), 10089–10092. http://doi.org/10.1063/1.464397

Davis, M. E., Hsieh, P. C., Takahashi, T., Song, Q., Zhang, S., Kamm, R. D., … Lee, R. T. (2006). Local myocardial insulin-like growth factor 1 (IGF-1) delivery with biotinylated peptide nanofibers improves cell therapy for myocardial infarction. *Proceedings of the National Academy of Sciences*, *103*(21), 8155–8160.

Davis, M. E., Motion, J. P. M., Narmoneva, D. A., Takahashi, T., Hakuno, D., Kamm, R. D., … Lee, R. T. (2005). Injectable Self-Assembling Peptide Nanofibers Create Intramyocardial Microenvironments for Endothelial Cells. *Circulation*, *111*(4), 442 –450. http://doi.org/10.1161/01.CIR.0000153847.47301.80

Deechongkit, S., Nguyen, H., Powers, E. T., Dawson, P. E., Gruebele, M., & Kelly, J. W. (2004). Context-dependent contributions of backbone hydrogen bonding to β-sheet folding energetics. *Nature*, *430*(6995), 101–105. http://doi.org/10.1038/nature02611

Deechongkit, S., You, S.-L., & Kelly, J. W. (2004). Synthesis of All Nineteen Appropriately Protected Chiral α-Hydroxy Acid Equivalents of the α-Amino Acids for Boc Solid-Phase Depsi-Peptide Synthesis. *Organic Letters*, *6*(4), 497–500. http://doi.org/10.1021/ol036102m

Douglas, S. M., Dietz, H., Liedl, T., Hogberg, B., Graf, F., & Shih, W. M. (2009). Self-assembly of DNA into nanoscale three-dimensional shapes. *Nature*, *459*(7245), 414–418. http://doi.org/10.1038/nature08016

Eckes, K. M., Mu, X., Ruehle, M. A., Ren, P., & Suggs, L. J. (2014). β Sheets Not Required: Combined Experimental and Computational Studies of Self-Assembly and Gelation of the Ester-Containing Analogue of an Fmoc-Dipeptide Hydrogelator. *Langmuir*, *30*(18), 5287–5296. http://doi.org/10.1021/la500679b

Edelman, M. J., Gandara, D. R., Hausner, P., Israel, V., Thornton, D., DeSanto, J., & Doyle, L. A. (2003). Phase 2 study of cryptophycin 52 (LY355703) in patients previously treated with platinum based chemotherapy for advanced non-small cell lung cancer. *Lung Cancer*, *39*(2), 197–199.

Eildal, J. N. N., Hultqvist, G., Balle, T., Stuhr-Hansen, N., Padrah, S., Gianni, S., … Jemth, P. (2013). Probing the Role of Backbone Hydrogen Bonds in Protein–Peptide Interactions by Amide-to-Ester Mutations. *Journal of the American Chemical Society*, *135*(35), 12998–13007. http://doi.org/10.1021/ja402875h

Elgersma, R. C., Meijneke, T., Posthuma, G., Rijkers, D. T. S., & Liskamp, R. M. J. (2006). Self-Assembly of Amylin(20–29) Amide-Bond Derivatives into Helical Ribbons and Peptide Nanotubes rather than Fibrils. *Chemistry - A European Journal*, *12*(14), 3714–3725. http://doi.org/10.1002/chem.200501374

Elgersma, R. C., Mulder, G. E., Posthuma, G., Rijkers, D. T. S., & Liskamp, R. M. J. (2008). Mirror image supramolecular helical tapes formed by the enantiomeric-depsipeptide derivatives of the amyloidogenic peptide amylin(20–29). *Tetrahedron Letters*, *49*(6), 987–991. http://doi.org/10.1016/j.tetlet.2007.12.021

England, P. M., Zhang, Y., Dougherty, D. A., & Lester, H. A. (1999). Backbone Mutations in Transmembrane Domains of a Ligand-Gated Ion Channel: Implications for the Mechanism of Gating. *Cell*, *96*(1), 89–98. http://doi.org/10.1016/S0092-8674(00)80962-9

Engler, A., Bacakova, L., Newman, C., Hategan, A., Griffin, M., & Discher, D. (2004). Substrate Compliance versus Ligand Density in Cell on Gel Responses. *Biophysical Journal*, *86*(1), 617–628. http://doi.org/10.1016/S0006-3495(04)74140-5

Engler, A. J., Sen, S., Sweeney, H. L., & Discher, D. E. (2006). Matrix Elasticity Directs Stem Cell Lineage Specification. *Cell*, *126*(4), 677–689. http://doi.org/10.1016/j.cell.2006.06.044

Estroff, L. A., & Hamilton, A. D. (2004). Water Gelation by Small Organic Molecules. *Chem. Rev.*, *104*(3), 1201–1218. http://doi.org/10.1021/cr0302049

Fan, W., Li, X., Qian, S., Wang, S., & Wu, Y. (2009). Enhanced Brain Targeting of Tegafur Using Novel Lactyl Cholesterol Liposome as a Carrier. *Letters in Drug Design & Discovery*, *6*(7), 542–547.

FASTSTATS - Heart Disease. (2012, December 4). Retrieved December 4, 2012, from http://www.cdc.gov/nchs/fastats/heart.htm

FDA Approval for Romidepsin. (n.d.). Retrieved February 20, 2015, from http://www.cancer.gov/cancertopics/druginfo/fda-romidepsin

Fitzpatrick, A. W. P., Debelouchina, G. T., Bayro, M. J., Clare, D. K., Caporini, M. A., Bajaj, V. S., … Dobson, C. M. (2013). Atomic structure and hierarchical assembly of a cross-β amyloid fibril. *Proceedings of the National Academy of Sciences*, *110*, 5468–5473. http://doi.org/10.1073/pnas.1219476110

Fleming, S., Frederix, P. W. J. M., Ramos Sasselli, I., Hunt, N. T., Ulijn, R. V., & Tuttle, T. (2013). Assessing the Utility of Infrared Spectroscopy as a Structural Diagnostic Tool for β-Sheets in Self-Assembling Aromatic Peptide Amphiphiles. *Langmuir*, *29*(30), 9510–9515. http://doi.org/10.1021/la400994v

García, A. E., & Onuchic, J. N. (2003). Folding a protein in a computer: An atomic description of the folding/unfolding of protein A. *Proceedings of the National Academy of Sciences*, *100*(24), 13898–13903. http://doi.org/10.1073/pnas.2335541100

Gazit, E. (2002). A possible role for π-stacking in the self-assembly of amyloid fibrils. *The FASEB Journal*, *16*(1), 77–83.

Gelain, F., Bottai, D., Vescovi, A., & Zhang, S. (2006). Designer Self-Assembling Peptide Nanofiber Scaffolds for Adult Mouse Neural Stem Cell 3-Dimensional Cultures. *PLoS ONE*, *1*(1), e119. http://doi.org/10.1371/journal.pone.0000119

Gelain, F., Unsworth, L. D., & Zhang, S. (2010). Slow and sustained release of active cytokines from self-assembling peptide scaffolds. *Journal of Controlled Release*, *145*(3), 231–239. http://doi.org/10.1016/j.jconrel.2010.04.026

Ghanaati, S., Webber, M. J., Unger, R. E., Orth, C., Hulvat, J. F., Kiehna, S. E., … Kirkpatrick, C. J. (2009). Dynamic in vivo biocompatibility of angiogenic peptide amphiphile nanofibers. *Biomaterials*, *30*(31), 6202–6212. http://doi.org/10.1016/j.biomaterials.2009.07.063

Giannis, A., & Kolter, T. (1993). Peptidomimetics for Receptor Ligands—Discovery, Development, and Medical Perspectives. *Angewandte Chemie International Edition in English*, *32*(9), 1244–1267. http://doi.org/10.1002/anie.199312441

Gonzalez-Muniz, R., Garcia-Lopez, M. T., Gomez-Monterrey, I., Herranz, R., Jimeno, M. L., Suarez-Gea, M. L., … Suzdak, P. (1995). Ketomethylene and

(cyanomethylene) amino pseudopeptide analogs of the C-terminal hexapeptide of neurotensin. *Journal of Medicinal Chemistry*, *38*(6), 1015–1021.

Gordon, D. J., & Meredith, S. C. (2003). Probing the Role of Backbone Hydrogen Bonding in β-Amyloid Fibrils with Inhibitor Peptides Containing Ester Bonds at Alternate Positions. *Biochemistry*, *42*(2), 475–485. http://doi.org/10.1021/bi0259857

Greenfield, M. A., Hoffman, J. R., Olvera de la Cruz, M., & Stupp, S. I. (2009). Tunable Mechanics of Peptide Nanofiber Gels. *Langmuir*, *26*(5), 3641–3647. http://doi.org/10.1021/la9030969

Guo, J., Wang, J., Anderson, J. C., & Schultz, P. G. (2008). Addition of an α-Hydroxy Acid to the Genetic Code of Bacteria. *Angewandte Chemie International Edition*, *47*(4), 722–725. http://doi.org/10.1002/anie.200704074

Hartgerink, J. D., Beniash, E., & Stupp, S. I. (2001). Self-Assembly and Mineralization of Peptide-Amphiphile Nanofibers. *Science*, *294*(5547), 1684 –1688. http://doi.org/10.1126/science.1063187

Hess, B. (2007). P-LINCS: A Parallel Linear Constraint Solver for Molecular Simulation. *J. Chem. Theory Comput.*, *4*(1), 116–122. http://doi.org/10.1021/ct700200b

Hess, B., Bekker, H., Berendsen, H. J. C., & Fraaije, J. G. E. M. (1997). LINCS: A linear constraint solver for molecular simulations. *Journal of Computational Chemistry*, *18*(12), 1463–1472. http://doi.org/10.1002/(SICI)1096-987X(199709)18:12<1463::AID-JCC4>3.0.CO;2-H

Hess, B., Kutzner, C., van der Spoel, D., & Lindahl, E. (2008). GROMACS 4: Algorithms for Highly Efficient, Load-Balanced, and Scalable Molecular Simulation. *J. Chem. Theory Comput.*, *4*(3), 435–447. http://doi.org/10.1021/ct700301q

Holmes, T. C., de Lacalle, S., Su, X., Liu, G., Rich, A., & Zhang, S. (2000). Extensive neurite outgrowth and active synapse formation on self-assembling peptide scaffolds. *Proceedings of the National Academy of Sciences*, *97*(12), 6728 –6733. http://doi.org/10.1073/pnas.97.12.6728

Horii, A., Wang, X., Gelain, F., & Zhang, S. (2007). Biological Designer Self-Assembling Peptide Nanofiber Scaffolds Significantly Enhance Osteoblast Proliferation, Differentiation and 3-D Migration. *PLoS ONE*, *2*(2), e190. http://doi.org/10.1371/journal.pone.0000190

Horne, W. S., & Gellman, S. H. (2008). Foldamers with Heterogeneous Backbones. *Accounts of Chemical Research*, *41*(10), 1399–1408. http://doi.org/10.1021/ar800009n

Houton, K. A., Morris, K. L., Chen, L., Schmidtmann, M., Jones, J. T. A., Serpell, L. C., … Adams, D. J. (2012). On Crystal versus Fiber Formation in Dipeptide

Hydrogelator Systems. *Langmuir*, *28*(25), 9797–9806. http://doi.org/10.1021/la301371q

Huebsch, N., Arany, P. R., Mao, A. S., Shvartsman, D., Ali, O. A., Bencherif, S. A., … Mooney, D. J. (2010). Harnessing traction-mediated manipulation of the cell/matrix interface to control stem-cell fate. *Nature Materials*, *9*(6), 518–526. http://doi.org/10.1038/nmat2732

Ingwall, R. T., & Goodman, M. (1974). Polydepsipeptides. III. Theoretical Conformational Analysis of Randomly Coiling and Ordered Depsipeptide Chains. *Macromolecules*, *7*(5), 598–605. http://doi.org/10.1021/ma60041a011

Jackson, M., & Mantsch, H. H. (1995). The Use and Misuse of FTIR Spectroscopy in the Determination of Protein Structure. *Critical Reviews in Biochemistry and Molecular Biology*, *30*(2), 95–120. http://doi.org/10.3109/10409239509085140

Jayawarna, V., Ali, M., Jowitt, T. A., Miller, A. F., Saiani, A., Gough, J. E., & Ulijn, R. V. (2006). Nanostructured Hydrogels for Three-Dimensional Cell Culture Through Self-Assembly of Fluorenylmethoxycarbonyl–Dipeptides. *Advanced Materials*, *18*(5), 611–614. http://doi.org/10.1002/adma.200501522

Jayawarna, V., Richardson, S. M., Hirst, A. R., Hodson, N. W., Saiani, A., Gough, J. E., & Ulijn, R. V. (2009). Introducing chemical functionality in Fmoc-peptide gels for cell culture. *Acta Biomater.*, *5*(3), 934–943. http://doi.org/10.1016/j.actbio.2009.01.006

Jenkins, C. L., Vasbinder, M. M., Miller, S. J., & Raines, R. T. (2005). Peptide Bond Isosteres: Ester or (*E*)-Alkene in the Backbone of the Collagen Triple Helix. *Organic Letters*, *7*(13), 2619–2622. http://doi.org/10.1021/ol050780m

Johnson, R. R., Johnson, A. T. C., & Klein, M. L. (2008). Probing the Structure of DNA−Carbon Nanotube Hybrids with Molecular Dynamics. *Nano Letters*, *8*(1), 69–75. http://doi.org/10.1021/nl071909j

Johnson, R. R., Kohlmeyer, A., Johnson, A. T. C., & Klein, M. L. (2009). Free Energy Landscape of a DNA−Carbon Nanotube Hybrid Using Replica Exchange Molecular Dynamics. *Nano Letters*, *9*(2), 537–541. http://doi.org/10.1021/nl802645d

Jorgensen, W. L., Briggs, J. M., & Gao, J. (1987). A priori calculations of pKa's for organic compounds in water. The pKa of ethane. *Journal of the American Chemical Society*, *109*, 6857–6858. http://doi.org/10.1021/ja00256a053

Jorgensen, W. L., Chandrasekhar, J., Madura, J. D., Impey, R. W., & Klein, M. L. (1983). Comparison of simple potential functions for simulating liquid water. *The Journal of Chemical Physics*, *79*(2), 926–935.

Jorgensen, W. L., Maxwell, D. S., & Tirado-Rives, J. (1996). Development and Testing of the OPLS All-Atom Force Field on Conformational Energetics and Properties

of Organic Liquids. *J. Am. Chem. Soc.*, *118*(45), 11225–11236. http://doi.org/10.1021/ja9621760

Jorgensen, W. L., & Schyman, P. (2012). Treatment of Halogen Bonding in the OPLS-AA Force Field: Application to Potent Anti-HIV Agents. *Journal of Chemical Theory and Computation*, *8*, 3895–3901. http://doi.org/10.1021/ct300180w

Jorgensen, W. L., & Tirado-Rives, J. (2005). Potential energy functions for atomic-level simulations of water and organic and biomolecular systems. *Proceedings of the National Academy of Sciences of the United States of America*, *102*(19), 6665–6670. http://doi.org/10.1073/pnas.0408037102

Kaminski, G. A., Friesner, R. A., Tirado-Rives, J., & Jorgensen, W. L. (2001). Evaluation and Reparametrization of the OPLS-AA Force Field for Proteins via Comparison with Accurate Quantum Chemical Calculations on Peptides†. *J. Phys. Chem. B*, *105*(28), 6474–6487. http://doi.org/10.1021/jp003919d

Kappe, C. O. (2004). Controlled Microwave Heating in Modern Organic Synthesis. *Angewandte Chemie International Edition*, *43*(46), 6250–6284. http://doi.org/10.1002/anie.200400655

Karplus, M., & McCammon, J. A. (2002). Molecular dynamics simulations of biomolecules. *Nat Struct Mol Biol*, *9*(9), 646–652. http://doi.org/10.1038/nsb0902-646

Khandelwal, G., & Bhyravabhotla, J. (2010). A Phenomenological Model for Predicting Melting Temperatures of DNA Sequences. *PLoS ONE*, *5*, e12433. http://doi.org/10.1371/journal.pone.0012433

Kim, J.-K., Anderson, J., Jun, H.-W., Repka, M. A., & Jo, S. (2009). Self-Assembling Peptide Amphiphile-Based Nanofiber Gel for Bioresponsive Cisplatin Delivery. *Molecular Pharmaceutics*, *6*(3), 978–985. http://doi.org/10.1021/mp900009n

Kirkpatrick, S., Gelatt, C. D., & Vecchi, M. P. (1983). Optimization by Simulated Annealing. *Science*, *220*(4598), 671 –680.

Kiso, Y. (1996). Design and synthesis of substrate-based peptidomimetic human immunodeficiency virus protease inhibitors containing the hydroxymethylcarbonyl isostere. *Peptide Science*, *40*(2), 235–244. http://doi.org/10.1002/(SICI)1097-0282(1996)40:2<235::AID-BIP3>3.0.CO;2-X

Knowles, T. P. J., Oppenheim, T. W., Buell, A. K., Chirgadze, D. Y., & Welland, M. E. (2010). Nanostructured films from hierarchical self-assembly of amyloidogenic proteins. *Nat Nano*, *5*, 204–207.

Ko, E., Liu, J., & Burgess, K. (2011). Minimalist and universal peptidomimetics. *Chemical Society Reviews*, *40*(8), 4411. http://doi.org/10.1039/c0cs00218f

Koh, J. T., Cornish, V. W., & Schultz, P. G. (1997). An Experimental Approach to Evaluating the Role of Backbone Interactions in Proteins Using Unnatural Amino

Acid Mutagenesis†. *Biochemistry*, *36*(38), 11314–11322. http://doi.org/10.1021/bi9707685

Konstam, M. A., Kramer, D. G., Patel, A. R., Maron, M. S., & Udelson, J. E. (2011). Left Ventricular Remodeling in Heart Failure: Current Concepts in Clinical Significance and Assessment. *JACC: Cardiovascular Imaging*, *4*(1), 98–108. http://doi.org/10.1016/j.jcmg.2010.10.008

Konstantinopoulos, P. A., Vandoros, G. P., & Papavassiliou, A. G. (2006). FK228 (depsipeptide): a HDAC inhibitor with pleiotropic antitumor activities. *Cancer Chemotherapy and Pharmacology*, *58*(5), 711–715. http://doi.org/10.1007/s00280-005-0182-5

Kopesky, P. W., Vanderploeg, E. J., Sandy, J. S., Kurz, B., & Grodzinsky, A. J. (2010a). Self-Assembling Peptide Hydrogels Modulate In Vitro Chondrogenesis of Bovine Bone Marrow Stromal Cells. *Tissue Engineering Part A*, *16*, 465–477. http://doi.org/10.1089/ten.tea.2009.0158

Kopesky, P. W., Vanderploeg, E. J., Sandy, J. S., Kurz, B., & Grodzinsky, A. J. (2010b). Self-Assembling Peptide Hydrogels Modulate In Vitro Chondrogenesis of Bovine Bone Marrow Stromal Cells. *Tissue Engineering Part A*, *16*, 465–477. http://doi.org/10.1089/ten.tea.2009.0158

Koutsopoulos, S., Unsworth, L. D., Nagai, Y., & Zhang, S. (2009). Controlled release of functional proteins through designer self-assembling peptide nanofiber hydrogel scaffold. *Proceedings of the National Academy of Sciences*, *106*(12), 4623 –4628. http://doi.org/10.1073/pnas.0807506106

Kuisle, O., Quiñoá, E., & Riguera, R. (1999). A General Methodology for Automated Solid-Phase Synthesis of Depsides and Depsipeptides. Preparation of a Valinomycin Analogue. *The Journal of Organic Chemistry*, *64*(22), 8063–8075. http://doi.org/10.1021/jo981580+

Kumar, S., Rosenberg, J. M., Bouzida, D., Swendsen, R. H., & Kollman, P. A. (1992). The weighted histogram analysis method for free-energy calculations on biomolecules. I. The method. *Journal of Computational Chemistry*, *13*, 1011–1021. http://doi.org/10.1002/jcc.540130812

Lakshminarayanan, R., Fan, D., Du, C., & Moradian-Oldak, J. (2007). The role of secondary structure in the entropically driven amelogenin self-assembly. *Biophysical Journal*, *93*(10), 3664–3674. http://doi.org/10.1529/biophysj.107.113936

Lau, K. H. A. (2014). Peptoids for biomaterials science. *Biomaterials Science*, *2*(5), 627–633. http://doi.org/10.1039/C3BM60269A

Lee, O.-S., Stupp, S. I., & Schatz, G. C. (2011). Atomistic Molecular Dynamics Simulations of Peptide Amphiphile Self-Assembly into Cylindrical Nanofibers.

Journal of the American Chemical Society, *133*(10), 3677–3683. http://doi.org/10.1021/ja110966y

Lemkul, J. A., & Bevan, D. R. (2010). Assessing the Stability of Alzheimer's Amyloid Protofibrils Using Molecular Dynamics. *The Journal of Physical Chemistry B*, *114*, 1652–1660. http://doi.org/10.1021/jp9110794

Le Novère, N. (2001). MELTING, computing the melting temperature of nucleic acid duplex. *Bioinformatics*, *17*, 1226–1227. http://doi.org/10.1093/bioinformatics/17.12.1226

Liang, G., Yang, Z., Zhang, R., Li, L., Fan, Y., Kuang, Y., … Xu, B. (2009). Supramolecular Hydrogel of a d-Amino Acid Dipeptide for Controlled Drug Release in Vivo†. *Langmuir*, *25*(15), 8419–8422. http://doi.org/10.1021/la804271d

Liang, J., Moore, R. E., Moher, E. D., Munroe, J. E., Al-awar Rima S., Hay, D. A., … others. (2005). Cryptophycins-309, 249 and other cryptophycin analogs: preclinical efficacy studies with mouse and human tumors. *Investigational New Drugs*, *23*(3), 213–224.

Li, J., Kuang, Y., Gao, Y., Du, X., Shi, J., & Xu, B. (2013). d-Amino Acids Boost the Selectivity and Confer Supramolecular Hydrogels of a Nonsteroidal Anti-Inflammatory Drug (NSAID). *Journal of the American Chemical Society*, *135*(2), 542–545. http://doi.org/10.1021/ja310019x

Li, J., Kuang, Y., Shi, J., Gao, Y., Zhou, J., & Xu, B. (2013). The conjugation of nonsteroidal anti-inflammatory drugs (NSAID) to small peptides for generating multifunctional supramolecular nanofibers/hydrogels. *Beilstein Journal of Organic Chemistry*, *9*, 908–917. http://doi.org/10.3762/bjoc.9.104

Ling, L. L., Schneider, T., Peoples, A. J., Spoering, A. L., Engels, I., Conlon, B. P., … Lewis, K. (2015). A new antibiotic kills pathogens without detectable resistance. *Nature*, *517*(7535), 455–459. http://doi.org/10.1038/nature14098

Li, W., Schlecker, A., & Ma, D. (2010). Total synthesis of antimicrobial and antitumor cyclic depsipeptides. *Chemical Communications*, *46*(30), 5403–5420. http://doi.org/10.1039/C0CC00629G

Li, X., Kuang, Y., Lin, H.-C., Gao, Y., Shi, J., & Xu, B. (2011). Supramolecular Nanofibers and Hydrogels of Nucleopeptides. *Angewandte Chemie International Edition*, *50*(40), 9365–9369. http://doi.org/10.1002/anie.201103641

Li, X., Kuang, Y., & Xu, B. (2012). "Molecular trinity" for soft nanomaterials: integrating nucleobases, amino acids, and glycosides to construct multifunctional hydrogelators. *Soft Matter*, *8*(10), 2801–2806. http://doi.org/10.1039/C2SM06920B

Mabey, W., & Mill, T. (1978). Critical review of hydrolysis of organic compounds in water under environmental conditions. *Journal of Physical and Chemical Reference Data*, *7*(2), 383–415. http://doi.org/doi:10.1063/1.555572

Maheshwari, G., Brown, G., Lauffenburger, D. A., Wells, A., & Griffith, L. G. (2000). Cell adhesion and motility depend on nanoscale RGD clustering. *Journal of Cell Science*, *113*(10), 1677–1686.

Mahler, A., Reches, M., Rechter, M., Cohen, S., & Gazit, E. (2006). Rigid, Self-Assembled Hydrogel Composed of a Modified Aromatic Dipeptide. *Advanced Materials*, *18*(11), 1365–1370. http://doi.org/10.1002/adma.200501765

Matson, J. B., & Stupp, S. I. (2011). Drug release from hydrazone-containing peptide amphiphiles. *Chem. Commun.*, *47*(28), 7962–7964. http://doi.org/10.1039/C1CC12570B

McCammon, J., Gelin, B., & Karplus, M. (1977). Dynamics of folded proteins. *Nature*, *267*(5612), 585–590. http://doi.org/10.1038/267585a0

McGaughey, G. B., Gagné, M., & Rappé, A. K. (1998). π-Stacking Interactions. *Journal of Biological Chemistry*, *273*(25), 15458–15463.

Modepalli, V. N., Rodriguez, A. L., Li, R., Pavuluri, S., Nicholas, K. R., Barrow, C. J., … Williams, R. J. (2014). In vitro response to functionalized self-assembled peptide scaffolds for three-dimensional cell culture. *Peptide Science*, *102*(2), 197–205. http://doi.org/10.1002/bip.22469

Moore, R. E. (1996). Cyclic peptides and depsipeptides from cyanobacteria: A review. *Journal of Industrial Microbiology*, *16*(2), 134–143. http://doi.org/10.1007/BF01570074

Munoz, B., Giam, C.-Z., & Wong, C.-H. (1994). α-Ketoamide Phe—Pro isostere as a new core structure for the inhibition of HIV protease. *Bioorganic & Medicinal Chemistry*, *2*(10), 1085–1090. http://doi.org/10.1016/S0968-0896(00)82058-1

Mu, X., Eckes, K. M., Nguyen, M. M., Suggs, L. J., & Ren, P. (2012). Experimental and Computational Studies Reveal an Alternative Supramolecular Structure for Fmoc-Dipeptide Self-Assembly. *Biomacromolecules*, *13*(11), 3562–3571. http://doi.org/10.1021/bm301007r

Nagai, Y., Unsworth, L. D., Koutsopoulos, S., & Zhang, S. (2006). Slow release of molecules in self-assembling peptide nanofiber scaffold. *Journal of Controlled Release*, *115*(1), 18–25. http://doi.org/10.1016/j.jconrel.2006.06.031

Nanotope, Inc. (2014). Retrieved February 27, 2015, from http://www.nanotope.com

Narmoneva, D. A., Oni, O., Sieminski, A. L., Zhang, S., Gertler, J. P., Kamm, R. D., & Lee, R. T. (2005). Self-assembling short oligopeptides and the promotion of angiogenesis. *Biomaterials*, *26*(23), 4837–4846. http://doi.org/10.1016/j.biomaterials.2005.01.005

Newman, D. J., & Cragg, G. M. (2004). Marine natural products and related compounds in clinical and advanced preclinical trials. *Journal of Natural Products*, *67*(8), 1216–1238.

Nguyen, M. M., Eckes, K. M., & Suggs, L. J. (2014). Charge and sequence effects on the self-assembly and subsequent hydrogelation of Fmoc-depsipeptides. *Soft Matter*, *10*(15), 2693. http://doi.org/10.1039/c4sm00009a

Nguyen, M. M., Ong, N., & Suggs, L. (2013). A general solid phase method for the synthesis of depsipeptides. *Organic & Biomolecular Chemistry*, *11*(7), 1167. http://doi.org/10.1039/c2ob26893k

Niece, K. L., Hartgerink, J. D., Donners, J. J. J. M., & Stupp, S. I. (2003). Self-Assembly Combining Two Bioactive Peptide-Amphiphile Molecules into Nanofibers by Electrostatic Attraction. *J. Am. Chem. Soc.*, *125*(24), 7146–7147. http://doi.org/10.1021/ja028215r

Ni, Y., Becquart, F., Chen, J., & Taha, M. (2013). Polyurea–Urethane Supramolecular Thermo-Reversible Networks. *Macromolecules*, *46*(3), 1066–1074. http://doi.org/10.1021/ma302421r

Nordén, B., Rodger, A., & Dafforn, T. (2010). *Linear Dichroism and Circular Dichroism: A Textbook on Polarized-Light Spectroscopy*. Royal Society of Chemistry.

Nymeyer, H., Gnanakaran, S., & García, A. E. (2004). Atomic Simulations of Protein Folding, Using the Replica Exchange Algorithm. In L. B. and M. L. Johnson (Ed.), *Methods in Enzymology* (Vol. 383, pp. 119–149). Academic Press. Retrieved from http://www.sciencedirect.com/science/article/pii/S0076687904830064

Orbach, R., Adler-Abramovich, L., Zigerson, S., Mironi-Harpaz, I., Seliktar, D., & Gazit, E. (2009). Self-Assembled Fmoc-Peptides as a Platform for the Formation of Nanostructures and Hydrogels. *Biomacromolecules*, *10*(9), 2646–2651. http://doi.org/10.1021/bm900584m

Ortoleva, P., Singharoy, A., & Pankavich, S. (2013). Hierarchical multiscale modeling of macromolecules and their assemblies. *Soft Matter*, *9*, 4319–4335. http://doi.org/10.1039/c3sm50176k

Page-McCaw, A., Ewald, A. J., & Werb, Z. (2007). Matrix metalloproteinases and the regulation of tissue remodelling. *Nature Reviews Molecular Cell Biology*, *8*(3), 221–233. http://doi.org/10.1038/nrm2125

Parchaňský, V., Kapitán, J., Kaminský, J., Šebestík, J., & Bouř, P. (2013). Ramachandran Plot for Alanine Dipeptide as Determined from Raman Optical Activity. *The Journal of Physical Chemistry Letters*, *4*(16), 2763–2768. http://doi.org/10.1021/jz401366j

Parrinello, M., & Rahman, A. (1981). Polymorphic transitions in single crystals: A new molecular dynamics method. *Journal of Applied Physics*, *52*(12), 7182–7190.

Pedersen, S. W., Pedersen, S. B., Anker, L., Hultqvist, G., Kristensen, A. S., Jemth, P., & Strømgaard, K. (2014). Probing backbone hydrogen bonding in PDZ/ligand interactions by protein amide-to-ester mutations. *Nature Communications*, *5*. http://doi.org/10.1038/ncomms4215

Pelham, R. J., & Wang, Y. (1997). Cell locomotion and focal adhesions are regulated by substrate flexibility. *Proceedings of the National Academy of Sciences*, *94*(25), 13661–13665.

Pellegrin, S., & Mellor, H. (2007). Actin stress fibres. *Journal of Cell Science*, *120*(20), 3491–3499. http://doi.org/10.1242/jcs.018473

Piehler, J., Brecht, A., Valiokas, R., Liedberg, B., & Gauglitz, G. (2000). A high-density poly(ethylene glycol) polymer brush for immobilization on glass-type surfaces. *Biosensors and Bioelectronics*, *15*(9–10), 473–481. http://doi.org/10.1016/S0956-5663(00)00104-4

Piekarz, R. L., Frye, R., Turner, M., Wright, J. J., Allen, S. L., Kirschbaum, M. H., … Bates, S. E. (2009). Phase II Multi-Institutional Trial of the Histone Deacetylase Inhibitor Romidepsin As Monotherapy for Patients With Cutaneous T-Cell Lymphoma. *Journal of Clinical Oncology*, *27*(32), 5410–5417. http://doi.org/10.1200/JCO.2008.21.6150

Ponder, J. W., & Richards, F. M. (1987). An efficient newton-like method for molecular mechanics energy minimization of large molecules. *Journal of Computational Chemistry*, *8*(7), 1016–1024. http://doi.org/10.1002/jcc.540080710

PuraMatrix. (2014). Retrieved February 26, 2015, from http://www.puramatrix.com/index.html

Qin, S.-Y., Pei, Y., Liu, X.-J., Zhuo, R.-X., & Zhang, X.-Z. (2013). Hierarchical self-assembly of a [small beta]-amyloid peptide derivative. *Journal of Materials Chemistry B*, *1*, 668–675. http://doi.org/10.1039/c2tb00105e

Raeburn, J., Cardoso, A. Z., & Adams, D. J. (2013). The importance of the self-assembly process to control mechanical properties of low molecular weight hydrogels. *Chemical Society Reviews*, *42*(12), 5143–5156. http://doi.org/10.1039/C3CS60030K

Raeburn, J., Pont, G., Chen, L., Cesbron, Y., Lévy, R., & Adams, D. J. (2012). Fmoc-diphenylalanine hydrogels: understanding the variability in reported mechanical properties. *Soft Matter*, *8*(4), 1168–1174. http://doi.org/10.1039/C1SM06929B

Reches, M., & Gazit, E. (2003). Casting Metal Nanowires Within Discrete Self-Assembled Peptide Nanotubes. *Science*, *300*(5619), 625 –627. http://doi.org/10.1126/science.1082387

Ren, P., & Ponder, J. W. (2003). Polarizable Atomic Multipole Water Model for Molecular Mechanics Simulation. *J. Phys. Chem. B*, *107*(24), 5933–5947. http://doi.org/10.1021/jp027815+

Richmond, T. J. (1984). Solvent accessible surface area and excluded volume in proteins: Analytical equations for overlapping spheres and implications for the hydrophobic effect. *Journal of Molecular Biology*, *178*(1), 63–89. http://doi.org/10.1016/0022-2836(84)90231-6

Ruoslahti, E., & Pierschbacher, M. D. (1986). Arg-Gly-Asp: a versatile cell recognition signal. *Cell*, *44*(4), 517–518.

Ryan, D. M., Anderson, S. B., & Nilsson, B. L. (2010). The influence of side-chain halogenation on the self-assembly and hydrogelation of Fmoc-phenylalanine derivatives. *Soft Matter*, *6*(14), 3220–3231. http://doi.org/10.1039/C0SM00018C

Ryan, E. A., Mockros, L. F., Weisel, J. W., & Lorand, L. (1999). Structural Origins of Fibrin Clot Rheology. *Biophysical Journal*, *77*(5), 2813–2826. http://doi.org/10.1016/S0006-3495(99)77113-4

Saha, B., Shindo, S., Irle, S., & Morokuma, K. (2009). Quantum Chemical Molecular Dynamics Simulations of Dynamic Fullerene Self-Assembly in Benzene Combustion. *ACS Nano*, *3*(8), 2241–2257. http://doi.org/10.1021/nn900494s

Schneider, A., Garlick, J. A., & Egles, C. (2008). Self-Assembling Peptide Nanofiber Scaffolds Accelerate Wound Healing. *PLoS ONE*, *3*(1), e1410. http://doi.org/10.1371/journal.pone.0001410

Sekton, B. (2010). Matrix metalloproteinases - an overview. *Research and Reports in Biology*, 1. http://doi.org/10.2147/RRB.S12043

Semino, C. E., Kasahara, J., Hayashi, Y., & Zhang, S. (2004). Entrapment of Migrating Hippocampal Neural Cells in Three-Dimensional Peptide Nanofiber Scaffold. *Tissue Engineering*, *10*, 643–655. http://doi.org/10.1089/107632704323061997

Shuman, R. T., Rothenberger, R. B., Campbell, C. S., Smith, G. F., Gifford-Moore, D. S., & Gesellchen, P. D. (1993). Highly selective tripeptide thrombin inhibitors. *Journal of Medicinal Chemistry*, *36*(3), 314–319.

Silva, G. A., Czeisler, C., Niece, K. L., Beniash, E., Harrington, D. A., Kessler, J. A., & Stupp, S. I. (2004). Selective Differentiation of Neural Progenitor Cells by High-Epitope Density Nanofibers. *Science*, *303*(5662), 1352 –1355. http://doi.org/10.1126/science.1093783

Silverstein, R. M. (1991). *Spectrometric Identification of Organic Compounds* (5th ed). New York: Wiley.

Singelyn, J. M., DeQuach, J. A., Seif-Naraghi, S. B., Littlefield, R. B., Schup-Magoffin, P. J., & Christman, K. L. (2009). Naturally derived myocardial matrix as an

injectable scaffold for cardiac tissue engineering. *Biomaterials*, *30*(29), 5409–5416. http://doi.org/10.1016/j.biomaterials.2009.06.045

Sivanathan, S., & Scherkenbeck, J. (2014). Cyclodepsipeptides: A Rich Source of Biologically Active Compounds for Drug Research. *Molecules*, *19*(8), 12368–12420. http://doi.org/10.3390/molecules190812368

Smith, A. M., Williams, R. J., Tang, C., Coppo, P., Collins, R. F., Turner, M. L., … Ulijn, R. V. (2008). Fmoc-Diphenylalanine Self Assembles to a Hydrogel via a Novel Architecture Based on π–π Interlocked β-Sheets. *Advanced Materials*, *20*(1), 37–41. http://doi.org/10.1002/adma.200701221

Smith, C. D., Zhang, X., Mooberry, S. L., Patterson, G. M. L., & Moore, R. E. (1994). Cryptophycin: A New Antimicrotubule Agent Active against Drug-resistant Cells. *Cancer Research*, *54*(14), 3779–3784.

Smith, D. K. (2009). Lost in translation? Chirality effects in the self-assembly of nanostructured gel-phase materials. *Chem. Soc. Rev.*, *38*(3), 684–694.

Solomon, S. D., Skali, H., Anavekar, N. S., Bourgoun, M., Barvik, S., Ghali, J. K., … Pfeffer, M. A. (2005). Changes in Ventricular Size and Function in Patients Treated With Valsartan, Captopril, or Both After Myocardial Infarction. *Circulation*, *111*(25), 3411–3419. http://doi.org/10.1161/CIRCULATIONAHA.104.508093

Soukasene, S., Toft, D. J., Moyer, T. J., Lu, H., Lee, H.-K., Standley, S. M., … Stupp, S. I. (2011). Antitumor Activity of Peptide Amphiphile Nanofiber-Encapsulated Camptothecin. *ACS Nano*, *5*(11), 9113–9121. http://doi.org/10.1021/nn203343z

Stevenson, J. P., Sun, W., Gallagher, M., Johnson, R., Vaughn, D., Schuchter, L., … others. (2002). Phase I trial of the cryptophycin analogue LY355703 administered as an intravenous infusion on a day 1 and 8 schedule every 21 days. *Clinical Cancer Research*, *8*(8), 2524–2529.

Stillinger, F. (1973). Structure in aqueous solutions of nonpolar solutes from the standpoint of scaled-particle theory. *Journal of Solution Chemistry*, *2*, 141–158. http://doi.org/10.1007/bf00651970

Sugita, Y., & Okamoto, Y. (1999). Replica-exchange molecular dynamics method for protein folding. *Chemical Physics Letters*, *314*(1–2), 141–151. http://doi.org/10.1016/S0009-2614(99)01123-9

Sun, S., & Bernstein, E. R. (1996). Aromatic van der Waals Clusters: Structure and Nonrigidity. *J. Phys. Chem.*, *100*(32), 13348–13366. http://doi.org/10.1021/jp960739o

Sun, S., Wong, J. T. Y., & Zhang, T.-Y. (2011). Effects of external electric fields on the self-assembly of phospholipids/water mixtures—coarse-grained molecular

dynamics simulations. *Soft Matter*, *7*(19), 9307–9310. http://doi.org/10.1039/C1SM05883E

Sutton, S., Campbell, N. L., Cooper, A. I., Kirkland, M., Frith, W. J., & Adams, D. J. (2009). Controlled Release from Modified Amino Acid Hydrogels Governed by Molecular Size or Network Dynamics. *Langmuir*, *25*(17), 10285–10291. http://doi.org/10.1021/la9011058

Svoboda, E. (n.d.). How Samuel Stupp Is Rebuilding Your Body, One Molecule at a Time. Retrieved February 27, 2015, from http://www.fastcompany.com/1715179/how-samuel-stupp-rebuilding-your-body-one-molecule-time

Tang, C., Smith, A. M., Collins, R. F., Ulijn, R. V., & Saiani, A. (2009). Fmoc-Diphenylalanine Self-Assembly Mechanism Induces Apparent pKa Shifts. *Langmuir*, *25*(16), 9447–9453. http://doi.org/10.1021/la900653q

Teplow, D. B., Lazo, N. D., Bitan, G., Bernstein, S., Wyttenbach, T., Bowers, M. T., … Stanley, H. E. (2006). Elucidating Amyloid β-Protein Folding and Assembly: A Multidisciplinary Approach. *Accounts of Chemical Research*, *39*(9), 635–645. http://doi.org/10.1021/ar050063s

Tian, Y. F., Hudalla, G. A., Han, H., & Collier, J. H. (2013). Controllably degradable β-sheet nanofibers and gels from self-assembling depsipeptides. *Biomaterials Science*, *1*(10), 1037. http://doi.org/10.1039/c3bm60161g

Tiec, C. L., Barrail, A., Goujard, C., & Taburet, D. A.-M. (2012). Clinical Pharmacokinetics and Summary of Efficacy and Tolerability of Atazanavir. *Clinical Pharmacokinetics*, *44*(10), 1035–1050. http://doi.org/10.2165/00003088-200544100-00003

Todd, S. J., Scurr, D. J., Gough, J. E., Alexander, M. R., & Ulijn, R. V. (2009). Enzyme-Activated RGD Ligands on Functionalized Poly(ethylene glycol) Monolayers: Surface Analysis and Cellular Response. *Langmuir*, *25*(13), 7533–7539. http://doi.org/10.1021/la900376h

Tycko, R. (2003). Insights into the Amyloid Folding Problem from Solid-State NMR. *Biochemistry*, *42*(11), 3151–3159. http://doi.org/10.1021/bi027378p

Tysseling-Mattiace, V. M., Sahni, V., Niece, K. L., Birch, D., Czeisler, C., Fehlings, M. G., … Kessler, J. A. (2008). Self-Assembling Nanofibers Inhibit Glial Scar Formation and Promote Axon Elongation after Spinal Cord Injury. *Journal of Neuroscience*, *28*(14), 3814–3823. http://doi.org/10.1523/JNEUROSCI.0143-08.2008

Van Gunsteren, W. F., & Berendsen, H. J. C. (1988). A Leap-frog Algorithm for Stochastic Dynamics. *Molecular Simulation*, *1*(3), 173–185. http://doi.org/10.1080/08927028808080941

Webber, M. J., Tongers, J., Newcomb, C. J., Marquardt, K.-T., Bauersachs, J., Losordo, D. W., & Stupp, S. I. (2011). Supramolecular nanostructures that mimic VEGF as a strategy for ischemic tissue repair. *Proceedings of the National Academy of Sciences*, *108*(33), 13438 –13443. http://doi.org/10.1073/pnas.1016546108

Whitesides, G. M., & Grzybowski, B. (2002). Self-Assembly at All Scales. *Science*, *295*, 2418–2421. http://doi.org/10.1126/science.1070821

Whitesides, G. M., Mathias, J. P., & Seto, C. T. (1991). Molecular self-assembly and nanochemistry: a chemical strategy for the synthesis of nanostructures. *Science*, *254*(5036), 1312–1319.

WHO | WHO Model Lists of Essential Medicines. (n.d.). Retrieved February 24, 2015, from http://www.who.int/medicines/publications/essentialmedicines/en/

Wiberg, K. B., & Laidig, K. E. (1987). Barriers to rotation adjacent to double bonds. 3. The carbon-oxygen barrier in formic acid, methyl formate, acetic acid, and methyl acetate. The origin of ester and amide resonance. *Journal of the American Chemical Society*, *109*(20), 5935–5943. http://doi.org/10.1021/ja00254a006

Williams, R. J., Hall, T. E., Glattauer, V., White, J., Pasic, P. J., Sorensen, A. B., … Hartley, P. G. (2011). The in vivo performance of an enzyme-assisted self-assembled peptide/protein hydrogel. *Biomaterials*, *32*(22), 5304–5310. http://doi.org/10.1016/j.biomaterials.2011.03.078

Wolf, M. G., Jongejan, J. A., Laman, J. D., & de Leeuw, S. W. (2008). Rapid Free Energy Calculation of Peptide Self-Assembly by REMD Umbrella Sampling. *The Journal of Physical Chemistry B*, *112*(43), 13493–13498. http://doi.org/10.1021/jp804285e

Wu, Y., Sellitti, C., Anderson, J. M., Hiltner, A., Lodoen, G. A., & Payet, C. R. (1992). An FTIR–ATR investigation of in vivo poly (ether urethane) degradation. *Journal of Applied Polymer Science*, *46*(2), 201–211.

Xu, L., Li, C., & Ng, K. Y. S. (2000). In-Situ Monitoring of Urethane Formation by FTIR and Raman Spectroscopy. *The Journal of Physical Chemistry A*, *104*(17), 3952–3957. http://doi.org/10.1021/jp992622g

Yang, Z., Gu, H., Fu, D., Gao, P., Lam, J. K., & Xu, B. (2004). Enzymatic Formation of Supramolecular Hydrogels. *Advanced Materials*, *16*(16), 1440–1444. http://doi.org/10.1002/adma.200400340

Yang, Z., Liang, G., Ma, M., Gao, Y., & Xu, B. (2007). Conjugates of naphthalene and dipeptides produce molecular hydrogelators with high efficiency of hydrogelation and superhelical nanofibers. *Journal of Materials Chemistry*, *17*(9), 850–854.

Yang, Z., Liang, G., Wang, L., & Xu, B. (2006). Using a Kinase/Phosphatase Switch to Regulate a Supramolecular Hydrogel and Forming the Supramolecular Hydrogel

in Vivo. *Journal of the American Chemical Society*, *128*(9), 3038–3043. http://doi.org/10.1021/ja057412y

Yu, T., Lee, O.-S., & Schatz, G. C. (2013). Steered Molecular Dynamics Studies of the Potential of Mean Force for Peptide Amphiphile Self-Assembly into Cylindrical Nanofibers. *The Journal of Physical Chemistry A*, *117*, 7453–7460. http://doi.org/10.1021/jp401508w

Yu, T., & Schatz, G. C. (2013). Free Energy Profile and Mechanism of Self-Assembly of Peptide Amphiphiles Based on a Collective Assembly Coordinate. *The Journal of Physical Chemistry B*, *117*, 9004–9013. http://doi.org/10.1021/jp404835q

Zelzer, M., Scurr, D. J., Alexander, M. R., & Ulijn, R. V. (2012). Development and Validation of a Fluorescence Method to Follow the Build-up of Short Peptide Sequences on Solid 2D Surfaces. *ACS Applied Materials & Interfaces*, *4*(1), 53–58. http://doi.org/10.1021/am2015266

Zhang, J., King, M., Suggs, L., & Ren, P. (2007). Molecular Modeling of Conformational Properties of Oligodepsipeptides. *Biomacromolecules*, *8*(10), 3015–3024. http://doi.org/10.1021/bm070244c

Zhang, S., Holmes, T. C., DiPersio, C. M., Hynes, R. O., Su, X., & Rich, A. (1995). Self-complementary oligopeptide matrices support mammalian cell attachment. *Biomaterials*, *16*(18), 1385–1393. http://doi.org/10.1016/0142-9612(95)96874-Y

Zhang, S., Holmes, T., Lockshin, C., & Rich, A. (1993). Spontaneous assembly of a self-complementary oligopeptide to form a stable macroscopic membrane. *Proceedings of the National Academy of Sciences*, *90*(8), 3334 –3338.

Zhang, S., Marini, D. M., Hwang, W., & Santoso, S. (2002). Design of nanostructured biological materials through self-assembly of peptides and proteins. *Current Opinion in Chemical Biology*, *6*(6), 865–871. http://doi.org/10.1016/S1367-5931(02)00391-5

Zhang, Y., Gu, H., Yang, Z., & Xu, B. (2003). Supramolecular Hydrogels Respond to Ligand–Receptor Interaction. *J. Am. Chem. Soc.*, *125*(45), 13680–13681. http://doi.org/10.1021/ja036817k

Zhang, Y., Kuang, Y., Gao, Y., & Xu, B. (2011). Versatile Small-Molecule Motifs for Self-Assembly in Water and the Formation of Biofunctional Supramolecular Hydrogels. *Langmuir*, *27*(2), 529–537. http://doi.org/10.1021/la1020324

Zhou, M., Smith, A. M., Das, A. K., Hodson, N. W., Collins, R. F., Ulijn, R. V., & Gough, J. E. (2009). Self-assembled peptide-based hydrogels as scaffolds for anchorage-dependent cells. *Biomaterials*, *30*(13), 2523–2530. http://doi.org/10.1016/j.biomaterials.2009.01.010

Zhou, M., Ulijn, R. V., & Gough, J. E. (2014). Extracellular matrix formation in self-assembled minimalistic bioactive hydrogels based on aromatic peptide

amphiphiles. *Journal of Tissue Engineering*, *5*, 2041731414531593. http://doi.org/10.1177/2041731414531593

Zhou, R. (2003). Exploring Protein Folding Free Energy Landscape: Replica Exchange Monte Carlo. In *AIP Conference Proceedings* (Vol. 690, pp. 406–408). AIP Publishing. http://doi.org/10.1063/1.1632168

Zhou, R. (2006). Replica exchange molecular dynamics method for protein folding simulation. In *Protein Folding Protocols* (pp. 205–223). Springer. Retrieved from http://link.springer.com/protocol/10.1385/1-59745-189-4:205

Vita

Kevin Michael Eckes was born in Reno, Nevada. He graduated from Edward C. Reed High School, in Sparks, Nevada, and matriculated at Cornell University in Ithaca, New York. There, he earned a Bachelor's of Science *cum laude* in Biological Engineering with a minor in Biomedical Engineering. He took a year after his undergraduate studies to work in the lab of Dr. Damien Faivre at the Max Planck Institute for Colloid and Interface Research (Institut für Kolloid- und Grenzflächenforschung) in Potsdam, Germany. Upon returning to the U.S., Kevin enrolled at the University of Texas at Austin. He was granted an NSF Graduate Research Fellowship in Spring 2012 to fund his doctoral studies and has received both an Endowed Presidential Fellowship and an Engineering Doctoral Fellowship from the Cockrell School of Engineering. Outside the realm of his scientific pursuits, Kevin is an avid musician who plays violin (primarily), piano, and guitar. He also enjoys cycling, cooking, international travel, coffee, motorcycles, and stimulating conversation with interesting people over good wine.

Permanent email: kevin.eckes@gmail.com

This dissertation was typed by the author.